U. PORTO

FEUP FACULDADE DE ENGENHARIA
UNIVERSIDADE DO PORTO

Vacuum-Assisted Vaginal Delivery: a Biomechanical Study

Ana Beatriz Chorão Estêvão

Mestrado em Engenharia Biomédica

Supervisor: Dulce Alves de Oliveira, PhD

Second Supervisor: Marco Paulo Lages Parente, PhD

July 19, 2021

Vacuum-Assisted Vaginal Delivery: a Biomechanical Study

Ana Beatriz Chorão Estêvão

Mestrado em Engenharia Biomédica

July 19, 2021

Resumo

O parto vaginal é considerado a principal causa de disfunção do pavimento pélvico, que pode levar ao prolapso dos órgãos pélvicos, a incontinência urinária, a incontinência fecal e a outros distúrbios pélvicos. Quando necessário, o instrumento para auxiliar na realização do parto vaginal é a ventosa, que é o dispositivo eleito na prática obstétrica moderna, principalmente pela segurança para o feto e pela menor probabilidade de morbidade materna. Durante o trabalho de parto, o feto tem que passar por diversos movimentos para atravessar com sucesso o canal de parto. Essa sequência de manobras pode causar lesões nos músculos do pavimento pélvico materno e nos ossos pélvicos devido às alterações biomecânicas, que não podem ser medidas *in vivo* por questões éticas e clínicas. Portanto, as simulações computacionais são a técnica usada para compreender estes processos biomecânicos.

Este trabalho tem como objetivo realizar uma análise biomecânica para estudar o impacto na musculatura do pavimento pélvico e nos ossos pélvicos do parto vaginal instrumentado (ventosa). Assim, para simular o parto vaginal assistido com a ventosa, foi utilizado um modelo de elementos finitos dos músculos do pavimento pélvico, dos ossos pélvicos, da cabeça do feto e da ventosa. No modelo dos ossos pélvicos, foram modeladas as articulações sacroilíacas, sacrococcígea e a sínfise púbica. Durante o segundo período do trabalho de parto foi simulada uma apresentação cefálica e uma posição occipito-anterior do feto. Deste modo, foram avaliados alongamentos, tensões e deformações na musculatura do pavimento pélvico. Também foi analisada a força na ventosa, a abertura da sínfise púbica e o movimento e rotação do cóccix e do sacro.

Os resultados obtidos demonstraram que nos músculos do pavimento pélvico ocorreu um alongamento de 1.7, sendo a parte inferior do músculo elevador do ânus, principalmente o pubo-coccígeo, o músculo mais afetado durante o parto e, portanto, onde as lesões são mais propensas a ocorrer. As forças obtidas para puxar a cabeça do feto foram ligeiramente superiores à força que o feto exerce sozinho num parto normal. Em relação aos ossos pélvicos, ocorreu um alargamento de 2.7 mm na sínfise púbica e uma rotação de aproximadamente 17° no cóccix, estando ambos nos valores admissíveis que podem ocorrer durante o trabalho de parto. Portanto, não ocorreu diástase da sínfise púbica nem fratura do cóccix, como pode ocorrer durante partos vaginais instrumentados. Comparando estes resultados com simulações realizadas em partos vaginais normais, não se verificaram grandes diferenças.

ii

Abstract

Vaginal delivery is considered to be the leading cause of pelvic floor dysfunction, which can lead to pelvic organ prolapse, urinary incontinence, fecal incontinence, and other pelvic disorders. When in need, the instrument to assist the mother in carrying out vaginal delivery is a vacuum extractor, which is the device of choice in modern obstetric practice, mainly because of the safety for the fetus and less probability of maternal morbidity. During labor, the fetus has to go through diverse movements in order to successfully pass through the birth canal. This sequence of maneuvers can cause damage to the maternal pelvic floor muscles and pelvic bones due to the biomechanical changes, which cannot be measured *in vivo* because of ethical and clinical reasons. Therefore, computational simulations are the technique used for solving these kinds of biomechanical processes.

This work aims at performing a biomechanical analysis to study the impact on the pelvic floor muscles and the pelvic bones during vaginal delivery with a vacuum extractor. Thus, to simulate the vacuum-assisted vaginal delivery, a finite element model of the pelvic floor muscles, the pelvic bones, the fetus head and the suction cup was used. In the pelvic bones model, the pubic symphysis, sacroiliac and sacrococcygeal joints were modeled. A vertex presentation and an occiput anterior position of the fetus during the second stage of labor were mimicked. Like this, stretches, stresses and strains were evaluated on the pelvic floor muscles. The force on the suction cup was also analyzed, as well as, the widening of the pubic symphysis and the movement and rotation of the coccyx and sacrum.

The results obtained demonstrate that a stretch ratio of 1.7 occurred in the pelvic floor muscles, being the inferior part of the levator ani muscle, especially the pubococcygeus muscle the most affected muscle during the delivery and so where injuries are most prone to occur. The forces obtained to pull the fetus head were slightly higher than the forces that the fetus does by itself in a normal delivery. Regarding the pelvic bones, a widening of 2.7 mm occurred in the pubic symphysis and a rotation of approximately $17°$ was obtained in the coccyx, both being in the permissible values that can occur during labor. Therefore, a diastasis of the symphysis pubic and a coccyx fracture did not occur, as it can happen during instrumental vaginal deliveries. Comparing these results with simulations performed with normal vaginal deliveries, there were no major differences.

iv

Acknowledgements

First, I would like to thank both of my supervisors, Professor Dulce Oliveira and Professor Marco Parente, for all the constant support and dedication given along this work. Even during the lockdown, they were always available to help me with any doubt I had and without their advice, I could not finish this project.

I am truly grateful to my parents, my sister, and my brother, always ready to encourage me and giving me the right words when I most needed them during my academic career. All this would not have been possible without them.

To my friends that accompanied me on this journey, I would like to thank them all, not only for the time that we spent working together but also for being able to relax and share fun moments in the most difficult times along these years.

I also would like to generally thank everyone who helped me directly or indirectly during this project.

Beatriz Estêvão

Contents

List of Figures

List of Tables

Abbreviations and Symbols

:	Double product
α	Activation variable
$\bar{\lambda}_f$	Fiber stretch ratio in the direction N of the underformed fiber
$\bar{C}$	Right Cauchy-Green strain tensor with the volume change eliminated
$\bar{F}$	Deformation gradient with the volume change eliminated
$\bar{I}_1^C$	First invariant of the right Cauchy-Green strain tensor with the volume change eliminated
λ	Stretch vector
φ	A configuration of a body B
Ψ	Helmholtz free-energy function
Ψ_f	Fiber part of the strain-energy function
Ψ_m	Ground matrix part of the strain-energy function
Ψ_{PE}	Passive elastic part of the fiber contribution of the strain-energy function
Ψ_{SE}	Active elastic part of the fiber contribution of the strain-energy function
Ψ_{vol}	Volumetric part of the strain-energy function
η	Virtual displacement or test function
σ	Cauchy stress tensor
τ	Kirchhoff stress tensor
$\cdot$	Scalar Product
$\delta\mathbf{C}$	Variation of the right Cauchy-Green deformation tensor
$\delta\mathbf{E}$	Variation of the Green-Lagrangian strain tensor
$\delta\mathbf{D}$	Virtual stretch rate
$\delta\mathbf{L}$	Virtual velocity gradient
$\delta\mathbf{u}$	Virtual displacement field
$\delta\mathbf{W}$	Virtual work
λ^M	Muscle stretch
μ	Shear modulus of linear elasticity
$\otimes$	Tensor product
ρ	Mass density in the deformed configuration

ρ_0	Mass density in the initial configuration
1	Second order unit tensor
b	Left Cauchy-Green deformation tensor
C	Right Cauchy-Green deformation tensor
E	Green-Lagrange strain tensor
e	Eulerian or Almansi strain tensor
F	Deformation gradient tensor
f	Force acting on the structure
$\mathbf{F}_{ext}$	External equivalent nodal forces
$\mathbf{F}_{int}$	Internal equivalent nodal forces
K	Stiffness matrix
N	Normal to the surface in the reference configuration
n	Normal to the surface in the deformed configuration
P	First Piola-Kirchhoff stress tensor
$\mathbf{R}_f$	Residual force
S	Second Piola-Kirchhoff stress tensor
T	Traction vector in the reference configuration
t	Traction vector in the deformed configuration
U	Right stretch tensor
u	Displacement vector
v	Velocity field
X	A particle belonging to the body B
x	Position of a particle X of B in the configuration φ
Π	Total potential potential
A,a	Parameters of the fiber part of the Martins constitutive model
B	A body
c,b	Parameters of the ground matrix part of the Martins constitutive model
c_{10}	Parameter of Neo-Hookean constituive model
D	Derivative operator
D_1	Penalty parameter of the penalty function to ensure incompressibility
dX	Material line element
dx	Spatial line element
dA	Surface element in the reference configuration
da	Surface element in the spatial configuration
dV	Volume element in the reference configuration

I_C	First invariant of the right Cauchy-Green train tensor
II_C	Second invariant of the right Cauchy-Green train tensor
III_C	Third invariant of the right Cauchy-Green train tensor
J	Jacobian
$N_i(\mathbf{X})$	Interpolation or basis functions
t	time
T_0^M	Maximum muscle tension at resting length
V	Volume of the body
N	Direction of the undeformed fiber
W	Strain energy function

ACOG	American College of Obstetrics and Gynecology
AP	Anteroposterior
AVD	Assisted Vaginal Delivery
CAD	Computer-Aided Design
CS	Cesarean Section
FE	Finite Element
FEM	Finite Element Method
FI	Fecal Incontinence
LAM	Levator Ani Muscles
LOA	Left Occiput Anterior
LOP	Left Occiput Posterior
LOT	Left Occiput Transverse
MRI	Magnetic Resonance Imaging
OA	Occiput Anterior
OP	Occiput Posterior
PFD	Pelvic Floor Dysfunction
PFM	Pelvic Floor Muscles
POP	Pelvic Organ Prolapse
ROA	Right Occiput Anterior
ROP	Right Occiput Posterior
ROT	Right Occiput Transverse
UI	Urinary Incontinence
VD	Vaginal Delivery
VE	Vacuum Extractor
WHO	World Health Organization

Chapter 1

Introduction

This chapter presents a global overview of vaginal deliveries, in particular, assisted vaginal deliveries. It also contains the motivations behind this work and the main objectives.

1.1 Context

The birth of a child is considered to many women a very significant, intense and demanding occasion in their lives. It is a natural and physiological process that can affect the woman positively or negatively, depending on their experiences. However, it is always considered a quite complex event so every childbirth should be as safe as possible [1, 2]. Unfortunately, and according to the World Health Organization (WHO), around the world more than 500 thousand mothers pass away because of problems during childbirth. Also, 2.6 million babies die every year during birth or even before birth [3, 4]. As a consequence, and as national development, reducing child and maternal mortality is essential [5]. Therefore, if any kind of problem arises during natural labor that causes the process to be interrupted or prolonged excessively, a situation of danger can happen not only for the baby but also for the mother. That requires specific measures to speed up birth, being assisted vaginal delivery (AVD) (by vacuum extraction or forceps) and cesarean section (CS) two of the interventions that intend to end these risky situations [6]. When a condition like this is anticipated during pregnancy or when its development is detected at the beginning of labor, a CS is usually performed. Recently, the percentage of deliveries by cesarean section has been increasing. In 2016, a research by WHO stated that these deliveries accounted for 25% in developed countries [7], which is significantly higher than the recommended 15% by WHO. Furthermore, when compared to vaginal delivery (VD), CS comes with extra risks since it is a surgical operation through the abdominal wall and uterine muscle [8, 9]. It can carry problems like considerable infection, the possibility of having a cardiac arrest, anesthetic complications, wound hematoma, hysterectomy, and also an elevated risk of bleeding [6, 8]. Thus, implementing a CS without being recommended is a great cause of concern, and that is why vaginal childbirth is usually recognized as the most frequent mode of delivery [1, 6].

Nevertheless, there are some cases in which problems only become unexpected after the beginning of labor, that is, although the cervix (the lowest portion of the uterus) is already dilated and the fetus' head is already engaged in the mother's pelvis, expulsion does not advance. In these unforeseen cases, doctors regularly resort to AVD with special instruments, which is a delivery in which the obstetrician uses a VE (ventouse) or forceps, in order to speed up the baby's expulsion and end the delivery as soon as possible [10]. The vacuum extraction is frequently applied in the first place because the traction force that the fetal scalp is subjected to is significantly lower than for forceps and these are only used when there is no progress with the vacuum [11]. In the last years, although the total rate of AVD (also named operative or instrumental VD) has been declining, the use of VE has been increasing, and it now accounts for nearly five times the rate of forceps-assisted vaginal births, as shown in Figure 1.1. The frequency of AVD depends on which country it is performed as well as the prevailing obstetric methods. In the US, the use of AVD was 3.1% in 2016, being 2.6% with vacuum-assisted vaginal delivery and 0.5% with forceps [12], while in 2020, the UK showed that 10% to 15% of women gave birth with AVD [13]. As a consequence, and mainly because of the safety of the fetus and fewer possibility of maternal morbidity, the vacuum extractor was declared in the literature to be the technique of choice in modern obstetric practice when in need of AVD [14].
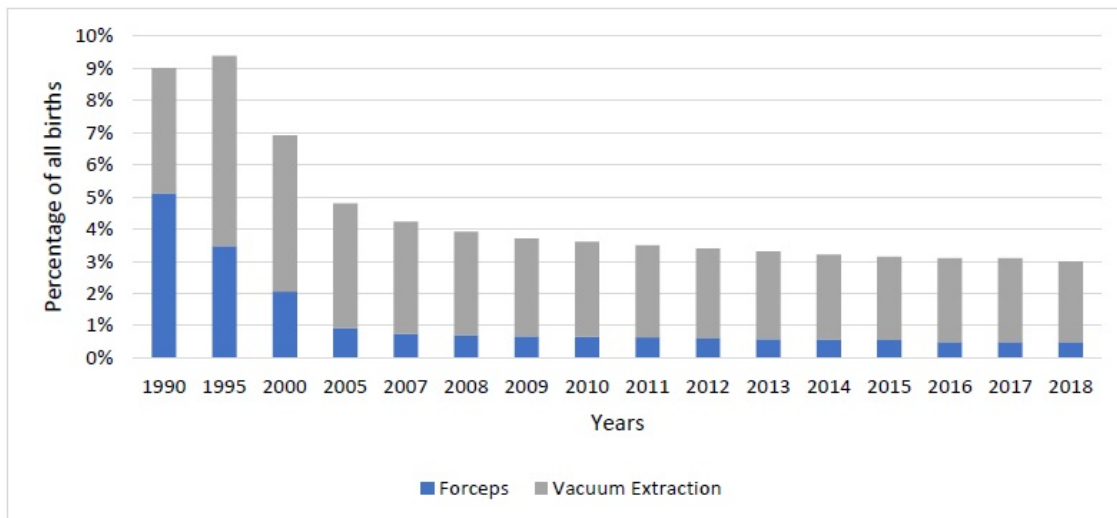
Figure 1.1: Assisted vaginal delivery by forceps or vacuum extraction in the US between 1990-2018 (adapted from [15]).

1.2 Motivation

Throughout pregnancy, because of the hormonal changes and elevated intra-abdominal pressure, the functions of the pelvic floor can be negatively affected [16]. During vaginal delivery, to facilitate the passage of the fetus through the birth canal, the maternal pelvis undergoes some modifications, as it may widening the pubic symphysis and some coccyx movement may occur, which

can affect the sacrococcygeal joint. Also, when the fetus passes from the womb through the cervix and the vagina, the pelvic floor muscles (PFM) go through a series of stretches and strains that can cause severe deformations and damage, and muscles can even rupture. These risks of injury that the PFM are subjected, make vaginal childbirth the leading cause of pelvic floor dysfunction (PFD) [16]. PFD occurs due to the reduction of support and suspension that the components of the levator ani muscle (LAM) of the PFM provide. This loss decreases muscular tonus and LAM becomes weaker, causing injuries to these structures [17]. Injuries usually happen when muscular or collagenous structures are stretched beyond their possible limits [18]. The symptoms of PFD can include chronic pelvic pain, pelvic organ prolapse (POP), urinary incontinence (UI), fecal incontinence (FI), or sexual dysfunction [19]. According to the definition of the International Continence Society (ICS), POP is the descent of one or more of the anterior vaginal wall, posterior vaginal wall, the uterus (cervix), or the apex of the vagina, UI is any complaint of involuntary loss of urine, and FI is the complaint of involuntary loss of feces [20]. This dysfunction represents a major public health problem due to its negative impact on the quality of life of various women and due to its high prevalence [21].

Statistics demonstrate that, in the United States, this disorder affects 24% of women [1] and that at least 11% of women will require surgery due to severe PFD during their lifetime [22]. In addition, 30 to 40% of women experience some degree of incontinence during their lifetime [23]. Several studies have proved that PFD also increases with age and affects 9.7% of women aged between 20-39 and 49.7% of women aged 80 and over [24]. Nygaard et al. [24] verified that the number of pregnancies also has an impact on the risk of having PFDs, affecting 18.4% of women with only one pregnancy, 24.6% of women with two pregnancies, and 32.4% of women with three or more pregnancies. As demonstrated by ultrasound and magnetic resonance imaging (MRI), after an instrumental vaginal delivery, PFM are at higher risk of injuries than after a spontaneous VD, increasing the risk of having PFD [25]. Researches also confirm that forceps delivery is associated with more damage on the LAM than vacuum delivery, and therefore rising the change of having PFD [26].

1.3   Objectives

The main goal of this study is to contribute to obtaining a better knowledge in the field of assisted vaginal delivery with a vacuum extractor. For this purpose, a biomechanical analysis in instrumented vaginal delivery with a vacuum extractor device, is going to be performed in order to observe the impact on the maternal pelvic floor muscles as well as in the female pelvis. To the best of our knowledge, there are only a few studies that use computer models to perform biomechanical simulations of vaginal deliveries, and those do not include a vacuum extractor to evaluate these impacts.

In this work, computer simulations are going to be developed in ABAQUS software in order to mimic a vertex presentation and an occiput anterior position of the fetus during the second stage of labor. For this, a validated computer model of the maternal pelvis is going to be used and a

model of a suction cup is going to be created in SOLIDWORKS software. The suction cup is then going to be placed in the correct position on the fetus' head and the simulation will occur so we can observe its impact on the mothers' PFM, like stresses, strains and stretches; analyze the widening of the pubic symphysis and the movement and rotation of the coccyx; the displacement of the sacrum and coccyx and also to observe the reaction force applied in the suction cup.

1.4   Outline

In addition to the Introduction, this work is structured in 5 more chapters.

Chapter 2 presents an explanation of the basics concepts needed to understand this study. This includes the anatomy of the maternal pelvis, the fetal head and the pelvic floor muscles. It also considers the labor mechanisms and a description of an instrumental vaginal delivery, in particular, vacuum-assisted delivery.

In chapter 3, the state of the art and the works that have already been developed in the area are described.

Chapter 4 introduces the fundamentals of the finite element method, like some solid mechanics kinematic concepts, some variational principles and constitutive equations. There is also an introduction on the software used in this work, the ABAQUS software.

Chapter 5 shows the finite element models that were used in this work and it also describes the constitutive models. The results obtained for the numerical simulation with the suction cup as well as the discussion of the simulation are also present.

Lastly, chapter 6 presents the mainly conclusions and it proposes some future work to improve the present study.

Chapter 2

Labor

In this chapter, a description about the basics concepts needed to understand this work are described.

2.1 Normal Labor

Labor, also known as vaginal delivery, can be defined as a sequence of events that end the pregnancy and concludes with the expulsion of the fetus, followed by the amniotic fluid, placenta and membranes through the birth canal [5, 9, 27]. It starts with the voluntary onset of regular uterine contractions which origins the effacement and the continuous dilation of the cervix and leads to the descent of the fetus [5, 27]. During labor, the fetal presentation has to adapt itself to the possible diameters of the pelvis, in order to get through the most favorable dimensions in the birth canal. Therefore, the delivery mechanism depends on the morphology and configuration of the maternal pelvis, fetal presentation, and also on uterine contractibility [10].

To successfully accomplish a safe vaginal delivery and to reduce complications to the mother and the baby, it is essential to have an adequate obstetric care. For that, the understanding of the interaction between uterine contractibility, the maternal pelvis (the passage), the fetus head (the passenger), the pelvic floor muscles, and the delivery mechanisms is crucial for a proper management of childbirth [27].

2.1.1 Maternal Pelvis

The female pelvis has essential functions like aiding in human locomotion, as the lower limbs carry the body weight through the pelvic girdle, it also supports abdominal organs by the muscles on the pelvic floor and by the pelvis itself. Another significant role is in childbirth, as the fetus must go through the birth canal, which is composed of the womb, cervix, vagina, and vulva that are placed in the pelvic girdle [28]. The bony pelvis is formed by four main bones, which are the two hip bones, also called innominate bones, the sacrum, and the coccyx. The innominate bones are joined to each other anteriorly by the pubic symphysis and to the sacrum posteriorly. Each of them is composed of the union between the ilium, ischium and pubis that are merged together

at the acetabulum, which articulates with the head of the femur [5, 9, 27]. The pelvis is generally divided into two regions: greater (or false) pelvis and in lesser (or true) pelvis, separated by an oblique plane, called the pelvic brim (or pelvic inlet), which forms a circumference that passes through the sacrum, the iliopectineal lines and the symphysis pubis [27, 29] (Figure 2.1). The true pelvis is the most important part of the obstetric area because it creates the path during childbirth. It contains the abdominal viscera and it is limited superiorly by the pelvic inlet and inferiorly by another imaginary plane, the pelvic outlet, and in the middle both include the pelvic cavity. The pelvic outlet (Figure 2.2) has a shape of a diamond [30] and is anteriorly bounded by the pubic symphysis, on each side by the ischial tuberosity and by the coccyx posteriorly. Above the pelvic inlet, the false pelvis is located [9, 27, 31].
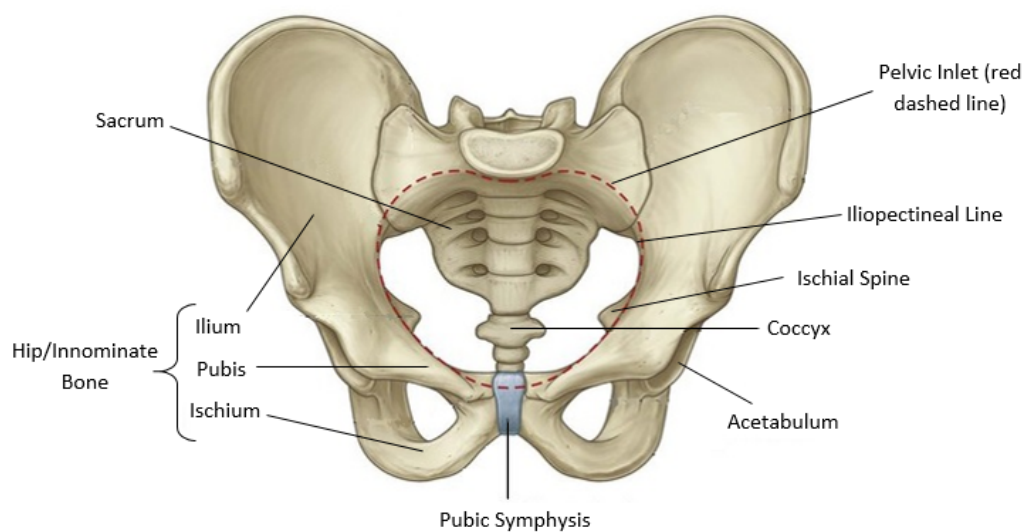
Figure 2.1: Anterior view of the female bony pelvis (adapted from [30]).
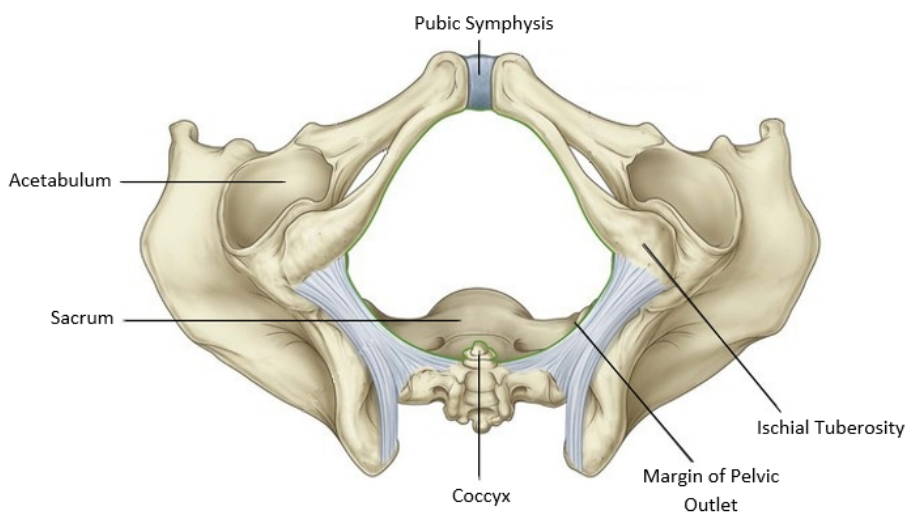
Figure 2.2: Pelvic outlet (adapted from [30]).

• **Pelvic joints and ligaments**

The pubic symphysis links the two hip bones anteriorly. It is a secondary cartilaginous joint that is covered by hyaline cartilage and connected by fibrocartilage, forming the interpubic disc. The pelvic joints are sustained by several ligaments. The ligaments present in the pubic symphysis joint is the superior pubic ligament, which strengthens the joint above and the inferior pubic ligament (or arcuate pubic ligament) which is located below the joint (Figure 2.3a). Although no noticeable movement happens in this joint, some widening of the pubic ligaments may occur during labor [30, 31]. Due to the hormones during pregnancy, pelvic laxity is increased and the separation of the pubic symphysis can happen. A normal symphysys pubic gap, in a nonpregnant woman, is between 4 to 5 mm but in the last months of pregnancy, a normal widening of 2 to 3 mm can occur, without pain. However, diastasis of the symphysis pubis can happen when the pubic symphysis gap is equal or larger to 10 mm and when a instrumental delivery is necessary, this gap can get even bigger [32, 33].

The sacroiliac is a synovial joint that is located between the sacral and iliac auricular surfaces. This joint surfaces are irregular which restricts its movement. The sacroiliac joint has 3 main ligaments: the anterior sacroiliac ligaments, which connect the bones above and below the pelvic inlet, forming the anterior part of the fibrous capsule; the interosseous sacroiliac ligaments which are a mass of the strongest ligaments that join the sacrum to the ilium postero superiorly, occupying the irregular spaces; and the posterior sacroiliac ligaments, being the most superficial fibres which cover the interosseous ligaments (Figure 2.3) [30, 31]. Ligaments are responsible for the stability of the sacroiliac joint. Together with the interosseous ligaments, the iliolumbar ligament counters any movement of the sacroiliac joint. To oppose the anterior rotation of the sacrum are the sacrotuberous and sacrospinous ligaments. The sacrotuberous ligament is mixed with the posterior sacroiliac ligament and is liked to the posterior superior and inferior of the iliac spines, to the lateral sacral crest and to the the lateral edges of the lower sacrum and upper coccyx. The sacrospinous ligament is attached to the margin of the sacrum and upper coccyx and goes to the ischial spines, anterior to the sacrotuberous ligament [31].

Like the pubic symphysis, the sacrococcygeal joint is a secondary cartilaginous joint that is located between the sacrum and the coccyx. It has a disc made of fibrocartilage, composed of hyaline cartilage. The ligaments that reinforce this joint are the anterior and posterior sacrococcygeal ligaments. In the last months of pregnancy and in labor, the pelvic ligaments become softer, allowing the the sacrococcygeal joint to move and the coccyx to have some rotation [31]. A normal coccyx can have between 5 to 22 degrees of rotation [34], however with an intrumental vaginal delivery the coccyx can have a rotation superior to 22 degrees and it can even fracture [35].
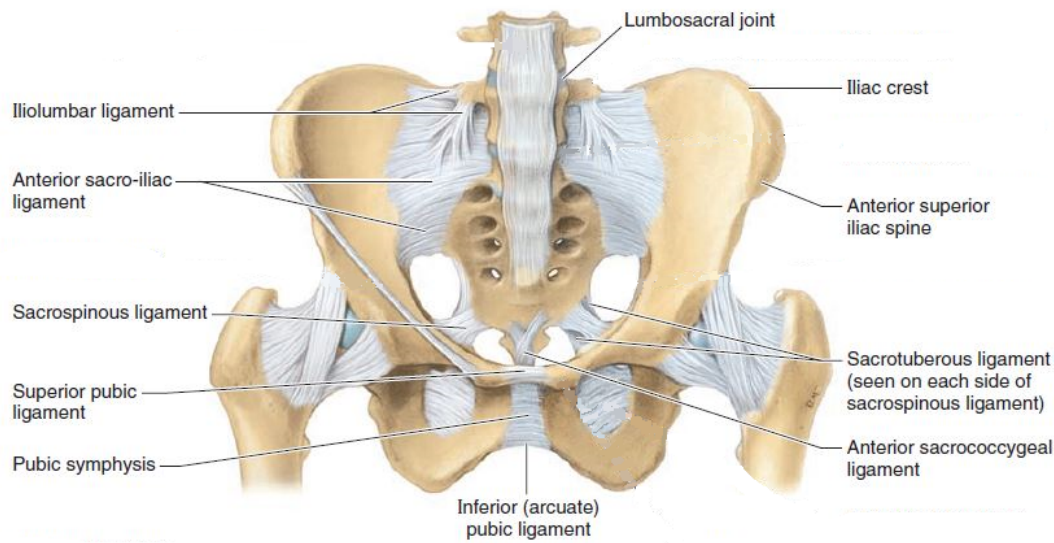
(a) Anterior view.
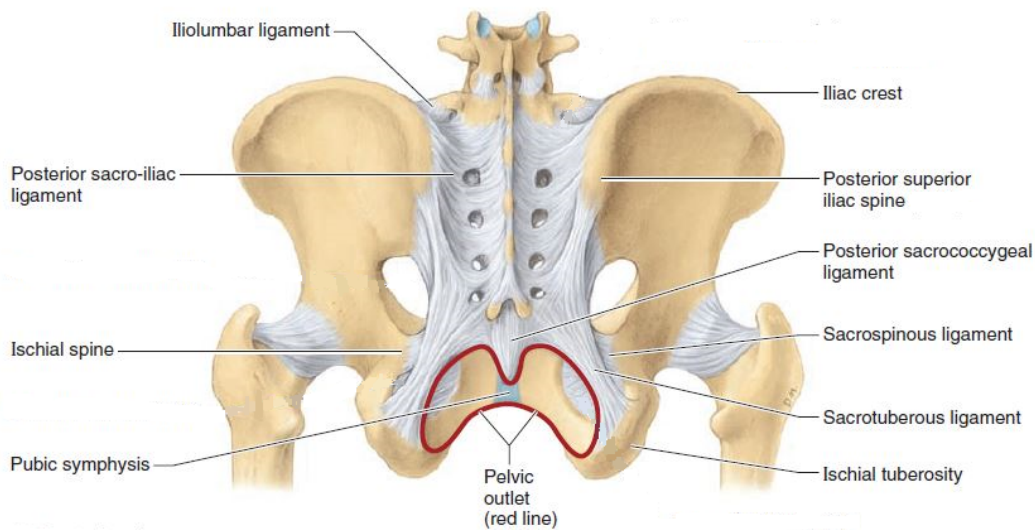
(b) Posterior view.

Figure 2.3: Ligaments and joints of the pelvis (adapted from [31]).

- **Pelvic planes and diameters**

There are four imaginary plans of the pelvis, that correspond to the main measurements for assessing the capacity of the maternal pelvis [36]. They are the inlet, the plane of greatest and least (midplane) diameter and the outlet (Figure 2.4). It is through these diameters that the fetus descends and goes through various movements in order to pass the challenging shape of the bony pelvis [27].

The pelvic inlet is composed of the anteroposterior diameter, which is a sagittal diameter that goes from the sacrum to the symphysis pubis; the transverse diameter is the widest diameter that links the iliopectineal lines; the oblique diameter that connects the sacroiliac joint and the opposite iliopectineal eminence (Figure 2.5a) [37]. In this diameter, there is also the anatomic conjugate which distances from the middle of the sacral promontory to the superior aspect of the pubic symphysis. The obstetric conjugate connects the middle of the sacral promontory to the posterior superior margin of the pubic symphysis and is the most important diameter since is where the fetus must pass through. The diagonal conjugate extends from the the sacral promontory to the inferior margin of the pubic symphysis (Figure 2.5b) [37].

(a) Sagittal view.

(b) Coronal view.
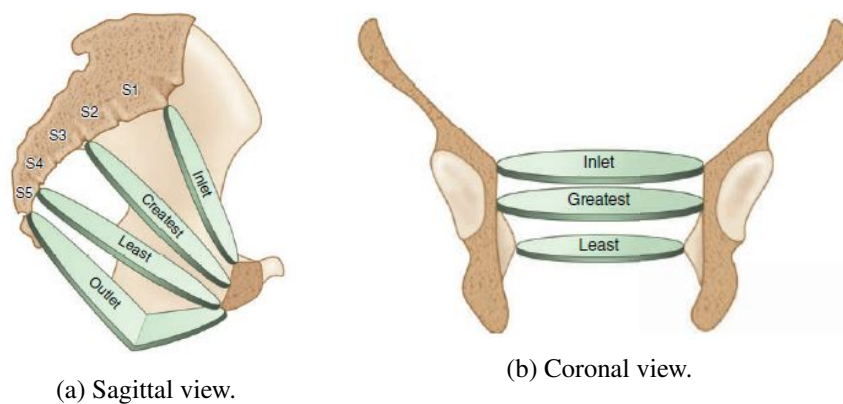
Figure 2.4: Pelvic planes [37].

(a) Anteroposterior view.

(b) Sagittal view.
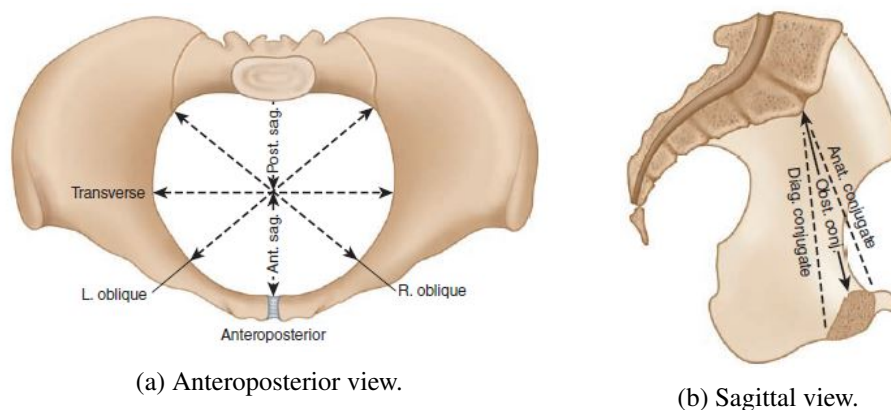
Figure 2.5: Pelvic inlet diameters [37].

In the plane of greatest diameter, the anteroposterior diameter goes from the midpoint of the posterior surface of the pubis to the junction of the second and third sacral vertebrae, while the transverse diameter extends through the lateral margins of the plane [37].

The midplane or plane of least diameter is the most important plane of the pelvis. In this plane, the anteroposterior diameter connects the lower part of the pubis to the junction of the fourth and fifth sacral vertebrae, while the transverse diameter extends between the ischial spines. The posterior sagittal diameter goes from midpoint of the bispinous diameter to the junction of the fourth and fifth sacral vertebrae (Figure 2.6) [37].

(a) Anteroposterior view.   (b) Sagittal view.
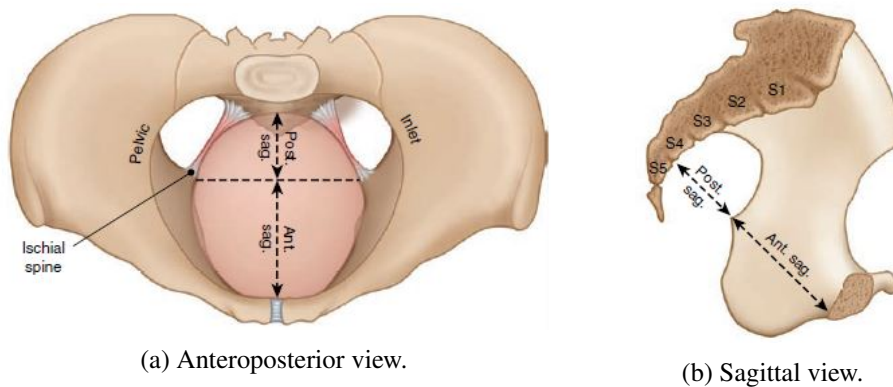
Figure 2.6: Midplane or plane of least diameters [37].

The pelvic outlet has four principal diameters. The anteroposterior diameter that extends from the apex of the coccyx to the midpoint of the lower pubic symphysis. The obstetric anteroposterior diameter connects the inferior margin of the pubis to the sacrococcygeal joint, while the transverse diameter has the distance of the ischial tuberosities at the lower borders of their medial surfaces. The posterior sagittal diameter extends from the middle of the transverse diameter to the sacrococcygeal joint (Figure 2.7) [37].

(a) Inferior view.   (b) Sagittal view.
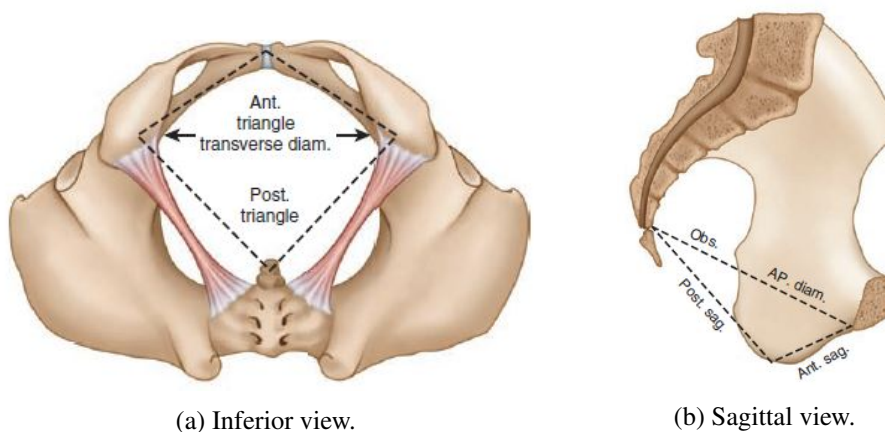
Figure 2.7: Pelvic outlet [37].

- **Pelvic Classification**

There are four main shapes that the female pelvis can be classified in, determined by the diameters of the inlet and pelvic cavity. Despite genetics, these shapes are also alleged to be different based on culture and environment. These shapes are gynecoid, anthropoid, android and platypelloid (Figure 2.8). The gynecoid pelvis is round and the most common one; the anthropoid has an oval inlet, a long and narrow pelvic cavity and the anteroposterior diameter is the broadest; the android, has an inlet with a shape of a heart and a thin outlet and the platypelloid shape has a flat inlet and the inlet anteroposterior diameter is shorter than a gynecoid pelvis but has a wider transverse diameter [9, 27].
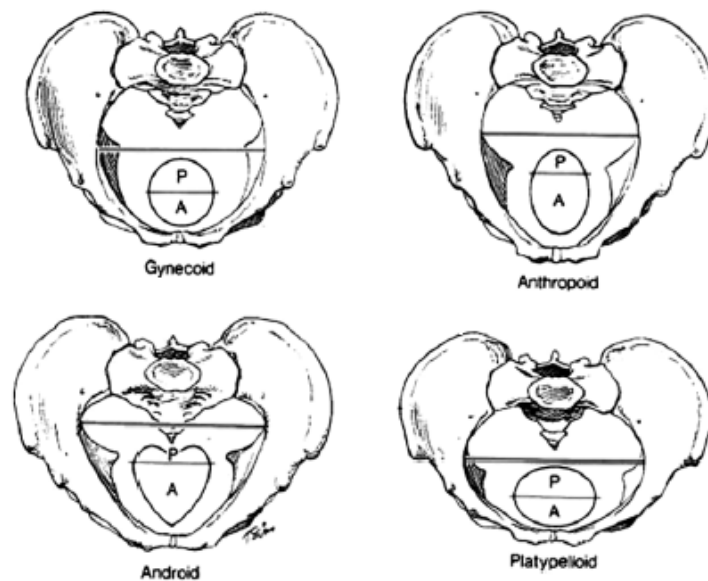
Figure 2.8: Different shapes of the female pelvis [9].

2.1.2 Fetal Head

The fetal skull is formed by five bones: two frontal bones, two parietal bones, and the occipital bone (Figure 2.9). The two parietal bones are separated by the sagittal suture, the frontal bones are separated by the frontal suture, the suture that separates the two frontal and the two parietal bones is called coronal suture and between the parietal bones and the occipital bone is the lambdoid suture. A fontanelle is a space composed of two or more sutures. The anterior fontanelle is made up of the sagittal, frontal and the two coronal sutures, while the posterior fontanelle is formed by the sagittal and the two lambdoid sutures (Figure 2.10) [5, 27].

Due to pressures and forces that the fetal head goes through as it descends in the birth canal, the anatomical connection between the skull bones is modified, enabling the fetus' head to arrange itself to the geometry of the birth canal. This process is named molding and it can decrease

the diameters of the fetal cranium. The fetal head is also divided into parts, in order to help in determining which presenting region is the lowest during examinations in vaginal delivery. The face is the part that goes from the nose to the chin. The brow is the region between the front of the anterior fontanelle and the nose, while the bregma is the region that covers the anterior fontanelle. The vertex is the region bounded by both fontanelles and it also covers the parietal bones and the part that is below the posterior fontanelle is called the occiput (Figure 2.9) [27].

During the course of labor, the fetal head takes different degrees of flexion that defines which area of the skull is presenting at the moment. Diameters of the presenting area are important and are presented in Figure 2.11. The relevant diameters are the suboccipitobregmatic (9,5 cm, vertex fully flexed), submentobregmatic (9,5 cm), mentovertical (13,5 cm), suboccipitofrontal (10,5 cm) and occipitofrontal (11,5 cm) [5, 27]. Depending on the degree that is presenting, due to the molding, the delivery may occur spontaneously, or an operative delivery has to be made [16].
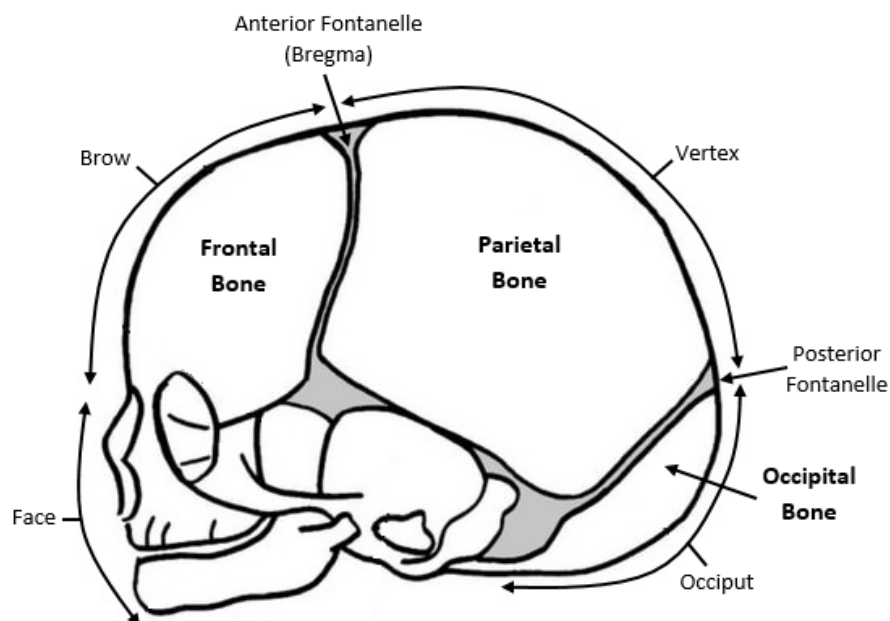
Figure 2.9: Fetal skull bones and regions (adapted from [27]).
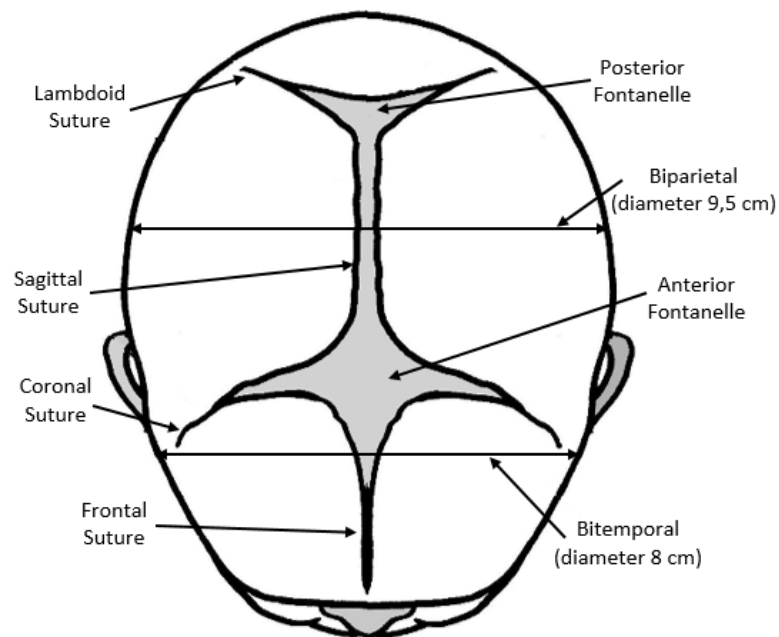
Figure 2.10: Sutures and fontanelles of the fetal skull (adapted from [27]).
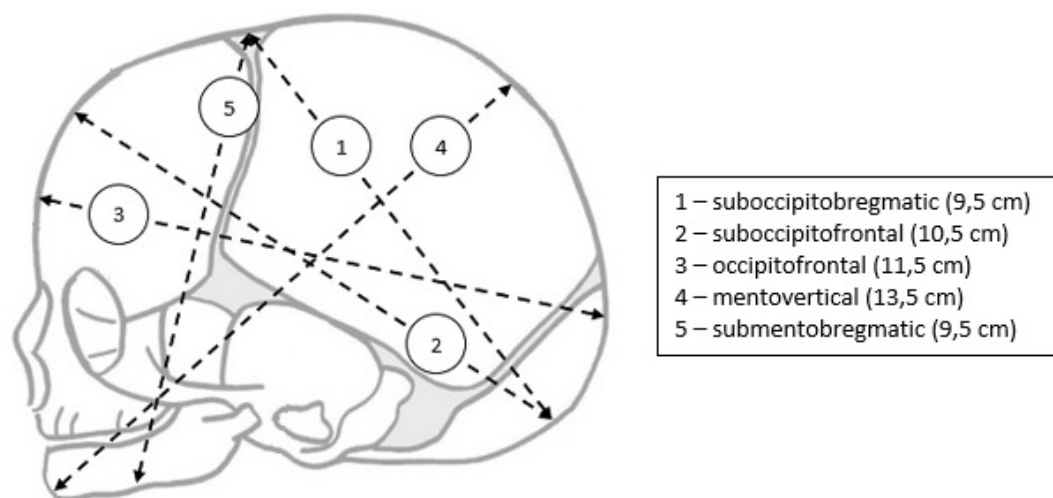
Figure 2.11: Fetal skull diameters (adapted from [27]).

2.1.3 Pelvic Floor Muscles (PFM)

The pelvic floor is a complex region of the pelvic cavity that consists of the pelvic organs (bladder, urethra, uterus, vagina, rectum), pelvic floor muscles (PFM), which support the pelvic organs by keeping them anatomically in their normal position, and connective tissues. PFM also have the function of resistance to augment the abdominal pressure when, for example, coughing or lifting

heavy weights as well as a continence mechanism to loosen and enable urination and defecation [19].

The female pelvic floor is comprised of the pelvic diaphragm, which has three main components: the levator ani muscle (LAM), coccygeus muscle, and the fascias that cover these muscles [29, 31, 38] (Figure 2.12). The coccygeus muscle has a triangular composition that is connected to the ischial spines posteriorly, on each side to a thickening in the internal obturator muscle, named the tendinous arch of levator ani, and to the lateral end of the sacrum and the coccyx [29, 31]. The levator ani muscle is the most important part of the pelvic floor and it is formed by the iliococcygeus, pubococcygeus and puborectalis muscles. The posterolateral part of the levator ani is the iliococcygeus that has its origin in the tendinous arch of the levator ani and the ischial spine. The pubococcygeus is the intermediate muscle that extends from the posterior surface of the pubic bone and the anterior part of the tendinous arch, while the lateral fibers are posteriorly inserting into the coccyx. The puborectalis is the thickest and the medial muscle of the levator ani. It originates from the posterior surface of the pubic bone and forms a muscular sling with the shape of a "U" (puborectal sling) which goes around the rectum and that is commonly termed as the urogenital hiatus [29, 31, 38], having the important function of keeping fecal continence. Collectively, the pubococcygeus and puborectalis muscles are referred to as the pubovisceral muscle.
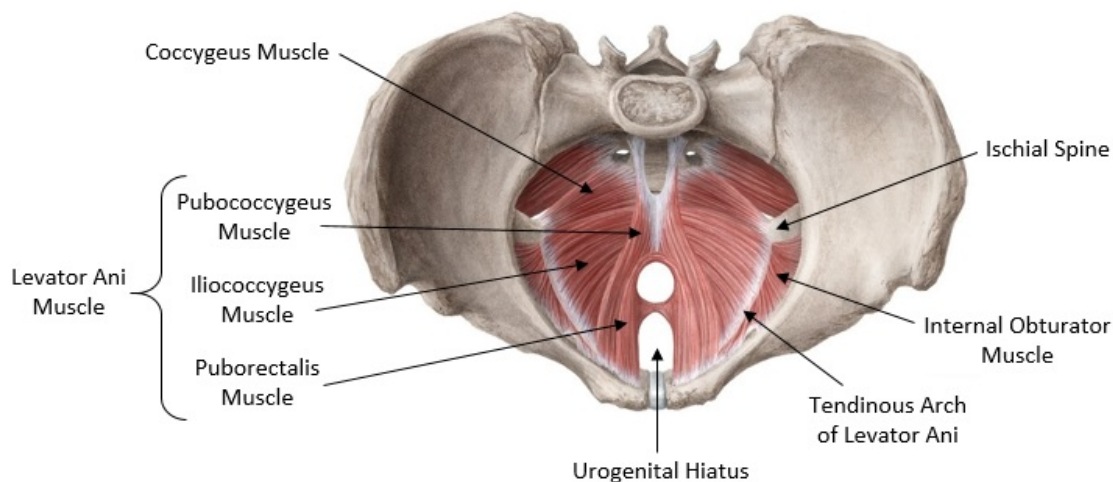
Figure 2.12: Female Pelvic Floor Muscles (PFM) (adapted from [39]).

2.1.4 Labor Mechanisms

To accomplish a safe and successful vaginal delivery, fetal variables such as lie, presentation, position, attitude, and asynclitism need to be addressed at the beginning of the first stage of labor.

Lie refers to the relation between the fetal longitudinal axis and the longitudinal axis of the uterus. The fetal lie can be either longitudinal, transverse, or oblique (Figure 2.13), but only the longitudinal lie can be safely vaginal delivered, in a singleton pregnancy [27, 40].

The presenting part of the fetus describes the portion of the fetus' body that is felt on vaginal examination. At term, the majority of the babies are presented by the vertex and in a longitudinal lie. The degree of flexion of the fetal head will determine the presentation, for instances, if a deflexed head will outcome in a brow or face presentation. In transverse or oblique fetal lies, the presenting part is typically the shoulder or, on rare occasions, the umbilical cord. Compound presentations are related to more than one part of the fetal body presenting together [27].

The fetus position is the relationship between the fetal presenting part and the maternal pelvis. Once the presentation of most fetuses is cephalic at term, the fetal occiput is the reference that is, if the occiput is directly anterior, the position is occiput anterior (OA); if the occiput is facing the mother's right side, the position is right occiput anterior (ROA). The different positions of a vertex presentation are demonstrated in Figure 2.14 [36].

Attitude describes the characteristic posture that the fetus assumes during the last weeks of pregnancy [27]. It is the relation of the fetal head and limbs to the fetal trunk (the degree of flexion and/or extension of the fetal head) [5].

Asynclitism happens when the sagittal suture is not directly central with the maternal pelvis. If the fetal head is rotated such that more parietal bone is present posteriorly, the sagittal suture is more anterior - mentioned as posterior asynclitism. On the other hand, anterior asynclitism occurs when more parietal bone presents anteriorly [36].
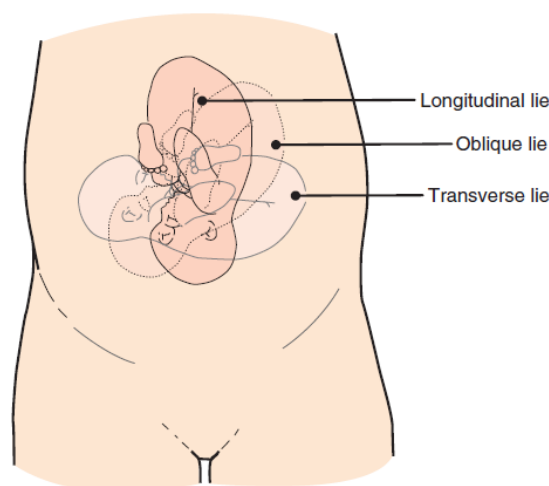
Figure 2.13: Examples of fetal lie [36].
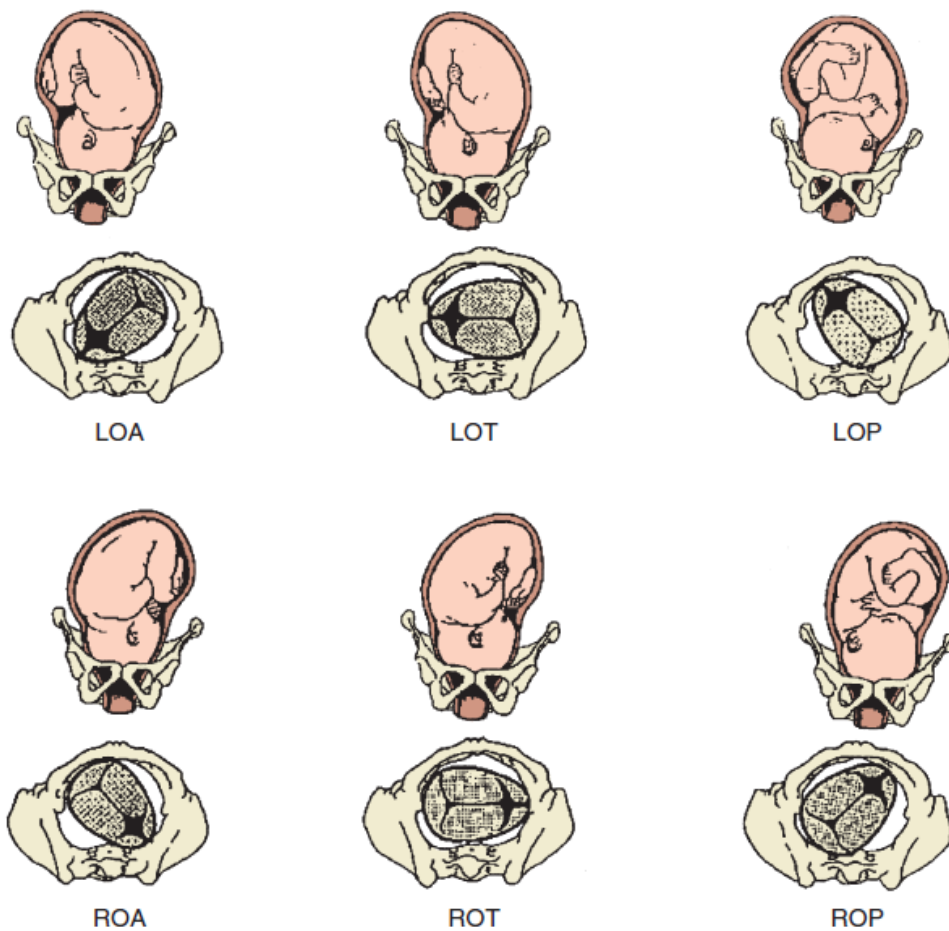
Figure 2.14: Fetal presentations and positions in labor. LOA: left occiput anterior; LOT: left occiput transverse; LOP: left occiput posterior; ROA: right occiput anterior; ROT: right occiput transverse; ROP: right occiput posterior [36].

The development of labor can be divided into three stages. The first stage initiates with the onset of regular uterine contractions which become more intense as labor develops and is completed with a full cervical dilation. The second stage of labor happens when the fetus passes through the birth canal and ends with its delivery. Lastly, the third stage is the time between the fetus delivery and the expulsion of the placenta and amniotic membranes out of the uterus [9, 19, 27].

Uterine contractions are essential for vaginal delivery. They are characterized by the frequency, intensity, and duration of the contractions. At the beginning of labor, these contractions reach an intensity of 1-2 kPa and rise to 7-8 kPa when the dilation of the cervix is almost complete, while during maternal pushing it can reach 10-20 kPa [16,41]. In the first stage of labor, as the dilation of the cervix progresses, not only the intensity but also the frequency of contractions increases until the delivery of the baby [10]. In an effective vaginal delivery, the fetal head descends as the cervix dilates and effaces, and for that, uterine contractions should have an adequate pattern [16, 41]. Otherwise, scalp edema (also known as caput succedaneum) and fetal head molding with the overlap of skull bones can happen [41].

In the second stage of labor, the way that the fetus descends through the birth canal depends on the maternal pelvis shape as well as the position that the child is lying. In an ideal labor, where the fetus is in the vertex position (with its head down), the widest diameter of the fetus' head has to negotiate with the widest diameter of the maternal pelvis into the most effective path. Hence, the baby goes through a sequence of maneuvers to pass through the maternal pelvis. First, it enters the pelvis with the occiput in the lateral position (occiput-transverse), because the transverse diameter is the widest of the pelvic inlet. Then, as it goes down through the pelvis, it rotates, and the occiput change to the anterior position (occiput-anterior). Lastly, the shoulders move around from the transverse position to the anterior-posterior position [5, 42]. This sequence of maneuvers is called labor mechanisms, and its cardinal movements describe the changes that the fetal head takes when passing through the birth canal (Figure 2.15) [27]. The seven cardinal movements that occur in a vertex presentation are:

- Engagement

- Descent

- Flexion

- Internal Rotation

- Extension

- External Rotation

- Expulsion

Engagement refers to the passage of the biparietal diameter of the fetal head (the largest diameter) into the true pelvis and below the pelvic inlet (Figure 2.15 - A). Usually, in most nulliparous pregnant women (women that have never given birth), the engagement movement occurs before the onset of labor, due to the action of the abdominal muscles that push the presentation part to the pelvis. In multiparous women (women that had at least one previous birth) and also some of the nulliparous women, the abdominal muscles are more relaxed and so engagement only takes place on the labor onset [27, 41].

The descent is the movement of the fetal head through the pelvis (Figure 2.15 - B). Its progress is typically evaluated by abdominal palpation and vaginal examination. It is measured by determining the tip of the fetal head position relative to an imaginary line on the level of the maternal ischial spines, labeled as 0 station [27, 43]. The pelvis has been divided into fifths of centimeters above and below the ischial spines. As the fetal head descends from the pelvic inlet towards the ischial spines, the stations are -5, -4, -3, -2, -1, while below the ischial spines the stations are +1, +2, +3, +4, +5 (Figure 2.16). In station +5, the fetal head is visible at the introitus [43, 44].

As the fetus' head comes down through the pelvis, it encounters a resistance presented by the soft tissues of the pelvic floor. At this moment, uterine contractions will cause the flexion of the fetal head which makes the occiput to become in contact with the pelvic floor. Flexion results in the contact between the fetal chin and the fetal chest allowing the presenting part of the fetus to

be the smallest diameter of the fetal head (the suboccipitobregmatic diameter) which proceeds on passing through the pelvis (Figure 2.15 - C) [27, 41].

In internal rotation, the fetal occiput gradually rotates so that it turns to the pubic symphysis (occiput-anterior position) since the anteroposterior diameter of the pelvic outlet is the widest one (Figure 2.15 - D). Then, in each uterine contraction, the fetus' head goes down, guided by the pelvis and the pelvic floor muscles. As it goes down, the fetus moves into the birth canal and after some time, the vertex becomes progressively visible at the vulva [10, 27, 41].

When the fetal head is at the level of the pelvic outlet, the occiput becomes in contact with the symphysis pubis, allowing the head to extend. The head is now out and will face the mother's back with the occiput anterior (Figure 2.15 - E) [27].

When the head is out, it returns to the position that it was in the birth canal. This new rotation is called external rotation (or restitution) and it is completed when the sagittal suture becomes in the transverse position, so that the back and shoulders that still are in the pelvic outlet, realign in the anteroposterior diameter (Figure 2.15 - F) [27].

After the shoulders come out, the torso of the baby's body is delivered (expulsion) by a lateral flexion movement (Figure 2.15 - G), and that defines the termination of the second stage of labor [10, 27].
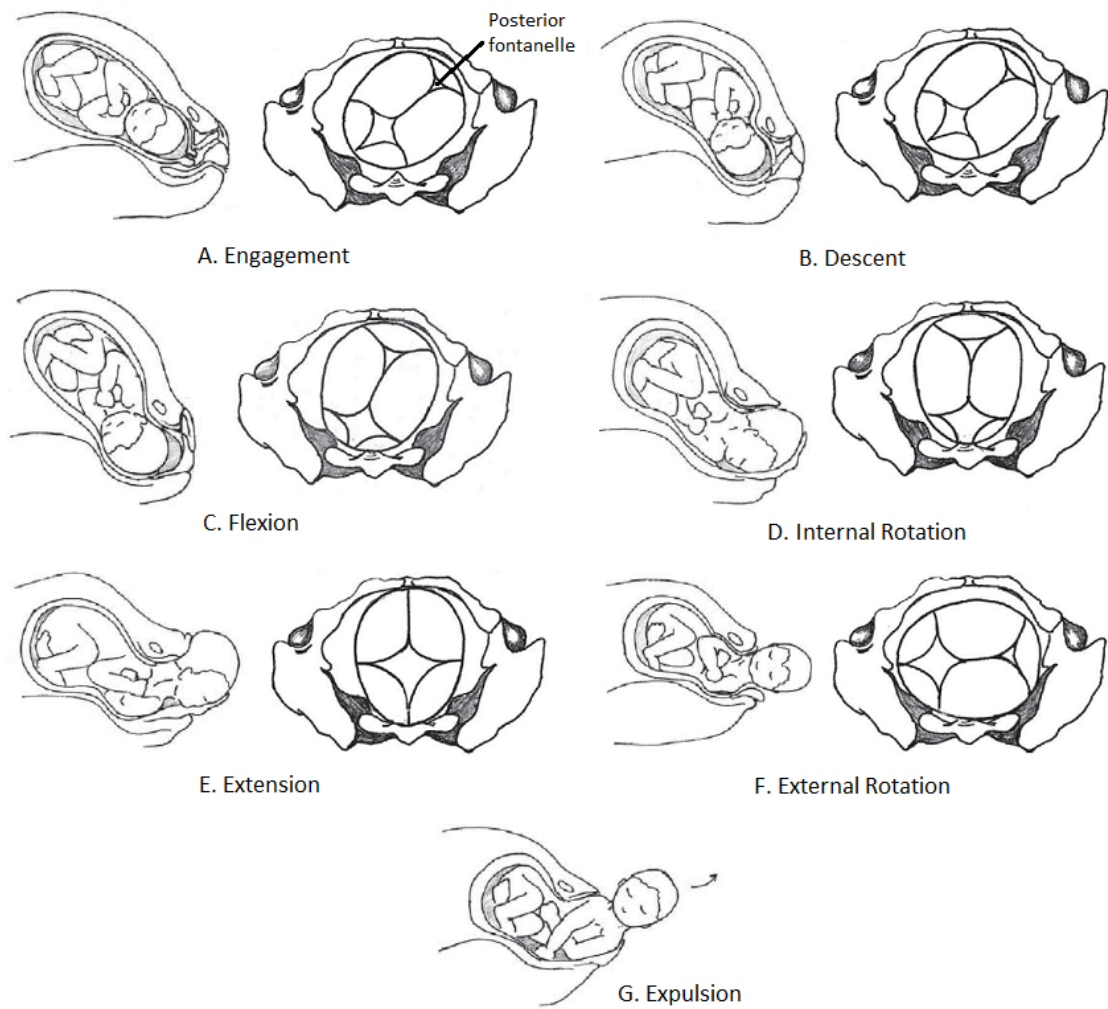
Figure 2.15: Cardinal movements of labor (adapted from [27]).
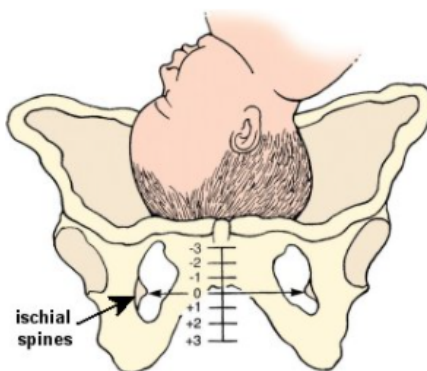
Figure 2.16: The pelvis divided into stations. The imaginary line on the ischial spines level is station 0 [45].

2.2 Instrumental Vaginal Delivery

Normal spontaneous vaginal delivery is the most common mode of delivery all over the world because of the low mortality and morbidity for the mother and the child [43]. However, during the second stage of labor, complications such as a prolonged second stage of labor, a non-reassuring fetal status, lack of effective maternal effort, maternal exhaustion, or a need to shorten the second stage of labor for maternal benefit can happen, and therefore, instrumental vaginal delivery is required [46, 47]. The American College of Obstetrics and Gynecology described (ACOG) a prolonged second stage of labor as the "lack of continuing progress for several hours". In nulliparous women, it is defined as the absence of progress for 3 hours with regional anesthesia or 2 hours without it. In multiparous women, it is considered prolonged labor after 2 hours with or 1 hour without regional anesthesia [43].

An instrumental VD or operative VD is a medical way of, during the second stage of labor, giving more mechanical support to the mother's contractions, providing additional force and guidance to the fetus [48]. The use of traction devices, typically, forceps or vacuum extractor devices are used to allow the obstetrician to increase the forces along the pelvic curve. The suction cup of the VE applies traction and suction on the fetal scalp, while the forceps support the parietal and malar bones of the fetus and employ traction, but also displace maternal tissues. When applied, both VE and forceps cause compression of the fetal head [46].

According to the ACOG, there are three classifications for operative vaginal deliveries, either with forceps or vacuum extractors, which are defined by the station of the leading bony point of the fetal head and the degree of rotation necessary for delivery [49]. Table 2.1 describes the outlet, low and mid classifications for instrumental vaginal deliveries.

Table 2.1: Classification of instrumental vaginal delivery [49].

Classification	Criteria
Outlet	• Fetal scalp is visible without separating the labia • Fetal skull has reached the pelvic floor • Fetal head is at or on the perineum • Sagittal suture is in an AP diameter or in the right or left occiput anterior or posterior position (rotation does not exceed 45°)
Low	• The leading point of the fetal skull is at station +2 or more and not on the pelvic floor. There are two subdivisions: (a) rotation of 45° or less, (b) rotation more than 45°
Mid	• The fetal head is engaged but the presenting part is above +2 station

When any complication mentioned above occurs, and the obstetrician decides that an instrumental vaginal delivery is going to take place, several criteria need to be satisfied before the delivery happens. Thus, the prerequisites and contraindications necessary for an instrumental vaginal delivery are presented in Table 2.2.

Table 2.2: Prerequisites and contraindications for instrumental vaginal delivery [36, 46].

Prerequisites	Contraindications
• The cervix is fully dilated, and the membranes ruptured • The fetus is in a vertex presentation • The fetus' head is fully engaged in the maternal pelvis • The exact position of the fetal head is known with certainty • Assessment of maternal pelvis is considered adequate • Consent has been obtained • Appropriate maternal analgesia is available • Maternal bladder is empty • Necessary support personnel and equipment are available • Operator has knowledge, experience, and the skills necessary to use the instruments • There is a backup plan and the operator is willing to abandon the procedure if necessary	Relative: • Unfavorable attitude of fetal head • Rotation > 45° from OA or OP (vacuum) • Mid-pelvic station • Fetal prematurity (below 34 weeks) Absolute: • Fetal malpresentation • Unengaged fetal head • Incomplete dilation of the cervix • Clinical evidence of cephalopelvic disproportion[1] • Fetal coagulopathy

2.2.1 Choice of Instruments

Both forceps and vacuum extractor devices are clinically acceptable for instrumental vaginal delivery because of the low likelihood of complications. The selection between the two devices should be based on the clinical circumstances and on the operator's experience, training, and comfort with the specific instrument. Some factors need to be taken into account, such as the availability of the instrument and if it is precisely operating, by ensuring that the vacuum device is working and that the forceps blades match [27]. Also, the degree of maternal analgesia and consideration of the advantages and disadvantages of each instrument should be validated, which are briefly presented in Table 2.3 [47]. Normally, it is considered that the vacuum extractor is safer to the mother due to the low risk of tissue injury to the birth canal, while a forceps delivery is safer to the fetus because of a lower occurrence of cephalohematoma and retinal hemorrhage [50].

Vacuum extractor and forceps are effective to deliver the fetus and reducing the time to delivery. However, if there is a complication in the application of the devices, if there is no substantial

---

[1]Cephalopelvic disproportion is a complication in pregnancy that occurs when the size of the pelvis is not suitable to enable the fetal head to negotiate the birth canal.

descent with each maternal pull or if the descent is not significant after three pulls and the baby has not been delivered after 15 to 20 min, the obstetrician should abandon the process [27].

Table 2.3: Advantages and disadvantages of vacuum extraction and forceps (adapted from [50]).

	Advantages	**Disadvantages**
Vacuum Extractor	• Technically easy to perform and learn • Can handle mal-rotation positions of the fetal head • Low maternal birth canal injury	• Weak pulling power • Suction cup can fail • Cup slips off if caput succedaneum is large • Inappropriate for premature delivery • Can cause complications in the fetal head
Forceps	• Fetus can be delivered in a short time • Strong pulling power • Delivery of the fetus is highly reliable • Can be performed with caput succedaneum	• Requires experience for technical proficiency • High risk of injury in the maternal birth canal • Risk of injury to the face and head of the fetus

2.2.2   Maternal and Fetal Complications

The application of an instrument during vaginal delivery should be as safe and effective as possible, otherwise maternal and fetal complications can happen due to the imperfect techniques and incorrect use of the device.

After an operative vaginal delivery, maternal complications are usually those of soft tissue trauma. Compared to a forceps delivery, maternal complications are less frequent and extensive when a vacuum is used [27]. The most common injuries include severe vaginal and perineal lacerations, vaginal hematomas, and third and fourth-degree perineal tears [27, 51]. Also, trauma to the pelvic floor muscles because of the use of the instruments, may contribute to urinary and anal dysfunction, and therefore the occurrence of urinary and fecal incontinence.

Although instrumental vaginal delivery is associated with risks, the absolute rate of fetal injury with forceps and vacuum extractor devices is low [49]. Fetal scalp injuries occur in many of these vaginal deliveries, though they generally are transient and of no clinical significance [27]. The possible injuries that the fetus is subjected to are craniofacial or intracranial injury and neurologic or cognitive effects. These complications are dependent on the instrument used. In a vacuum delivery, traction with a suction cup is applied to the fetal scalp, which can lead to retinal hemorrhages, a cephalohematoma, and subgaleal or intracranial hemorrhage. With the use of forceps, injures include facial lacerations, facial nerve paralysis, skull fracture, and intracranial hemorrhage [36, 49].

Summing up, forceps and vacuum both have different complications that are associated with. However, the use of either device is related to relatively low rates of major morbidity and mortality, being an excellent option when in need of an assisted delivery [49].

2.3   Vacuum-Assisted Delivery

As mentioned in chapter 1, in the last years, there was a decrease in the use of forceps delivery, making the vacuum extractor device the technique of choice for assisted vaginal delivery, because of the low risk of injury for the mother and also due to its technical ease [50] and effectiveness in ending the second stage of labor. Vacuum-Assisted Vaginal Delivery consists of placing on the fetal scalp, a suction cup that is attached with a tube to a vacuum font and a handle, which applies traction to the cup [27]. Vacuum extractors, also named ventouse, are available as manual or electrical equipment, and both have a regulator valve and pressure gauge where the development of negative pressure can be monitored. These devices are classified by the material that the suction cup is made of, including metal, semi-rigid, and soft (plastic/silicone) cups [36, 52]. The soft cup is a flexible funnel cup and the rigid cup is a firm mushroom-shaped cup (M cup) [47]. A meta-analysis that compared soft and rigid suction cups showed that the soft cups were more likely to fail because of more frequent detachments (pop-offs) but were associated with fewer scalp injuries, and the risk of maternal injury did not increase [47].

Even though James Young Simpson is known for describing the first vacuum device, in 1849, the instrument only became acceptable in the 1950s with the design of the Swedish obstetrician Tage Malmström [53]. The Malmström vacuum device has a cup with a shape of a stainless steel disc with a suction tubing, and a traction metal chain attached on the center of the upper surface of the cup (Figure 2.17) [27, 47]. Although it has some limitations, like causing bruising to the fetal head due to the metal cup and it failed when OP delivery was attempted, it is still in use, and the suction cups are available in three diameters of 40, 50, and 60 mm [53]. Bird modified the Malmström vacuum extractor (Figure 2.18) by separating the suction cup and the traction systems, allowing the placement of the cup to be closer to the occiput in OP and lateral positions [27, 53].

The most recent vacuum extractor is the Kiwi Omnicup Vacuum Device developed by Clinical Innovations. It comprises a hand pump-traction system directly applied to the suction cup [27], which is made of rigid plastic and has a diameter of 50 mm [47]. Moreover, it has a flexible stem and a low-profile cup that enables placement over the fetal head flexion point, regardless of the fetal head position, and has the capacity to correct the malposition of the fetal head easily [51] (Figure 2.19).

<div style="text-align: center;">(a)   (b)</div>

Figure 2.17: Malmström vacuum extractor. (a) Stainless steel suction cup with the three diameters [47]. (b) Manual operated vacuum [53].

<div style="text-align: center;">(b)</div>

<div style="text-align: center;">(a)</div>

Figure 2.18: Bird modified vacuum extractor. (a) Suction cup and traction handle. (b) Metal suction cup with a separation of traction chain and the vacuum port [53].
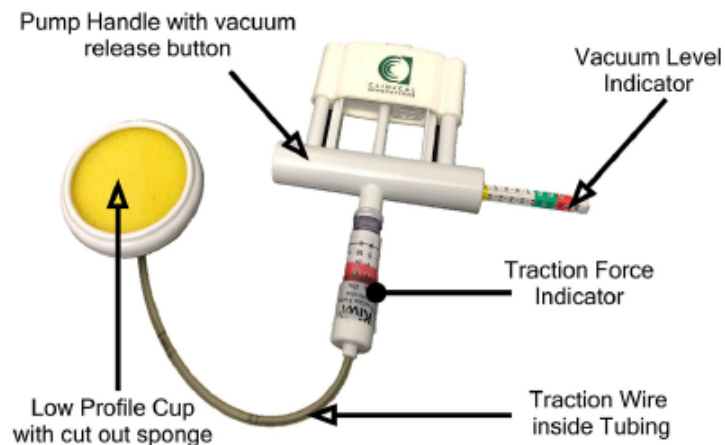
Figure 2.19: Kiwi Omnicup Vacuum Extractor [48].

2.3.1 Application in the fetal head

After satisfying the prerequisites presented in Table 2.2, the vacuum extractor device can be applied to the baby's head. The proper placement of the suction cup in the fetus' scalp and the traction within the pelvic axis is a crucial first step to complete a successful vacuum-assisted vaginal delivery [36]. The center of the suction cup should be placed on the flexion point (or pivot point), which is located on the sagittal suture 3 cm anteriorly to the posterior fontanelle (Figure 2.20a). Application on this point favors flexion of the fetal head presenting the ideal fetal head diameter, the suboccipitobregmatic, to the maternal pelvis [27]. It also promotes descent and rotation of the vertex when traction is applied which can low the risk of injury to the fetus as well as the maternal birth canal tissues [47]. When there is incorrect placement of the suction cup, on an asynclitic head, the fetal head will present a larger diameter, resulting in a different distribution of forces, which increases the complexity and risk of failure or can cause fetal injury [27, 36].

After the placement of the suction cup, as demonstrated in Figure 2.20b, there should be ensured that there is no maternal tissue is between the fetus head and the cup [49], which can cause the detachment of the cup and some maternal injuries. Once the correct position of the cup has been confirmed, suction can be applied by gradual increments. Vacuum negative pressures should first be raised to 100 to 150 mmHg in order to maintain the cup's position [47] and posteriorly, it is recommended to increase vacuum suction pressures to 500-600 mmHg and traction follows, parallel to uterine contractions [51]. Lower suction pressures rise the chance of cup detachment, but conversely, pressures above 600 mmHg increase the risk of fetal scalp trauma and hemorrhages. Once the fetal head is visible at the introitus (process named crowning), suction should cease, the vacuum cup removed and the remainder of the delivery of the baby is like any vaginal delivery [5]. The procedure is recommended to be achieved with no more than 3 sets of pulls and a maximum of 2 to 3 cup detachments [47], with a restricted time of no longer than 15 minutes [27].

In Figure 2.21, the procedure in order to complete a vacuum-assisted vaginal delivery can be observed.

F = Flexion Point
P = Posterior Fontanelle

(a)

(b)
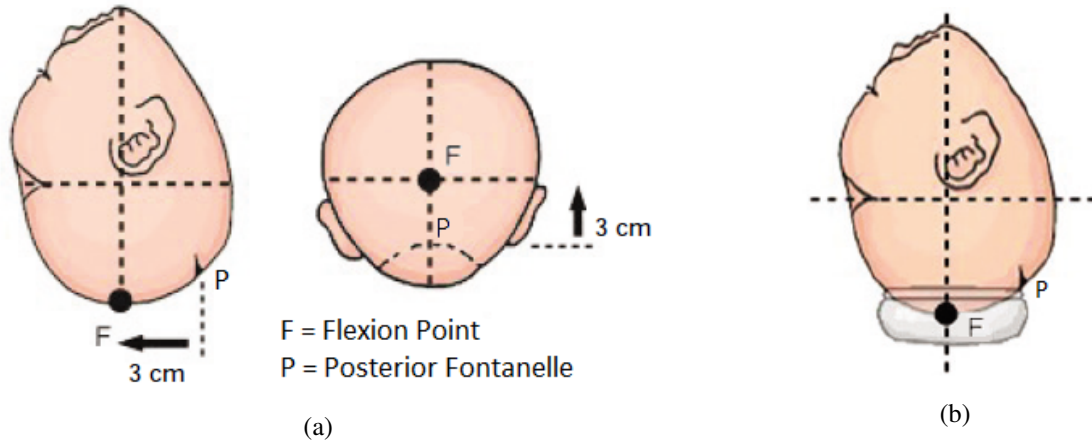
Figure 2.20: (a) Flexion point. (b) Correct placement of the suction cup, with the center on the flexion point (F) and its border on the posterior fontanelle (P) (adapted from [54]).

A. Locating the flexion point

B. Retracting the perineum and inserting the suction cup

C. Placing the cup over the flexion point

D. Applying traction to bring the head down to the perineum

E. Applying traction

F. Changing the direction of traction following the curve of the birth canal

G. Delivering the fetal head (hand protects the perineum)
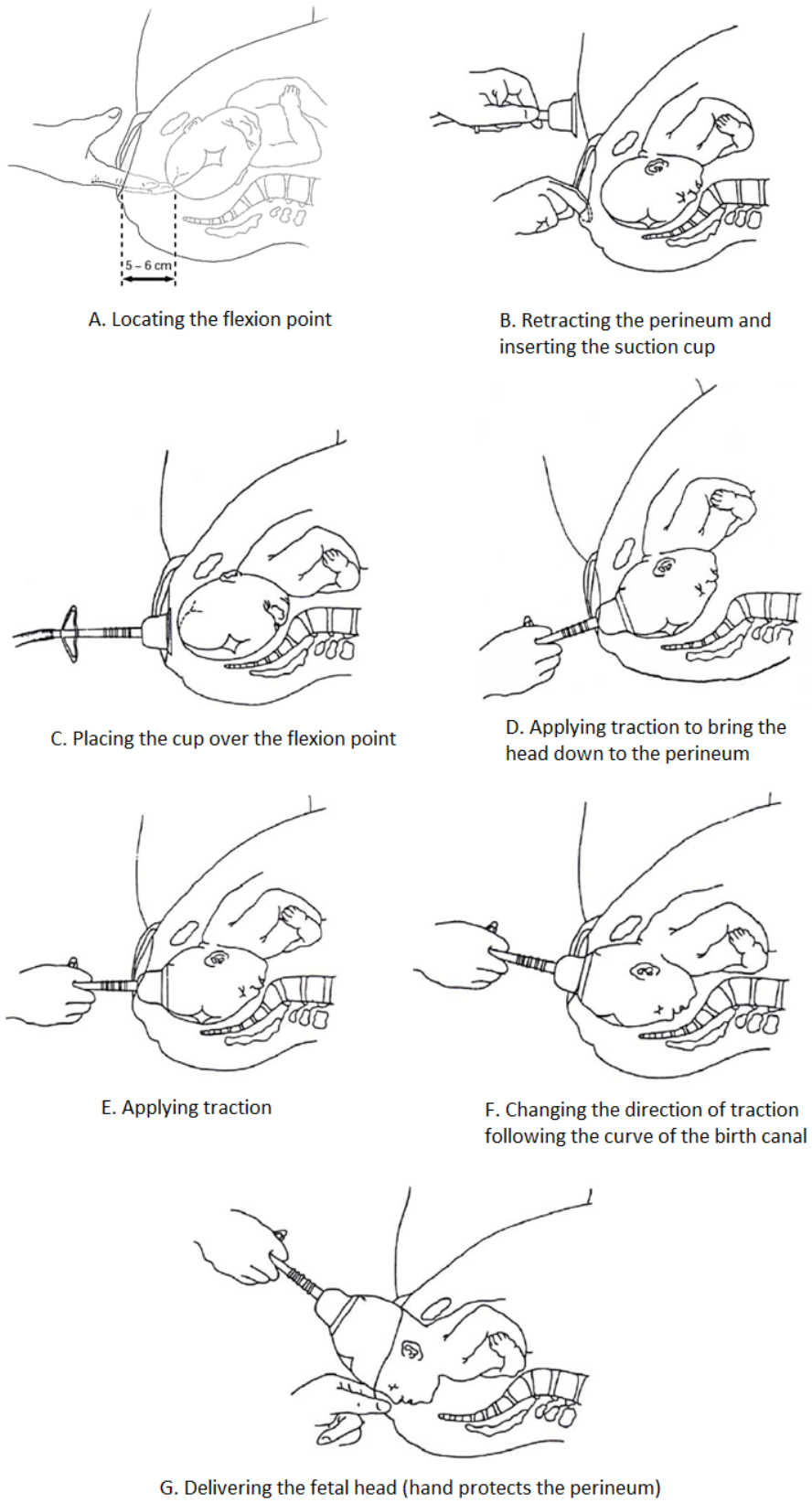
Figure 2.21: Procedure for vacuum-assisted vaginal delivery [4].

Chapter 3

Literature Review

This chapter reviews the current state of the art regarding the area of vaginal delivery and its impact on the pelvic structures as well as the main method used to assess it, providing knowledge of what has already been studied in the field.

3.1 Pelvic Floor Dysfunctions and Vaginal Delivery

The movements that the fetus has to do in order to pass through the maternal pelvis, causes great damage to the bony pelvis and to the pelvic floor muscles. Those injuries, in a near future, can be in the origin of pelvic floor dysfunctions such as pelvic pain, POP, UI, and FI. This is the reason why vaginal delivery is the number one cause of PFD.

Regarding the bony pelvis, it was already mentioned that the pubic symphysis gap can get wider as labor occurs. Its normal size gap is 4 to 5 mm and a widening of 2 to 3 mm is considered normal, but a widening of 10 mm or more is considered a pubic symphysis diastasis. However, this gap size can get bigger than 10 mm in an operative delivery, just like Sujana et al. [32] proved. In their study, two women who had an instrumental delivery reported a pubic symphysis diastasis after a difficult vaginal delivery. In one patient, a ventouse was used but it was unsuccessful, so delivery was performed using forceps. This patient had a widening of the pubic symphysis of 30 mm. The other patient had a vacuum assisted delivery and on the X-ray examination, a pubic symphysis gap of 25 mm was demonstrated. To study the coccyx, Maigne et al. [35] showed that after an instrumental vaginal delivery there is a possibility (5.3%) that the coccxy may fracture.

Several observational studies and investigations with magnetic resonance imaging (MRI) and three-dimensional (3D) ultrasound have been developed to study pelvic floor dysfunctions. After vaginal delivery, PFM suffer major damage, and according to a study by Rahmanou et al. [26], 46.4% women provided evidence of having at least one symptom of PFD. It has been proved that PFD increases with age, affecting 9.7% of women aged between 20-39 years and 49.7% of women aged 80 and over [24]. Rahmanou et al. [26] also stated that advanced maternal age comes with a significant risk of PFD with an odds ratio (OR) of 1.064, for each increasing year after 18 years old. Some studies have also settled that PFDs increase with the number of childbirths, meaning

that PFDs are more frequent in multiparous women when compared to nulliparous women. Having 0, 1, 2, and 3 or more deliveries, the percentage of women who reported at least one symptom of PFD was 12.8%, 18.4%, 24.6%, and 32.4%, respectively [24]. Similarly, Kepenekci et al. [55] claimed that the risk of UI and other PFD increased with the number of parturitions.

Lately, PFD studies have focused on the role of levator ani muscle injuries after VD. LAM avulsion, is the detachment of the puborectalis muscle from its insertion on the inferior pubic bone [56, 57] and is the most important muscle injury. Shek et al. [58] concluded that after vaginal delivery the levator hiatus enlarges, especially after an avulsion injury, increasing the hiatal area by 28%. The same research group found that the stretch ratio (defined as the ratio of tissue length under stretch to the original tissue length [18]) required for VD was 1.47 and also that LAM fibers can increase their distension between 25 and 245% [59].

Pelvic floor dysfunction also varies with the mode of delivery. Hilde et al. [25] conducted a study where after normal and instrumental VD, PFM was reduced in strength by 54% and 66% and in endurance by 53% and 65%, respectively. Comparing the two assisted vaginal delivery techniques, in several studies, forceps delivery was associated with a higher prevalence for LAM avulsion and therefore PFM trauma, compared to vacuum delivery [26, 56, 57, 60–66]. Memon et al. [65] revealed that the prevalence of LAM avulsion was 49% with forceps and 18% with vacuum delivery, while Kearney et al. [63] found that 66% of women who had a forceps delivery had LAM injury compared with 25% of delivery with a vacuum extractor and 10.7% of women with a spontaneous VD. Cassadó et al. [57] declared a predominance of LAM avulsion of 7.8% in spontaneous delivery, 28.8% in vacuum-assisted, and 51.1% in forceps-assisted delivery. Also, compared with spontaneous delivery, the OR for LAM avulsion was 12.31 with forceps and 4.78 with vacuum-assisted delivery. However, García-Mejido et al. [67] found no significant difference when comparing the rate of LAM avulsion between Malmstrom's vacuum extractor delivery and the Kielland forceps delivery.

Regarding vacuum-assisted vaginal deliveries, Garcia-Mejido et al. [68] observed that LAM avulsion was increased with vacuum-assisted delivery (9.6% in normal VD vs. 34.2% in vacuum-assisted delivery) and that the levator hiatal area was larger than in normal VD, supporting Shek et al. [58]. On the contrary, Peschers et al. [69] reported that vacuum-assisted delivery is associated with more sphincter defects but not with more harm to PFM than normal VD. Likewise, Michalec et al. [70] noticed that delivery with a VE leads to a longer levator-urethra gap but not to an elevated LAM avulsion. It was also found by Jundt et al. [71] that vacuum-assisted delivery causes higher bladder neck mobility compared to normal vaginal delivery. Ashwa et al. [72] observed that in an occipito-posterior (OP) position, there is a higher rate of vacuum cup detachment with a vacuum-assisted VD. Two of the most frequently used vacuum extractors are the Malmstrom's VE and the Kiwi Omnicup VE. Turkmen, S. studied the two vacuum extractors and concluded that both are safe for assisted VD, although the Kiwi device presents more advantages than the Malmstrom's suction cup [52]. However, González-Diaz and García-Mejido et al. [73, 74] didn't found a higher risk of LAM with the Malmstrom's vacuum in comparison to the Kiwi's Omnicup.

All these PFM injuries can be easily detected and assessed by ultrasound and MRI. Nevertheless, additional investigations are necessary to understand if this type of trauma is frequent or severe enough to demand a change in clinical practice [19].

3.2 Computational Simulations

During labor, due to the arrangements of the fetus through the birth canal, the maternal pelvic floor goes through some biomechanical changes that cause damage to the pelvic floor muscles. These changes cannot be quantified *in vivo* because of ethical and clinical reasons. However, medical imaging and computational models are valuable tools that help in the analysis of complex processes and systems which cannot be observed directly [18, 19]. Although magnetic resonance imaging and 3D/4D ultrasound can identify injuries in PFM, they lack resolution and structures are poorly detailed [75], therefore the biomechanical process of childbirth and the mechanism of labor are still not fully understood [16]. Nevertheless, computational models are a non-invasive method that can be achieved through MRI or 3D ultrasound images and also consider the geometry of structures, like the pelvic bone, the PFM and the fetus as well as their mechanical properties. As most biomechanical studies, to approach these models in order to perceive the biomechanical interactions of these structures, the finite element method (FEM) is frequently used as a quantitative analysis to carry out simulations [76]. To better understand the whole evolution of childbirth and to prevent complicated cases of labor, computational simulations of childbirth are performed and forces and stresses on the PFM and other structures can be predicted [16, 41].

3.2.1 Introduction to the Finite Element Method (FEM)

In the field of science and engineering, there are diverse physical problems that are described by mathematical relationships, namely the partial differential equations. In cases with elaborate geometries and other physical restrictions, obtaining a direct solution to these equations is sometimes not achievable [18]. Therefore, the finite element method (FEM) is the computational method used for solving those engineering and mathematical models' problems. It was developed in the 1950s to investigate complicated systems that were subjected to mechanical loads [44]. The FEM consists of subdividing continuous problems (systems) into smaller and simpler parts, called finite elements, keeping the same properties of the original model and taking into consideration the geometry of the system, the behavior of the material structures, and the loading conditions applied [77]. The finite elements are joined together and the points where they connect are called nodes. This method uses the nodes system to convert the model structure into a grid, which is usually named a mesh. In this way, stresses, strains, displacements, and forces can be measured quantitatively and qualitatively, giving a response to the mechanical load or displacements. Numerical simulations with the FEM can be solved in just a few seconds or it can last weeks, depending on the complexity of the problem and on the computational resources that are available at the moment [18].

The FEM allows to model any geometries and indirectly estimate their mechanical behavior under any circumstances. During childbirth, the interactions between the fetus and the maternal pelvis can be considered a biomechanical process. This technique has been widely applied in this area, in order to study the impact on the pelvic floor muscles during vaginal delivery, showing effective results [44].

3.2.2 Biomechanical Vaginal Delivery Simulations

Biomechanical vaginal delivery simulations can exhibit the effects on the pelvic floor muscles when the fetus passes through the birth canal, from a mechanical point of view [16]. These simulations have been studied for a while and several childbirth models have been developed. Research groups use the FEM to study the second stage of labor, in particular, to predict the impact on the PFM, which in the future may be the cause of pelvic floor dysfunctions.

To study the biomechanical vaginal delivery trauma, Lien et al. [78] developed a 3D computer model of the levator ani muscles (LAM) using MRI images of a 34-year-old nulliparous woman. The model aid to quantify the stretch induced in the PFM as the fetal head model, with a shape of a sphere, passed and stretched the muscles. They reported a stretch ratio of 3.26 in the medial portion of the pubococcygeus muscle, which exceeds by 217% the largest noninjurious stretch value of 1.5, also mentioned in this study. They concluded that the pubococcygeus muscle is the LAM at greater risk of stretch related injuries during childbirth and also that muscle stretch ratios were directly proportional to the fetal head diameter. In 2007, Parente and Martins et al. developed a finite element (FE) model of the PFM, obtained from a cadaver dissection, the bony pelvis, and the fetus [79, 80]. The numerical simulations of the vaginal delivery were performed with the fetus in a vertex presentation and in an occipito-anterior (OA) position. They found a maximum value of stretch ratio in the PFM of 1.63, which occurred during the fetal head extension, and that exceeds the noninjurious stretch of 1.5 [78]. Similar to Lien et al. [78], they concluded that PFM are subjected to high deformations during the second stage of labor and that the pubococcygeus muscle is submitted to the largest values of stretch, being at greater risk of damage. Hoyte and colleagues [81] used MRI images of a 21-year-old nulligravida woman to obtain a computer model based on the FEM of a bony pelvis, obturator internus, and LAM for simulation. They also used a sphere with a 9 cm diameter to mimic the fetal head that passed through the maternal pelvis to simulate vaginal delivery. A maximum stretch ratio of 3.5 was achieved in the posteromedial puborectalis, supporting the studies of Lien, Parente and Martins [78–80]. In another study accomplished by Lien et al. [23], they updated their previous model by adding pudendal nerve branches in order to determine the increase in the length of the nerves, which is commonly found in women with PFD. Between all the pudendal nerve branches, the maximum strain was obtained in the inferior rectal branch with a value of 35%, while the perineal nerve branch innervating the anal sphincter reached 33%, which can cause permanent damage. In 2013, Noritomi et al. [82] used MRI images to model the PFM and used a 90 mm diameter fetus head to achieve the distribution of stress and strain across the PFM. Results proved that higher stresses occurred around the tendinous arch and in the midpoint of the pubococcygeus muscle, concluding that these areas are at critical risk.

More recently, Krofta and colleagues [83] developed an MRI based model of the pelvic structures from a 25-year-old nulliparous woman and also a fetus to simulate changes in the LAM during childbirth. Higher stresses were found at the beginning of fetal head extension in the puboviseral and puborectal, while LAM had a maximum value of stretch ratio of 2.5, which is consistent with the range of 1.63 [79, 80] to 3.5 [81] found in this literature review. Oliveira et al. [84], in 2016, used the model previously applied by Parente et al. [79] to estimate the damage in the PFM by mechanical effects during vaginal delivery. They come to the conclusion that PFM are damaged, especially during fetus head extension, and that the puborectalis is the component of the LAM most vulnerable to injuries.

To demonstrate the influence of different material parameters on the PFM with the same numerical simulation, Parente et al. [85] used their prior FE model assuming two new materials sets: one with a stiffer behavior and the other had a softer behavior. They found that the strains obtained in the PFM were very similar in the different materials since higher strain values mostly rely on the dimensions of the fetal head. Moreover, they also showed that the maximum principal stresses had large differences because of the exponential behavior of the material. In 2012, Jing et al. [86] verified strains and stresses in an anisotropic, viscous-hyperelastic FE model to assess the levator muscles during the second stage of labor. In their model, a material constitutive relations resultant from biaxial tests of human PFM was applied. An MRI of a fetus at 40 weeks as gestation was also used. The findings indicated that higher stresses arisen near the levator hiatus, specifically at the puboviseral muscle enthesis. In addition, the average levator hiatus stretch ratio was 3.55, which was similar to the value referred by Hoyte et al. [81], but higher than the values predicted by Lien et al. [78], Parente and Martins et al. [79, 80]. Li et al. [76] compared two different constitutive relations for the LAM: one exponential and another Neo-Hookean (linear) forms. The exponential relation had much stiffening at higher strains to reproduce conventional soft tissue behavior. The results indicated that when increasing nonlinearity, that is, when increasing the rate of tissue stiffening, a 56% higher force was necessary for delivery in the exponential model. Also, the maximum stretch ratio across the muscle had a more homogeneous distribution. One year later, the same research team investigated the effect of mechanical anisotropy, that is the different properties along the fiber direction versus non-fiber direction on the LAM during a simulated vaginal delivery [87]. From MRI images, they created two meshes of the PFM, while the fetus skull was obtained in the literature. Modifying the relative stiffness between the fibers and the matrix component, the force required for delivery decreased as the fiber anisotropy increased. Just like the Parente et al. study [85], the overall maximum stretch ratio was located in the dorsal-caudal aspect of the LAM (puborectalis muscle). Recently, Vila Pouca et al. [88] used a visco-hyperelastic constitutive model, since viscoelasticity is a property of the PFM and is time dependent, which can lead to rate-dependent responses. Comparing with the elastic response, viscoelasticity augments tissue stiffness which increases strength, explaining the higher efforts related to precipitous childbirths. In the same year, the group of Vila Pouca et al. [89] add a continuum mechanics damage to the prior model and discover that properties of tissue relaxation provide to reduce damage levels, sustaining the theory of delayed pushing in the second stage of labor. In the same study,

results revealed that the pubovisceral muscle presented approximately 30% of fully damaged fiber elements, being the most LAM affected.

In order to analyze the effect of muscle hypertrophy (in the absence of muscle activation), Li et al. compared the mechanical response of PFM models, from MRI images, of an athlete and a non-athlete [90]. Results showed that a greater force was necessary for delivery with the athlete model compared to the non-athlete, increasing by 45% the peak value. This difference can be due to the fact that athletes possess a greater muscle tone and therefore require more effort during vaginal delivery [91]. Additionally, in both models, the overall maximum stretches ratios were acquired at the muscle insertions to the pubis, with muscle elongations of more than 3.2 times their original length, consistent with previous studies [78, 81, 86]. In 2010, Parente et al. studied, for the first time, the PFM activation [44] by adding it to their previous model. The results demonstrated that higher values of forces were needed against fetal descent when increasing PFM activation because the muscle becomes stiffer. That indicates that pelvic floor muscle activation may represent an obstacle to the fetal descent and also it increases the risk for PFM injuries.

For the purpose of evaluating the malposition of the fetus, Parente et al. verified the consequences of an occipito-posterior malposition of the fetus by analyzing the stretch on the PFM when compared to the normal OA position [40, 92]. The computational simulations exhibit a maximum stretch on the PFM of 1.73 when presenting an OP malposition compared to 1.63 in the normal position, leading to the conclusion that a malposition of the fetus during VD results in higher deformations of the PFM, which increases the risk of PFM injuries. Moreover, the LAM and the pubococcygeus muscle were the PFM subjected to these elevated values of stretch. Supporting the previous study, Silva, M. [93], in her master thesis, also demonstrated that in the OP malposition, the forces on the PFM are higher and obtained a stretch ratio of 1.70, exceeding the value of 1.5 [78], in which permanent damage on the PFM appears.

Numerical simulations can also attempt to prevent PFM injuries by studying some strategies of the effectiveness of childbirth. Parente et al. investigated the influence of fetal head flexion on pelvic floor stress and forces during VD, using their 3D computational FE model [94]. By simulating the cardinal movements, stresses on the PFM and forces against the fetal head descendent were obtained with different degrees of head flexion. They found that lower values of opposite forces against the fetal descent and lower stresses on the PFM were connected to an increase in the degrees of the fetal head flexion. A fully fetal head flexion only required half of the maximum values of forces of the poor head flexion, which insinuates that a complete fetal head flexion during vaginal delivery can simplify birth as well as protecting the pelvic floor. To also prevent PFM injuries, Silva et al. [95] inquired about the influence of the fetus head molding on the PFM by comparing a rigid and a deformable fetus head, with cranial sutures. The simulation of the fetus passing the birth canal with the deformable head produced a reduction of 17.3% on the forces on the PFM and a diminution of 1.86% in the PFM stretches, reaching a stretch ratio of 1.504. They conclude that as the fetal deformable head showed lesser values, the molding of the fetus head reduces the stretches on PFM and so less risk of injuries.

3.2.3   Biomechanical Vacuum-Assisted Vaginal Delivery Simulations

When normal spontaneous vaginal delivery is impossible to achieve, due to maternal exhaustion making no labor progress or any problem with the fetus, a vacuum delivery is usually performed. The suction cup of the vacuum extractor is placed in the fetal head and traction force is applied, coinciding with uterine contractions and a push [96]. Computation simulations with vacuum extractors have already been accomplished with the view of studying the impact of the suction cup in the fetus head and also its impact while passing through the PFM.

To develop his master thesis, Gaspar R. [10] resorted to numerical simulations based on the finite element method to studied vacuum-assisted delivery. He used the pelvis, the PFM, and the fetus computational models of Parente et al. [40] and performed numerical simulations with a FE model of the Kiwi vacuum extractor to inquire the impact on the PFM and also on the fetus head. With the fetus presenting a vertex and an OA position, results showed a 1.55 stretch ratio on the PFM being the pubococcygeus muscle submitted to the higher values of stretch and strain, reinforcing the previous studies. Regarding the suction cup, for a vertical displacement of the fetal head of 40 mm the maximum values of force, stress and logarithmic strain exerted by the suction cup on the fetal head were 12.3 N, 1.812 MPa, and 0.216, respectively.

In order to evaluate the effect of the incorrect position of the vacuum extractor, Lapeer et al. [11] developed a computer-based simulation with a finite element analysis of the fetal skull bones, fontanelles, and the suction cup. Simulations with a correct placement of the suction cup and with an incorrect placement were performed with and without fetal head molding. The overall maximum value of deformation and rotation of the fetus, with an incorrect vacuum extractor position, was 7.01 mm and 0.69 rads, respectively. Whereas, with a correct position of the suction cup, the values for deformation and rotations were 3.15 mm and 0.35 rads, respectively. When adding the molding effect to the numerical simulations, all these values were aggravated.

3.3   Conclusions

Even though there are questions that still demand some more specific answers, this literature review showed that substantial progress has been accomplished in the field of vaginal deliveries. According to the literature, age, the number of parity, mode of delivery, history of pelvic surgery, malposition of the fetus, and genetics are some of the most frequent risks for developing PFD [97]. It was also shown that forceps delivery increases the risk of LAM avulsion compared to vacuum delivery. Computational simulations of childbirth predicted forces and stresses on the PFM, being the pubovisceral muscle of the LAM the one that suffers from the largest stretch ratio, ranging from 1.63 to 3.55, which is much higher than the permissible noninjurious length stretch value of 1.5. Although the studies presented in this chapter regarding the biomechanical vacuum-assisted vaginal delivery demonstrate promising results, there is still a lack of knowledge about the impact of vacuum extractors in the bony pelvis, the PFM and in the fetus head, with numerical simulations.

Chapter 4

Finite Element Method

4.1 Introduction

Just as mentioned in chapter 3, the finite element method is a computational method that solves engineering and mathematical problems mainly from differential equations. Since the majority of biomedical engineering problems can't seem to find a solution *in vivo* due to ethical and clinical issues, computational modeling is a valuable tool that aids in the analysis of such complex processes.

The finite element method is one of the most important developments in numerical analysis and the most widely used and versatile method to simulate deformable solids. It is very important to consider the analysis and determination of the effects of mechanical stresses, strains and interactions of different components in complex geometries by reducing them into a finite number of elements with simple geometries. Thus, this chapter presents the basic fundamentals of the finite element method.

4.2 Kinematics Concepts

4.2.1 Continuum Bodies

A macroscopic system involves continuum bodies (or just continuum) which have macroscopic dimensions and quantities. In macroscopic studies the continuum body mass and volume are continuous functions of continuum particles. These systems are described with a continuum approach which leads to the continuum theory. In this theory, a fundamental assumption affirms that a given body B, can be seen as having a continuous distribution of matter in space and time. It is imagined as a constitution of a (continuous) set of particles, represented by $P \in B$. This continuum body, which can change its shape is called a deformable body [98].

Figure 4.1 shows the general motion of a deformable body. A body B with a particle $P \in B$ is described and are in a region of the three-dimensional Euclidean space at a given instant of time t. The continuum body B changes its position in space from one instant of time to another, and the placement of the body B is described by $\varphi(B)$ of the continuum B [98].
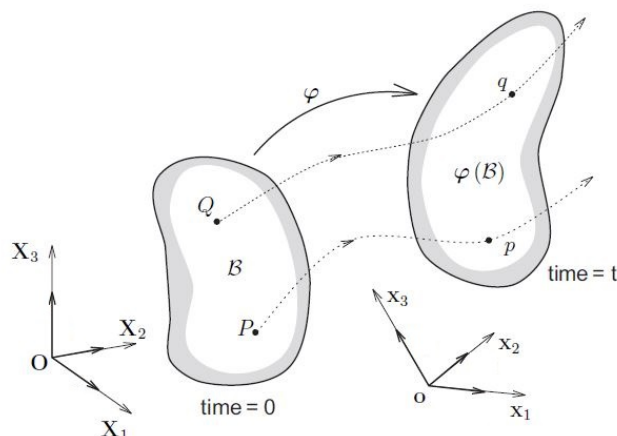
Figure 4.1: General motion of a deformable body, with points P and Q (adapted from [40]).

A configuration of the body *B* is then a one-to-one mapping, which puts all the particles of *B* in the Euclidean space. The motion of the continuum body *B* is then a temporally parametric series which is associated with the vector field φ that defines the new location x of a particle X for a fixed time *t*:

$$x = \varphi(X) \tag{4.1}$$

Considering a given particle X which occupies the position (x, *t*), in a given time instance, its position, which is associated with the place x at time *t* is given by the equation:

$$X = \varphi^{-1}(x) \tag{4.2}$$

4.2.2   Material and Spatial Descriptions

When it comes to the finite deformation analysis, a deliberate distinction is required among the coordinate systems that can be chosen to describe the behavior of the body whose motion is in account. The material description (also called referential) is a characterization of the motion, or any other quantity, that concerns the material coordinates (X_1, X_2, X_3) and time *t*, given by equation 4.1. In the material description, which is also often mentioned as the Lagrangian description, when a particle is in motion, what happens to it is studied. The Eulerian (or spatial) description is a characterization of the motion, or any other quantity, that concerns the spatial coordinates (x_1, x_2, x_3) and time *t*, given by 4.2. In the spatial description, it is observed what happens to a point in space as the time is changing [40].

4.2.3   Deformation Gradient

When a continuum is in motion from the reference configuration to some actual configuration, a deformation on the body will occur, which can change its shape, position and orientation.

The deformation gradient $\mathbf{F}$ is the fundamental kinematic tensor in the finite deformation that characterizes changes of a material element during motion. It is involved in all equations relating quantities before deformation to the corresponding quantities after (or during) deformation. It is a tensor that can present the relative spatial position of two neighboring particles after deformation, just like particles p and q represented in Figure 4.1. $\mathbf{F}$ maps elemental vectors of the reference configuration to elemental vectors in the spatial configuration. This tensor associates to a material line element $d\mathrm{X}$ in B the spatial line element $d\mathrm{x}$ in φ (B), which leads to relationship between the differential elements $d\mathrm{X}$ and $d\mathrm{x}$:

$$dx = \mathbf{F}dX \tag{4.3}$$

Since $\mathbf{F}$ is a linear operator, equation 4.3 is also linear, meaning that if $\mathbf{F} = 1$, $d\mathrm{X}$ is going to have the same value as $d\mathrm{x}$ $(d\mathrm{X} = d\mathrm{x})$, meaning no deformation is observed. To maintain the continuous structure in B during the deformation, the determinant deformation gradient must be positive:

$$J = det\mathbf{F} > 0, \tag{4.4}$$

where J is the Jacobian determinant of $\mathbf{F}$.

4.2.4 Strain Measures

Changes of material elements during motion are characterized by the deformation gradient. Is it now required to determine these changes in terms of strain tensors related with both reference or current configuration. Considering the change in the scalar product of two elemental vectors dX_1 and dX_2 that deform to dx_1 and dx_2, stretching (change in length) and the changes in the enclosed angle between the two vectors will be involved. Therefore, in equation 4.3, the spatial scalar product $dx_1 \cdot dx_2$ can be written with the designation of the material vectors dX_1 and dX_2:

$$dx_1 \cdot dx_2 = dX_1 \cdot \mathbf{C}dX_2, \tag{4.5}$$

where $\mathbf{C}$ corresponds to the right Cauchy-Green deformation tensor, known as material tensor quantity which is an important strain measure in material coordinates, that is given in terms of the deformation gradient as $\mathbf{F}$:

$$\mathbf{C} = \mathbf{F}^T\mathbf{F} \tag{4.6}$$

As another option, the initial material scalar product $dX_1 \cdot dX_2$ can be viewed in terms of the spatial vectors dx_1 and dx_2:

$$dX_1 \cdot dX_2 = dx_1 \cdot b^{-1}dx_2, \tag{4.7}$$

where b corresponds to the left Cauchy-Green or Finger deformation tensor, being a spatial tensor quantity:

$$b = \mathbf{F}\mathbf{F}^T \tag{4.8}$$

The change in scalar product can be written in terms of the material vectors dX_1 and dX_2 as:

$$\frac{1}{2}(dx_1 \cdot dx_2 - dX_1 \cdot dX_2) = dX_1 \cdot \mathbf{E}dX_2, \tag{4.9}$$

where $\mathbf{E}$ is a material tensor defined as the Green-Lagrange strain tensor:

$$\mathbf{E} = \frac{1}{2}(\mathbf{F}^T\mathbf{F}) = \frac{1}{2}(\mathbf{C} - 1) \tag{4.10}$$

The same change in scalar product can be written with reference to the spatial elemental vectors dx_1 and dx_2 and the Eulerian or Almansi strain tensor e as:

$$\frac{1}{2}(dx_1 \cdot dx_2 - dX_1 \cdot dX_2) = dx_1 \cdot edx_2, \tag{4.11}$$

where e equals to:

$$e = \frac{1}{2}(1 - b^{-1}) \tag{4.12}$$

4.2.5   Stress Tensors

The motion and deformation described until now causes interactions between the material and the neighboring material in the interior part of the body. These interactions lead to stress, which is responsible for the deformation of material and has a physical dimension force per unit of area. It is also one of the most important quantities in solid mechanics.

In linear analysis, there was no need to differentiate the deformed from the undeformed area, as an infinitesimal deformation occurred. However, when a large deformation occurs, it is relevant to make clear what area is used in defining stress, because depending on the area, the definition of stress changes [98, 99]

To define the concept of stress it is necessary to consider a general deformable body during a finite motion. For this body, a traction vector $\mathbf{t}$ can be described using the area of the differential element Δa normal to the unit vector $\mathbf{n}$ and the resultant force on the area Δf:

$$\mathbf{t} = \lim_{\Delta a \to 0} \frac{\Delta f}{\Delta a} = \sigma\mathbf{n}, \tag{4.13}$$

where σ denotes a symmetric spatial tensor known as the Cauchy stress tensor which refers to the current deformed geometry as a reference for both the force and area.

Another stress vector **T**, can be also defined, considering the same force (Δf), a differential area ΔA and the unit normal **N** in the undeformed geometry as:

$$\mathbf{T} = \lim_{\Delta A \to 0} \frac{\Delta f}{\Delta A} = \mathbf{P}^T \mathbf{N}, \tag{4.14}$$

where **P** is the first Piola-Kirchhoff stress tensor. Unlike from the Cauchy stress, the first Piola-Kirchhoff stress is not symmetric. It refers to the force in the deformed geometry and the area in the undeformed geometry.

The correlation between the Cauchy stress tensor (σ) and the first Piola-Kirchhoff stress tensor (**P**) can be obtained:

$$\mathbf{P} = J\sigma\mathbf{F}^{-T} \tag{4.15}$$

As said, the first Piola-Kirchhoff stress tensor is not symmetric, once the deformation gradient is also not symmetric. With this inconvenient property, the definition of the Second Piola-Kirchhoff **S** stress tensor appeared, which is already symmetric:

$$\mathbf{S} = \mathbf{P}\mathbf{F}^{-T} = J\mathbf{F}^{-1}\sigma\mathbf{F}^{-T} \tag{4.16}$$

On the deformed configuration, the Kirchhoff stress tensor τ is also often used and it is described as the "push forward" of **S** to the deformed configuration

$$\tau = J\sigma = \mathbf{F}\mathbf{S}\mathbf{F}^T \tag{4.17}$$

4.3 Variational Principles

4.3.1 Principle of Virtual Work

Usually, the finite element formulation is settled as a weak form regarding the differential equations. In solid mechanics this implies the use of the virtual work equation. Several problems in computational mechanics need to discover an approximate (finite element) solution for forces, deformations and other variables when a solid body is subjected to different events [99].

Consider a deformable solid that is subjected to the loading that induces a displacement **u**(x) and a velocity field v(x). The loading comprises a prescribed displacement on part of the boundary (S_1), together with a traction **t** applied to the rest of the boundary (S_2) and it induces a Cauchy stress σ_{ij} [100].

The principle of conservation of linear momentum says that the rate of change of the total linear momentum of a continuum medium is the same as the vector sum of all external forces acting on the body. Therefore, the following equation of motion, also called Cauchy's Equation of Motion can be written:

$$\frac{\partial\sigma}{\partial x} + \mathbf{f} = \rho\frac{\partial^2\mathbf{u}}{\partial t^2} \tag{4.18}$$

where σ is the Cauchy stress distribution, $\mathbf{f}$ represents the body force vector (per unit volume), ρ is the mass density of the deformed solid and $\mathbf{u}$ is a displacement vector.

The principle of virtual work forms the basis for the finite element method and corresponds to the equilibrium of the work done by internal and external forces with small, arbitrary, virtual displacements that satisfy kinematic constraints. It is another method of expressing partial differential equations for linear moment balance in an equivalent integral form [100].

To express this principle a continuous and differentiable velocity field $\delta v(x)$ is required, satisfying $\delta v = 0$ on S_1, corresponding to an arbitrary vector field. Therefore, the virtual velocity gradient and virtual stretch rate can be written as the following equations:

$$\text{Virtual velocity gradient: } \delta\mathbf{L} = \frac{\partial \delta v}{\partial x} \tag{4.19}$$

$$\text{Virtual stretch rate: } \delta\mathbf{D} = \frac{1}{2}\left(\frac{\partial \delta v}{\partial x} + \left(\frac{\partial \delta v}{\partial x}\right)^T \right) \tag{4.20}$$

As a result, the principle of virtual work can be now written, taking into account that the stress, body force and traction are in equilibrium if, and only if, the rate of the work done by Cauchy stresses on the rate of deformation of any virtual velocity field are equal to the rate of work done by the traction and body forces acting on the body (external forces). Thus, it can be denoted as:

$$\int_V \sigma : \delta\mathbf{D}\, dV + \int_V \rho \frac{dv}{dt} \delta v\, dV = \int_V \mathbf{f}\delta v\, dV + \int_{S_2} t\delta v\, dA \tag{4.21}$$

Applying the Gauss's theorem along with equation 4.21 is currently possible. The theorem is a quality relationship between surface integrals and volume integrals:

$$\int_S \mathbf{n} \cdot ()\, dS = \int_V \frac{\partial}{\partial x} \cdot ()\, dV \tag{4.22}$$

where ( ) is any continuous function-scalar, vector or tensor. Also, some statements regarding the properties of the Cauchy Stress can be used:

$$\sigma_{ij}\delta D_{ij} = \frac{1}{2}\sigma_{ij}\left(\frac{\partial \delta v_i}{\partial x_j} + \frac{\partial \delta v_j}{\partial x_i} \right) = \frac{1}{2}\left(\sigma_{ji}\frac{\partial \delta v_i}{\partial x_j} + \sigma_{ji}\frac{\partial \delta v_j}{\partial x_i} \right) = \sigma_{ji}\frac{\partial \delta v_i}{\partial x_j} \tag{4.23}$$

being,

$$\sigma_{ji}\frac{\partial \delta v_i}{\partial x_j} = \frac{\partial}{\partial x_j}(\sigma_{ji}\delta v_i) - \frac{\partial \sigma_{ji}}{\partial x_j}\delta v_i \tag{4.24}$$

Substituting the latter equation in the principle virtual work equation 4.21, it becomes:

$$\int_V \sigma : \delta\mathbf{D}\, dV = \int_V \frac{\partial \sigma \delta v}{\partial x}\, dV - \int_V \frac{\partial \sigma}{\partial x}\delta v\, dV \tag{4.25}$$

Applying the Guass's theorem to first term on the right-hand side of the principle of virtual work and replacing it, we get:

$$\int_{S_2} (\boldsymbol{\sigma} \cdot \mathbf{n}) \, \delta v \, dA - \int_V \frac{\partial \boldsymbol{\sigma}}{\partial x} \delta v \, dV + \int_V \rho \frac{dv}{dt} \delta v \, dV = \int_V \mathbf{f} \delta v \, dV + \int_{S_2} \mathbf{t} \delta v \, dA \qquad (4.26)$$

Regarding equation 4.13, the following is obtained:

$$\int_V \mathbf{f} \delta v \, dV + \int_V \frac{\partial \boldsymbol{\sigma}}{\partial x} \delta v \, dV = \int_V \rho \frac{dv}{dt} \delta v \, dV \qquad (4.27)$$

4.3.2   Principle of Minimum Potential Energy

In the principle of virtual work, stresses are considered without their connections to the strains. Here, we assume a conservative mechanical system requiring the presence of an energy Π for both stresses and loads [98].

When working with hyperelastic materials, a strain energy function W describes the elastic energy stored in a body B. Based on this, the minimum principle of the total elastic potential can be written and we have to consider the potential energy of the forces applied. The main application of this principle is to make approximate solutions to linear elastic boundary value problems, which will form the basis of the FEM in linear elasticity. The minimum of total potential energy, Π, is given as:

$$\Pi(\boldsymbol{\varphi}) = \int_B \Big[W(\mathbf{C}) - \rho_0 b \cdot \boldsymbol{\varphi} \Big] \, dV - \int_{\partial B_\sigma} \mathbf{t} \cdot \boldsymbol{\varphi} \, dA \qquad (4.28)$$

where $\mathbf{C}$ and b represent the right and left Cauchy-Green deformation tensor, respectively, and ρ_0 the density in the undeformed configuration.

From all the possible deformation states $\boldsymbol{\varphi}$ the one that minimizes Π is the solution for the problem. The minimum can be shown by a variation of equation 4.28 and it can be written by applying the directional derivative D, which leads to the first variation of Π:

$$\delta \Pi = D\, \Pi\, (\boldsymbol{\varphi}) \cdot \eta \qquad (4.29)$$

where η is a vector valued function also called a virtual displacement.

Writing equation 4.29 in an explicit form it is obtained:

$$D\, \Pi\, (\boldsymbol{\varphi}) \cdot \eta = \int_B \left[\frac{\partial W}{\partial C} \cdot \delta C - \rho b \cdot \eta \right] dV - \int_{\partial B_\sigma} \mathbf{t} \cdot \eta \, dA = 0 \qquad (4.30)$$

The variation of the right Cauchy-Green tensor $\delta \mathbf{C}$ can easily be expressed in terms of the Green-Lagrange strain tensor: $2\, \delta \mathbf{C} = \delta \mathbf{E}$. While, the partial derivative of W with respect to $\mathbf{C}$ leads to the second Piola-Kirchhoff stress tensor $\mathbf{S}$, with: $2\, \partial W / \partial \mathbf{C}$.

4.4   Constitutive Equations

The deformation of a material can cause stresses that are produced in the body, and it is now needed to express the stresses which are related to material straining. These relation depend on the type of the material that is being considerate and are called constitutive equations. A constitutive equations defines the state of stress at any point $\mathbf{x}$ of a continuum body at time t. The intention of constitutive models is to develop mathematical models that can represent the real behavior of matter. Although there are several material descriptions, in here constitutive equations are going to be established with hyperelastic materials, mainly due to its simplicity [99].

4.4.1   Hyperelastic Materials

Elastic materials are those for which the constitutive behavior is only a function of the current state of deformation. Under such conditions, any stress measure at a particle is a function of the current deformation gradient $\mathbf{F}$ associatedwith that particle. When the work done by the stresses during a deformation process is dependent only on the initial state at time t_0 and the final configuration at time t, the behavior of the material is said to be path-independent and the material is named hyperelastic [99].

For a hyperelastic material, the elastic energy stored in a body B is characterized by the strain energy function W and the first Piola-Kirchhoff stress tensor can be calculated as:

$$P = \frac{\partial W(\mathbf{F})}{\partial \mathbf{F}} \tag{4.31}$$

Taking into account the symmetric Cauchy stress tensor $\sigma = J^{-1}\mathbf{P}\mathbf{F}^T = \sigma^T$, it is obtained:

$$\sigma = J^{-1}\mathbf{F}\left(\frac{\partial W(\mathbf{F})}{\partial \mathbf{F}}\right)^T \tag{4.32}$$

The strain-energy function can be represented in equivalent forms. The strain energy generated by motion is assumed to be objective, which means that after a translation and rotation of the stretched body, the amount of energy stored is unchanged. Hence, it can be said that a hyperelastic material depends on the stretching part of $\mathbf{F}$, i.e. the symmetric right stretch tensor $\mathbf{U}$.

Employing the transformation rule for the deformation gradient, we see that W cannot be an arbitrary function of $\mathbf{F}$ and must obey the restriction:

$$W(\mathbf{F}) = W(\mathbf{C}) = W(\mathbf{E}) \tag{4.33}$$

where $\mathbf{C} = \mathbf{U}^2$ and $\mathbf{E} = (\mathbf{U}^2 - 1)/2$. It is possible to reduce the constitutive equations for hyperelastic materials at finite strains. Therefore:

$$\left(\frac{\partial W(\mathbf{F})}{\partial \mathbf{F}}\right)^T = 2\,\frac{\partial W(\mathbf{C})}{\partial \mathbf{C}}\,\mathbf{F}^T \tag{4.34}$$

which gives an important reduced form of the constitutive equation for hyperelastic materials:

$$\boldsymbol{\sigma} = J^{-1}\mathbf{F}\left(\frac{\partial W(\mathbf{F})}{\partial \mathbf{F}}\right)^{T} = 2J^{-1}\mathbf{F}\frac{\partial W(\mathbf{C})}{\partial \mathbf{C}}\,\mathbf{F}^{T} \tag{4.35}$$

Piola-Kirchhoff stress tensors **P** (not symmetric) and **S** (symmetric) may get alternative expressions:

$$\mathbf{P} = 2\mathbf{F}\frac{\partial W(\mathbf{C})}{\partial \mathbf{C}} \tag{4.36}$$

$$\mathbf{S} = 2\frac{\partial W(\mathbf{C})}{\partial \mathbf{C}} = \frac{\partial W(\mathbf{E})}{\partial \mathbf{E}} \tag{4.37}$$

4.4.1.1 Isotropic Hyperelastic Materials

Isotropy is a property that a material can posses that is defined by the physical idea that the response of the material is identical in any material direction. One example of an (approximately) isotropic material with a wide range of applications is rubber [98]. This implies that the constitutive relation between W and **C** must be independent of the coordinate system chosen and W must only be a function of the invariants of **C** as the following isotropic tensor function:

$$W(\mathbf{C}) = W(I_C, II_C, III_C) \tag{4.38}$$

where I_C, II_C, III_C are the invariants of the right Cauchy-Green train tensor, **C**.

As a result of the isotropic restriction, the second Piola–Kirchhoff stress tensor can be rewritten from equation 4.29 as:

$$S = 2\left[\left(\frac{\partial W}{\partial I_C} + I_C\frac{\partial W}{\partial II_C}\right)1 - \frac{\partial W}{\partial II_C}\,\mathbf{C} + III_C\frac{\partial W}{\partial III_C}\,\mathbf{C}^{-1}\right] \tag{4.39}$$

where 1 is the second order identity tensor. The following results for the derivative of invariants with respect to tensors were obtained by deriving equation 4.39

$$\frac{\partial I_C}{\partial \mathbf{C}} = 1, \quad \frac{\partial II_C}{\partial \mathbf{C}} = I_C\,1 - \mathbf{C}, \quad \frac{\partial III_C}{\partial \mathbf{C}} = III_C\,\mathbf{C}^{-1} \tag{4.40}$$

4.5 Linearization of the Equilibrium Equations

Variational principles such as the principle of virtual work, which establishes the equilibrium equations, are generally nonlinear in the unknown displacement vector field **u**. For a given material and loading conditions, its solution is given by a deformed configuration in a state of equilibrium. To obtain this new equilibrium position, the Netwon-Raphson iterative solution is applied, being necessary to linearize the equilibrium equations such as the virtual work [99].

4.5.1   Discretized Equilibrium Equations

The displacement field **u** can be approximated by interpolation functions, where *n* represents the number of nodes per element, given as:

$$\mathbf{u}(x) \approx \sum_{i=1}^{n} N_i(\mathbf{X})\mathbf{u}_i \tag{4.41}$$

where **X** is the position vector at the beginning of each iteration, $N_i(\mathbf{X})$ represents the shape functions defined within the finite element and $\mathbf{u}_i$ defines the unknown nodal displacement. Taking into consideration the interpolation of equation 4.41 and that the virtual field $\delta\mathbf{u}$ must be compatible with all kinematics constraints, it can be written as:

$$\delta\mathbf{u} \approx \sum_{i=1}^{n} N_i(\mathbf{X})\delta\mathbf{u}_i \tag{4.42}$$

Furthermore, the virtual work (δW) equation 4.21 can be rewritten in terms of the virtual displacement:

$$\delta W = \int_V \boldsymbol{\sigma} : \delta e \, dV - \int_V \mathbf{f} \cdot \delta\mathbf{u} \, dV - \int_{S_2} \mathbf{t} \cdot \delta\mathbf{u} \, dA \tag{4.43}$$

This last equation can be approximated by a variation over the finite set of $\delta\mathbf{u}_i$, from the discretization process. Therefore, for an arbitrary node (a) of the element (e), it can be defined as:

$$\delta W^{(e)} = \int_{V^{(e)}} \boldsymbol{\sigma} : (\delta u_a \otimes N_a) \, dV - \int_{V^{(e)}} \mathbf{f} \cdot (N_a \delta\mathbf{u}_a) \, dV - \int_{S_2^{(e)}} \mathbf{t} \cdot (N_a \delta\mathbf{u}_a) \, dA \tag{4.44}$$

Hence, equation 4.44 can be changed, since the virtual nodal displacement is independent of the integration. In addition, the virtual work per element (e) per node (a) can be expressed in terms of internal and external equivalent nodal forces $\mathbf{F}_{int\ a}^{(e)}$ and $\mathbf{F}_{ext\ a}^{(e)}$, respectively:

$$\delta W^{(e)} = \delta\mathbf{u}_a \cdot \left(\int_{V^{(e)}} \sigma N_a dV - \int_{V^{(e)}} N_a \mathbf{f} dV - \int_{S_2^{(e)}} N_a \mathbf{t} dA \right) = \delta\mathbf{u}_a \cdot (\mathbf{F}_{int\ a}^{(e)} - \mathbf{F}_{ext\ a}^{(e)}) \tag{4.45}$$

where $\mathbf{F}_{int\ a}^{(e)} = \int_{V^{(e)}} \sigma N_a dV$ and $\mathbf{F}_{ext\ a}^{(e)} = \int_{V^{(e)}} N_a \mathbf{f} dV - \int_{S_2^{(e)}} N_a \mathbf{t} dA$.

Due to the fact that the virtual work equation must be satisfied for any arbitrary virtual displacement and the equilibrium conditions require that $\delta W^e = 0$, the discretized equilibrium equations, in terms of nodal residual force $\mathbf{R}_{f\ a}^{(e)}$, arise as:

$$\mathbf{R}_{f\ a}^{(e)} = (\mathbf{F}_{int\ a}^{(e)} - \mathbf{F}_{ext\ a}^{(e)}) = 0 \tag{4.46}$$

Posterior to getting the sum of the contribution of every nodes and elements, which corresponds to the assembling process, the global equilibrium equation in the discretized form can be

written as:

$$\mathbf{R}_f = (\mathbf{F}_{int} - \mathbf{F}_{ext}) = 0 \tag{4.47}$$

4.5.2   Linearization of the Virtual Work Principle

In order to linearize the principle of virtual work, we have to recall section 4.3.1. Taking into consideration a trial solution Φ_k, it can be linearized in the direction of an increment $\Delta\mathbf{u}$ in φ_k as:

$$\delta W(\Phi_k, \delta\mathbf{u}) + D_{\Delta u}\delta W(\Phi_k, \delta\mathbf{u}) = 0 \tag{4.48}$$

where, like mentioned above, D is the directional derivative of the virtual work equation at Φ_k in the direction of $\Delta\mathbf{u}$. Therefore, to get both internal and external forces together into equilibrium, it is required in the Newton-Raphson procedure to adjust the configuration Φ_k. The linearization of the equilibrium equation will be denoted considering the internal and external work components as:

$$D_{\Delta u}\delta W(\Phi_k, \delta\mathbf{u}) = D_{\Delta u}\delta W_{int}(\Phi_k, \delta\mathbf{u}) - D_{\Delta u}\delta W_{ext}(\Phi_k, \delta\mathbf{u}) = 0 \tag{4.49}$$

The final expression of the directional derivate can be written in the discretized form as:

$$D_{\Delta u}\delta W(\Phi_k, \delta\mathbf{u}) = \delta\mathbf{u}^T \mathbf{K} \, \mathbf{u} \tag{4.50}$$

where $\mathbf{K}$ represents the stiffness matrix and $\mathbf{K} = \frac{\partial \Delta\sigma}{\partial \Delta\varepsilon}$.

Considering equation 4.47 and replacing equation 4.50 in equation 4.48, we get:

$$\mathbf{R}_f + \mathbf{K} \, \mathbf{u} = 0 \tag{4.51}$$

that gives the basis of the iterative Newton-Raphson scheme, that can be structured as:

$$\mathbf{K} \, \mathbf{u} = -\mathbf{R}_f(x_k); \; x_{k+1} = x_k + \mathbf{u} \tag{4.52}$$

4.6   ABAQUS software

To perform the finite element simulations on this work, the ABAQUS software was used. ABAQUS is a software for finite element analysis and computer-aided engineering. It has several products, but in this study, the most used was the ABAQUS/CAE, or "Complete ABAQUS Environment", which can be used to model and analyze mechanical components and assemblies and also to visualizing the finite element analysis result.

A complete finite element analysis includes three principal stages:

- Pre-processing or modeling, which involves creating an input file that contains a design for a finite element analyzer.

- Processing or finite element analysis, that produces an output visual file.

- Post-processing, which generates an output visual file.

The first stage can also be developed by other compatible CAD software, like for example SOLIDWORKS. ABAQUS/CAE is capable of processing all these stages.

Regarding the complex mechanical modeling of soft human tissues, the ABAQUS software comprises a user subroutine, called UMAT, that allows the user to develop is own model to have in consideration specific constitutive equations to calculate the stiffness matrix and the stresses.

Chapter 5

Numerical Simulations

5.1 Finite Element Models

As most biomechanical studies, the finite element method is used in computational simulations to study the biomechanics changes of the mother's pelvic floor during vaginal delivery. Thus, in this work, the finite element method is going to be used to develop biomechanical computer simulations in order to study the impact on the PFM and in the bony pelvis in a vacuum-vaginal assisted delivery. Like mentioned in chapter 3, although providing promising results, few works had been done in the area of assisted vaginal delivery, especially with vacuum extractors, since forceps fell out of use. However, as far as we know, these studies do not include a vacuum extractor to evaluate the effect on both the maternal PFM and on the pelvic bones after labor. Therefore, to the vacuum-assisted vaginal delivery process, geometric models that represent the maternal pelvic anatomy such as the pelvic bones and the pelvic floor muscles and also a model of the fetus' head are necessary. The finite element model of the suction cup of the vacuum extractor will also be essential to the simulation. This way, it is going to be possible to evaluate stretches and deformations on the PFM as well as in the pelvic bones during the passage of the fetus through the birth canal with the aid of a ventouse.

5.1.1 Pelvic Floor Muscles Finite Element Model

Just like mentioned in chapter 2, the pelvic floor is composed by a group of muscles and fascias of the female urogenital region. Throughout pregnancy, these muscles along with the abdominal muscles are those that support the fetus' weight, which creates an overload during the several months, making normal labor violent for these muscles [93].

In this work, the finite element model of the pelvic floor muscles was already developed by Parente et al. in [79] and it was modeled using hexahedral elements with an hybrid formulation (C3D8H). It was built using a geometrical data point-set obtained from cadaver measurements by Janda et al. [101] and is represented in Figure 5.1. All measurements were performed on a

woman's corpse, that was obtained for scientific investigation mainly because it didn't present any known pathologies of the pelvic floor.

Figure 5.1: Pelvic floor muscles finite element model.

5.1.2   Pelvic Bones Finite Element Model

The maternal pelvic bones support the abdominal organs by the pelvic floor muscles and consist of four bones: two hip bones, the sacrum and the coccyx (Figure 2.5). For the pelvic girdle finite element model, all four bones were included, as well as, the main pelvic ligaments which are demonstrated in Figure 5.2. This model was developed by Borges et al. [102] and rigid triangular shell elements with reduced integration (S3R) were used. This is an important model in defining the boundary conditions between this structure and the pelvic floor muscles. Like this, it is possible to know which PFM nodes are fixed and which are left free.

Regarding the pelvic ligaments, the main ones were modeled in the pubic symphysis and in the sacroiliac joints. Several linear truss elements (T3D2) were used to simulate the anterior, interosseous and posterior sacroiliac ligaments, the sacrospinous and sacrotuberous ligaments and in the pubic symphysis, the superior and inferior pubic ligaments. In addition, 3D solid element were added to the pelvic joints, so that they could have a better movement. To simulate the synovial part of the sacroiliac joint, a group of wedges elements were added, while to simulate the interpubic disc of the pubic symphysis, another group of 3D solid elements were added [102].

Between the sacrum and the coccyx, the sacrococcygeal joint is located, which can move in order to increase the anteroposterior diameter of the pelvis during labor, being easier for the fetus to pass through. However, the coccyx can only move if there is no surface (a bed, for instances) under the mother, which is the case in this simulation. In Figure 5.3, the finite element model of the sacrum and coccyx is represented in light blue, whereas in dark blue is the sacrococcygeal joint. Every modeling details as well as the maternal pelvic diameters are fully described by Borges et al. in [102]. According to this model, the initial pubic symphysis gap is 4.05 mm.

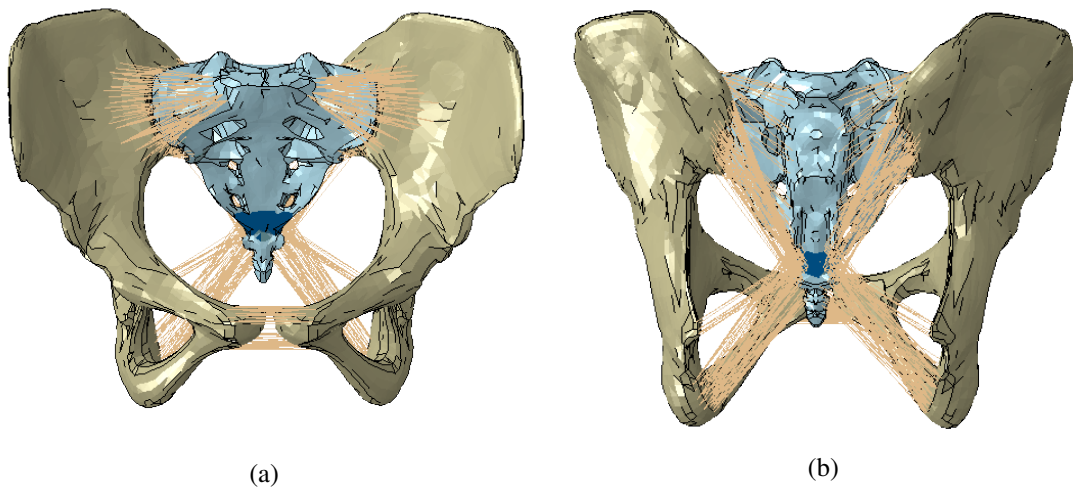(a)   (b)

Figure 5.2: Pelvis finite element model. (a) anterior and (b) posterior view.

Figure 5.3: Sacrum and coccyx finite element model in light blue and the sacrococcygeal joint in dark blue.

To obtain the desired finite element model for the fetus to pass through during the vaginal delivery simulation, the pelvic floor muscles and the pelvic bones models were joined together. To do that, an upgrade was made to the PFM model. Two meshes were added to the model to correctly support the pelvic floor muscles, and are represented in light grey in Figure 5.4. These represent the structures that carry the pelvic floor which are divided in three sections, where the lateral meshes corresponds to the arcus tendinous, obturator fascia and the obturator internus and the posterior mesh to the different connections between the sacrum and the PFM. Figure 5.4 presents the modified pelvic floor muscle model attached with the pelvic bones model.
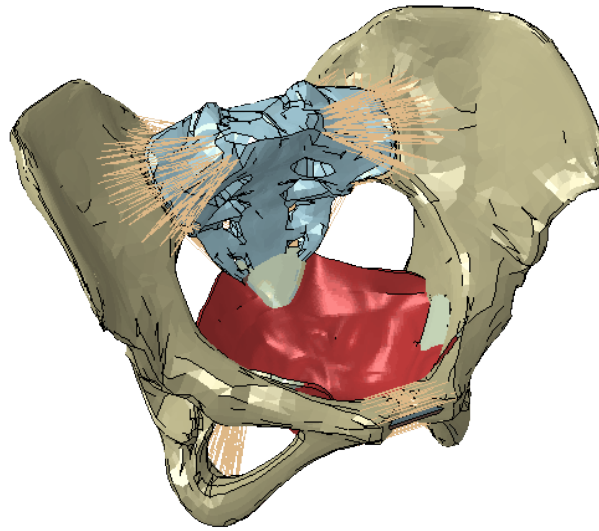
Figure 5.4: The models of pelvic bones and PFM joined together.

5.1.3 Fetus Head Finite Element Model

To perform childbirth simulations, a model of a fetus is essential, since it is this model that will cause an impact on the PFM and pelvic bones during the delivery. To simplify the simulations, only the fetal head was modeled since it is the most massive structure. Figure 5.5 shows the finite element model of the fetal head used in this work, which is formed by tetrahedral elements and it was developed by Parente et al. [79]. The dimensions of the fetus model were adjusted so that the fetal head diameters correspond with the literature for a full-term fetus as shown in Figure 2.11.

Figure 5.5: Fetal head finite element model.

5.1.4 Vacuum Extractor Finite Element Model
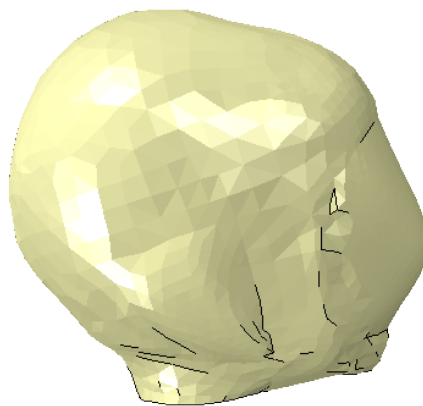
The vacuum extractor used in this work was the Kiwi Omnicup Vacuum Device developed by Clinic Innovations. This was the instrument of choice because it is one of the most used VE in Portugal and also because it is available at FEUP.

Since there are no measures available in the literature to create the Kiwi suction cup model, besides its diameter (50 mm [47]), the measures of the Kiwi suction cup used by Roriz, G. [10] in his master thesis were also used in this simulation.

5.1.4.1 Creation of the suction cup mesh

Before creating the mesh of a model, it is necessary to design the model in a CAD environment. Figure 5.6 shows the main measures, in millimeters, required to create the model. For designing the Kiwi suction cup in 3D, the software SOLIDWORKS was used, and the model obtained can be observed in Figure 5.7.

Afterwards, the 3D Kiwi model was imported to the ABAQUS software, and there, a mesh of the object was created using tetrahedral elements, which can be seen in Figure 5.8. Although hexahedral elements are more accurate in computer simulations, the suction cup is not a structure where results will be read, hence the choice for the tetrahedral elements. The Kiwi suction cup mesh contains 7146 linear tetrahedral elements of type C3D4 and 13553 nodes.
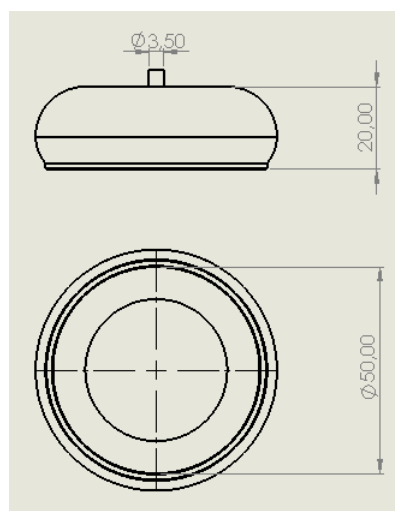

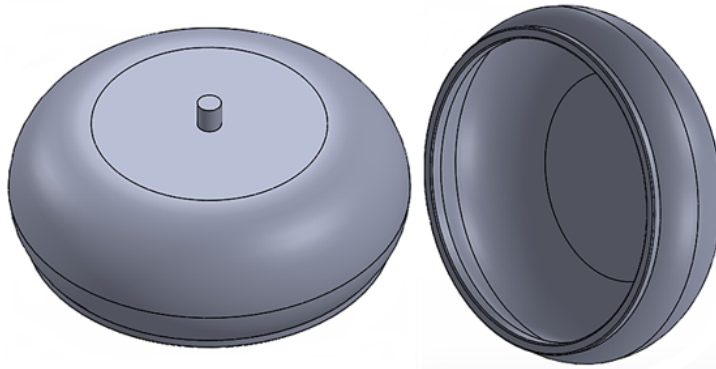Figure 5.6: Main measures of the Kiwi suction cup model in 2D.

Figure 5.7: Model of the Kiwi suction cup in 3D, obtained using SOLIDWORKS software.
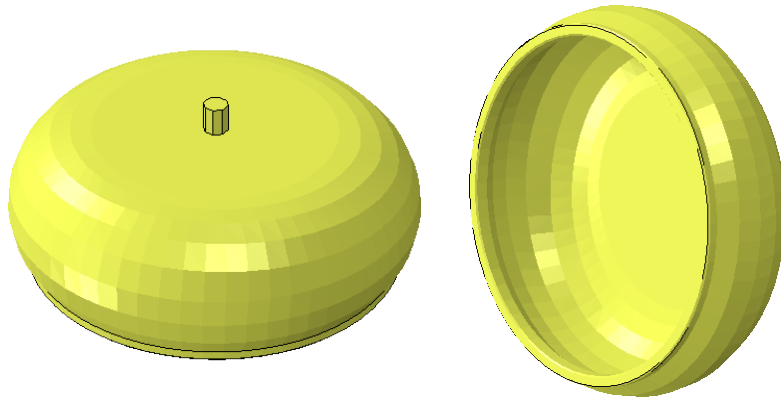

Figure 5.8: Finite element mesh of the Kiwi suction cup, obtained using ABAQUS software.

5.2 Constitutive Models

The muscle tissue is a complex structure that has a complex mechanical behavior. They are made of collagen fibers that are covered by an extracelular matrix. These soft tissues usually possess material and geometric characteristics that are considered nonlinear. Therefore and because it is possible to analyze a lot of mechanical properties, the theory of continuum mechanics was used in order to control the PFM deformation.

To explain the muscle behavior, simulations of both passive and active finite strain responses of the muscle were performed using a Helmholtz free-energy function (Ψ). Parts of the tissue microstructure were considered such as: the extracellular matrix that provides the tissue strength and resilience (Ψ_m); both passive (Ψ_{PE}) and active (Ψ_{SE}) parts of the fibers (Ψ_f), which are in control of muscle contraction and (Ψ_{vol}) which is the volumetric contribution to enforce the incompressibility condition. Thus, the quasi-incompressible transversely isotropic hyperelastic model, was the constitutive model implemented in this work to represent these physical properties. This model was already been successfully used by Martins et al. [80] and by Parente et al. [40]

and equation 5.1 describes the strain energy function, per unit volume:

$$\Psi = \Psi_m(\bar{I}_1^C) + \Psi_f(\bar{\lambda}_f, \alpha) + \Psi_{vol}(J) \tag{5.1}$$

where:

$$\Psi_m = c\left[e^{b(\bar{I}_1^C - 3)} - 1\right] \tag{5.2}$$

$$\Psi_f = \overbrace{A\left[e^{a(\bar{\lambda}_f - 1)^2} - 1\right]}^{\Psi_{PE}} + \overbrace{T_0^M \int_1^{\bar{\lambda}_f} f_{SE}(\lambda^M, \alpha)\, d\lambda^M}^{\Psi_{SE}} \tag{5.3}$$

$$\Psi_{vol} = \frac{1}{D_1}(J-1)^2 \tag{5.4}$$

In these equations, c, b, A, a, D_1 and T_0^M are constants, whereas $\bar{I}_1^C$ is the first invariant of the right Cauchy-Green strain tensor, $\mathbf{C}$, with the volume change eliminated, like:

$$\bar{I}_1^C = tr(\bar{\mathbf{C}}) = tr(\bar{\mathbf{F}}^T \bar{\mathbf{F}}) = J^{-\frac{2}{3}} tr(\mathbf{C}) \tag{5.5}$$

where $\bar{\mathbf{F}}$ is the deformation gradient with the volume change eliminated and J the volume change, $\bar{\mathbf{F}} = J^{-1/3}\mathbf{F}$.

Also $\bar{\lambda}_f$ represents the fiber stretch ratio in the direction $\mathbf{N}$ of the undeformed configuration:

$$\bar{\lambda}_f = \sqrt{\mathbf{N}^T \bar{C} \mathbf{N}} = \sqrt{\bar{C} : (N \otimes N)} \tag{5.6}$$

where $\otimes$ represents the tensor product.

In equation 5.3, to obtain the function $f_{SE}(\lambda^M, \alpha)$, the following expression was used:

$$f_{SE} = \alpha \begin{cases} 1 - 4(\lambda^M - 1)^2, & for \quad 0.5 < \lambda^M < 1.5 \\ 0, & otherwise \end{cases} \tag{5.7}$$

which means that for values of $0.5 \geq \lambda^M \geq 1.5$, the muscle does not produces energy. The level of activation is controlled by the internal variable $\alpha \in [0,1]$.

The constitutive parameters used in this model were the ones in Parente et al. [85] which are described in table 5.1.

For the meshes that were added to support the pelvic floor muscles, a model that had already been used in other numerical studies, the Neo-Hookean constitutive model, was applied. This constitutive model is a basic and trustworthy formulation of a hyperelastic model [103] and it is described by equation 5.8.

$$\Psi(\mathbf{C}) = c_{10}(\bar{I}_1^C - 3) + \Psi_{vol}(J) \tag{5.8}$$

in which $c_{10} = \frac{\mu}{2}$, and μ is a constant representing the shear modulus of linear elasticity.

Table 5.1: Constitutive material parameters for the PFM [85].

Material Parameters
$c = 1.85 \times 10^{-2}$ MPa
$b = 1.173$
$A = 2.80 \times 10^{-2}$ MPa
$a = 0.6215$
$D_1 = 1 \times 10^{-4}$ MPa^{-1}
$T_0^M = 0.682$ Pa

As for the pelvic bones, in order to reduce bone deformation and to facilitate the simulation convergence, they were considered rigid structures, except for the sacrum and the coccyx, since there is a mobility in the sacrococcygeal joint. Cortical and trabelcular bones were considered in the pelvic model, being the cortical bone made of a stronger and denser material and the trabelcular a more spongy with more porous in the bone. The material properties assigned to these two bones are represented in Table 5.2 and were obtained in Borges et al. study [102].

The sacroiliac joint, which connect the sacrum to the ilium, is a synovial joint that can make pregnancy and labor easier due to the ligaments involved that allow this joint to move. Conversely, the pubic symphysis is a nonsynovial joint, which can barely manage to move. The ligaments that enable these joints to move were modeled by Borges et al. [102] and their materials properties are presented in Table 5.2.

To simulate the pubic symphysis, the synovial part of the sacroiliac joints and the sacrococcygeal joint, a Neo-Hookean constitutive model was applied in the 3D solid elements, taking into consideration the material properties of the medial collateral ligament of the knee, since there are few data on the mechanical properties of the pubic ligaments [102].

The material assigned to the fetus head model was a high stiffness material, so that the fetus head is considered rigid when compared with the pelvic floor, like in other successfully numerical simulations [84, 102]. Since the goal of this work is to evaluate deformations on the PFM and on the pelvic bones and not on the fetus head, with this material property, the deformations of the fetus are reduced and the simulations will be easier to converge.

Regarding the suction cup of the vacuum extractor, it was also considered of a rigid material, so that it can pull the fetus' head once both are connected.

Table 5.2: Material parameters for the bones and ligaments [102].

		Young's Modulus [MPa]	Poisson Coefficient
Bones	Cortical	6140	0.3
	Trabecular	1400	0.3
Ligaments	Sacroiliac	350	0.495
	Sacrospinous	29	0.495
	Sacrotuberous	33	0.495
	Superior Pubic	19	0.495
	Inferior Pubic	20	0.495

5.3   Boundary Conditions

For the pelvic floor muscles boundary conditions, a tie constraint was applied between the two supporting structures meshes and the pubic bones. Also, the nodes that represent the different connections between the PFM and the sacrum were considered fixed (Figure 5.9).
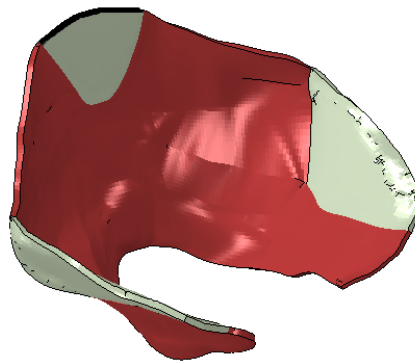

Figure 5.9: Pelvic floor muscles finite element model showing the fixed nodes in black.

Regarding the pelvic bone, the sacrum nodes in the articular faces were fixed and another tie constraint was applied between the sacrospinous and sacrotuberous ligaments and the pelvic bones.

At a first stage, the fetus movements were entire controlled. To control these movements, a reference node was assigned in the middle of the fetus head to an element with rigid properties. Like this, the flexion and extension of the fetal head, corresponding to the cardinal movements can be made by controlling displacements and rotations of that node, causing the vertical descend of the fetus. Figure 5.10 shows the fetal head finite element model with the location of the reference node.

In a second phase, once the prerequisites were fulfilled in order to place the vacuum extractor in the fetus' head, the descend of the fetus was no longer controlled by the reference node on the head, but instead by a reference node in the suction cup. This reference node was placed in the center of the suction cup, where in the real model, the traction wire is connected. Figure 5.10 illustrates the suction cup model with the assigned reference node. To maintain the fetus' head and the suction cup connected during the simulations, a tie constraint was used between the two surfaces so that once attached to each other one can no longer separate from the other until the end of the simulation, that is, after the total passage of the fetus head through the pelvic floor.
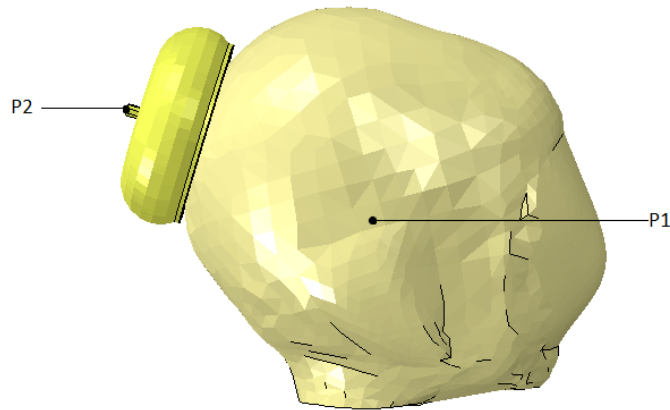
Figure 5.10: Reference nodes assigned to the fetus head (P1) and to the suction cup (P2), used to control the fetus movements.

5.4   Results and Discussion of a Vacuum-Assisted Vaginal Delivery

During vaginal delivery, the maternal pelvis undergoes some modifications, facilitating the passage of the fetus through the birth canal. Therefore, in this work, a simulation of a vacuum-assisted vaginal delivery was performed to mimic the second stage of labor with the fetus in a vertex presentation and in an occiput anterior position, which is the most common position. To develop the numerical simulation, the ABAQUS software was used. Thus, stresses, strains and stretches were analyzed in the PFM; while in the vacuum extractor the force was evaluated; in the pelvic bones, the widening of the pubic symphysis gap and the stresses in the pubic ligaments were observed as well as the movement and rotation of coccyx and also the stresses in the sacrum and coccyx.

Just like stated in chapter 2, the fetus' head must be fully engaged in the maternal pelvis in order to safely place the suction cup. Before being engaged, the fetus must descend through the pelvic canal by performing some movements, called cardinal movements of labor. When the fetus was engaged in the maternal pelvis, the suction cup was correctly placed in the flexion point of the fetus head, as shown in Figure 5.11. From this point, the reference node of the suction cup controlled the fetus movements while the remaining degrees of freedom were left free, in order to conclude the last cardinal movements and the expulsion of the fetus. A normal force was applied to the reference node of the suction cup to make the fetus descend through the birth canal until the fetal head was visible at the introitus. Throughout the simulation, due to the pelvic bones and pelvic floor, some constraints were forced to the fetus movements, so to counter that, a left OA position was used to successfully complete the simulation.

Figure 5.11: Suction cup placed in the flexion point.

5.4.1 Pelvic Floor Muscles

In order to obtain the stretches, stresses and strains on the pelvic floor muscles during the simulation, four different levels along the muscles were defined. Figure 5.12 demonstrate the position of the curves as well as their initial length. These four levels were defined where the levator ani muscle and the pubococcygeus muscles are located. The scale of the levels, named the normalized length, ranges from 0 to 1, where the maximum and minimum values correspond to the PFM extremities and 0.5 to the middle value.

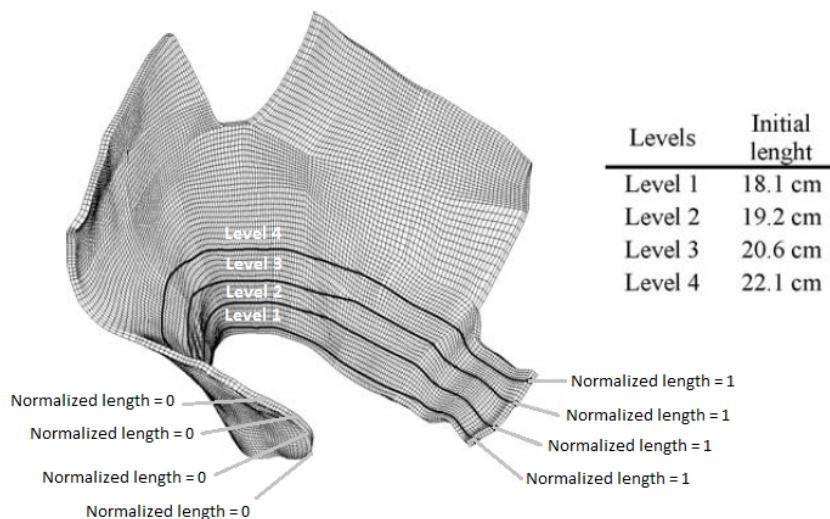| Levels	Initial lenght
Level 1	18.1 cm
Level 2	19.2 cm
Level 3	20.6 cm
Level 4	22.1 cm

Figure 5.12: Different levels to evaluate stretches, stresses and strains on the pelvic floor muscles.

Knowing the curve's initial length, it is possible to obtain the PFM stretch ratio for each level. Like already mentioned, the stretch ratio is calculated as the ratio between the current tissue length and the original tissue length. Figure 5.13 shows the stretch ratio obtained in the four different levels along the pelvic floor muscles during the descent of the fetus head.
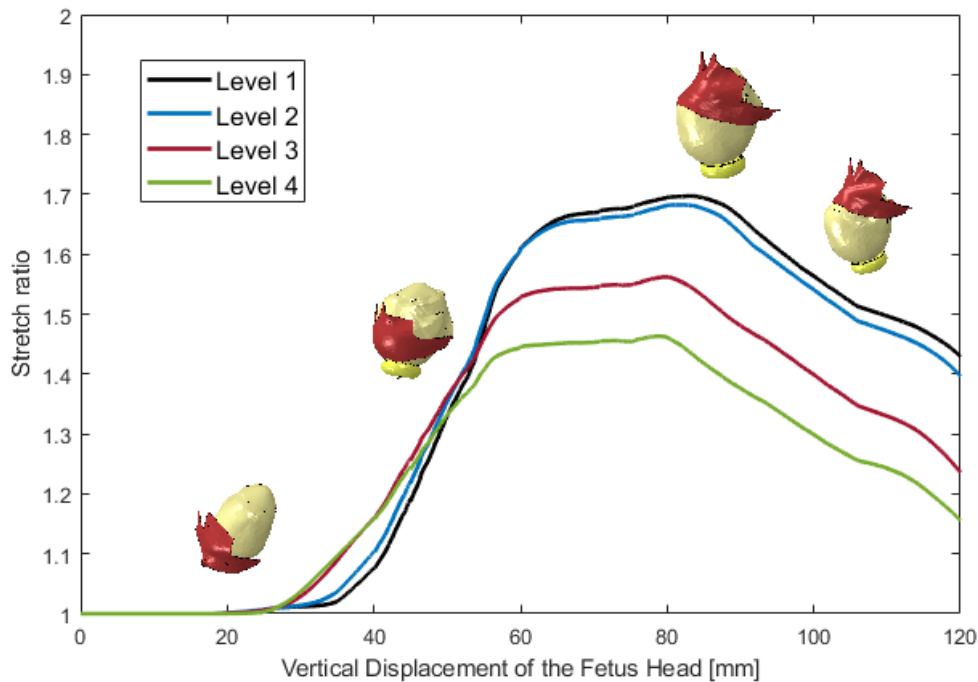

Figure 5.13: Stretch ratio calculated in the four different levels along the pelvic floor muscles during the descent of the fetus head.

The maximum stretch ratio was obtained in curve level 1 with a value of approximately 1.7 for a fetal head descent of approximately 83 mm. It can also be noted that the maximum value for each level decreases as the curve levels are higher, meaning that the lower part of the levator ani muscle, especially the pubococcygeus muscle is subjected to the higher values of stretch. In addition, it can also be observed that the peak of stretch varies with the vertical displacement of the fetus head. The lower the level, the higher the stretch peak, and the greater the displacement of the fetal head. This can be explained because the larger diameter of the fetal head reaches the upper levels of the pelvic floor muscles at an earlier stage (lower fetal descent).

In Figure 5.14 the stretch ratio calculated for level 1 along the PFM is presented, as well as the stretch ratio obtained in Parente et al. [79] and in Borges et al. [102] studies, both on level 1. Parente et al. [79] calculated the stretch ratio during a normal delivery and obtained a maximum value of 1.63, however, this value was for a vertical displacement of the fetus head of approximately 60 mm. This difference can be explained due to the restrictions forced by the maternal pelvis and also because in this simulation a left occiput anterior position was performed, while in the study by Parente et al., a normal occiput anterior position took place. Nonetheless, Borges et al. [102],

obtained a similar value of stretch ratio in curve level 1, using the same strategy as in this study but with a normal delivery.
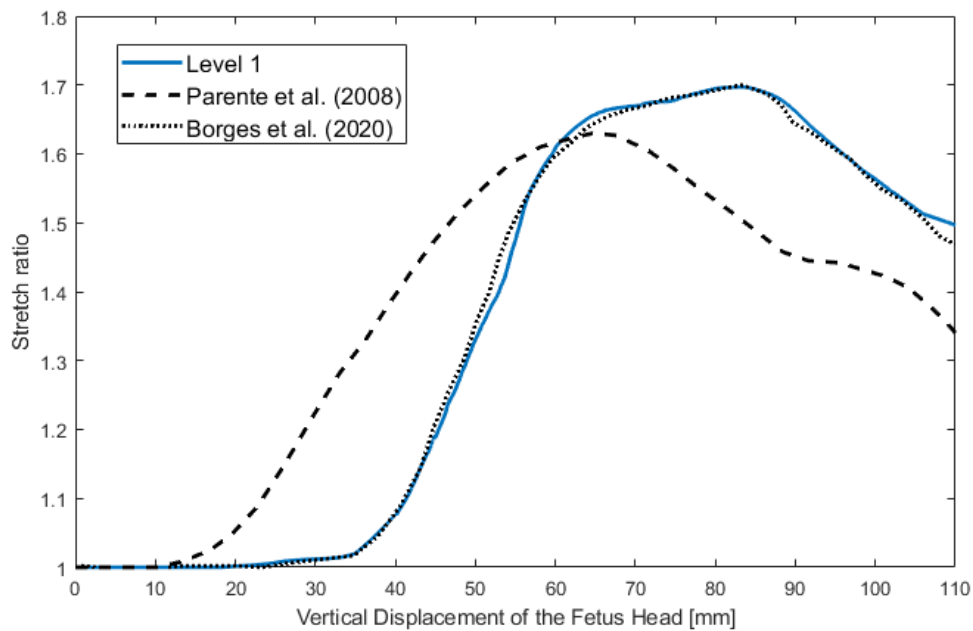

Figure 5.14: Stretch ratio calculated in the level 1 curve along the pelvic floor muscles during the descent of the fetus head compared with other studies.

The maximum principal stresses were also analyzed in the different levels along the PFM. The stresses were evaluated for a vertical displacement of the fetus head of 83 mm, which was the maximum value obtained in the stretch ratio, and therefore where stresses are predictably higher. The results of the maximum principal stresses are represented in Figure 5.15.

In both levels 1 and 2, the level extremities present high values of stresses due to the boundary conditions applied in the PFM, corresponding to the attachment of levator ani muscle and the pubococcygeal muscle to the pelvic bones. However, there is another peak stress that stands out, which is located in the middle of the level length of the PFM. This maximum value is approximately 2 MPa in the first two levels. In the other levels, the maximum stresses are lower, although also appearing approximately in the middle length, confirming that the lower parts of the muscle are subjected to higher stresses. In comparison with Borges et al. [102], where a normal delivery was performed, the maximum values are similar, since in their study they also obtained a value of approximately 2 MPa in the middle length.

Figure 5.15: Maximum principal stresses obtained along the normalized length in the four different levels of the pelvic floor muscles for a vertical displacement of the fetus head of 83 mm.

The distribution of the maximum principal stresses can be observed in Figure 5.16 for a vertical displacement of the fetus head of 75 mm, 83 mm and 90 mm. These figures show the stresses that the PFM suffer, through the descent of the fetus and it can be confirmed that higher stresses are shown in a vertical descent of 83 mm. It can also be observed that the posterior part of the levator ani muscle, more specifically the pubococcygeal muscle, is the one where the maximum value of stresses appears.

Figure 5.16: Distribution of the maximum principal stresses obtained along the pelvic floor muscles for a vertical displacement of the fetus head of a) 75 mm, b) 83 mm and c) 90 mm.

The logarithmic maximum principal strains evaluated in the four different levels of the pelvic floor muscles are shown in Figure 5.17 and were also obtained for a vertical displacement of the fetus head of 83 mm. As expected, the evolution of strains is similar to the stresses evolution, hence the maximum principal strains occur at the same normalized length of nearly 0.5, like in the maximum principal stresses. The maximum strain value for the first two levels is approximately 0.7, and as predicted this number is lower in levels 3 and 4. Parente et al. [79] obtained a maximum strain value of 0.67 for a normal delivery, which is similar to this study.

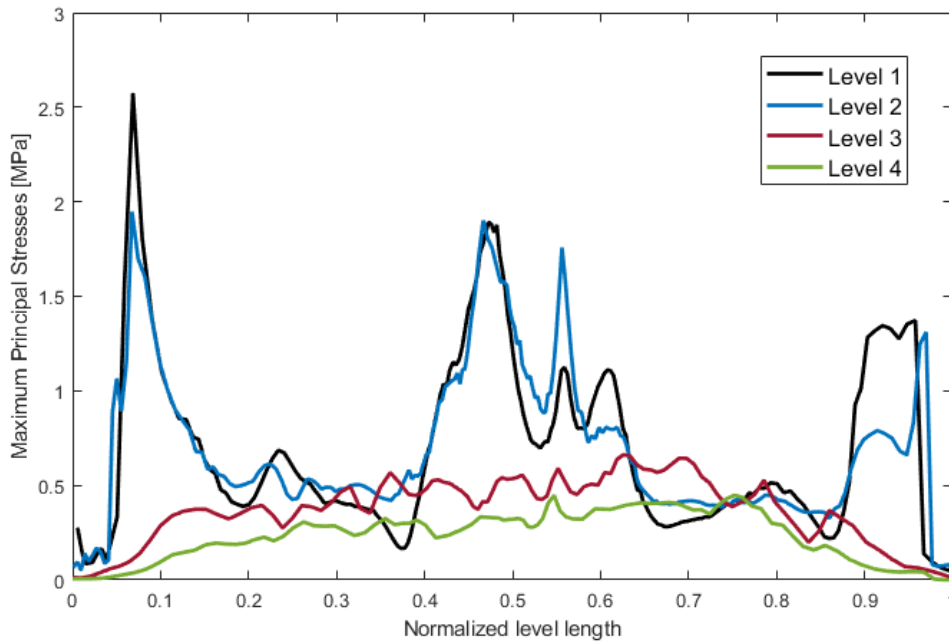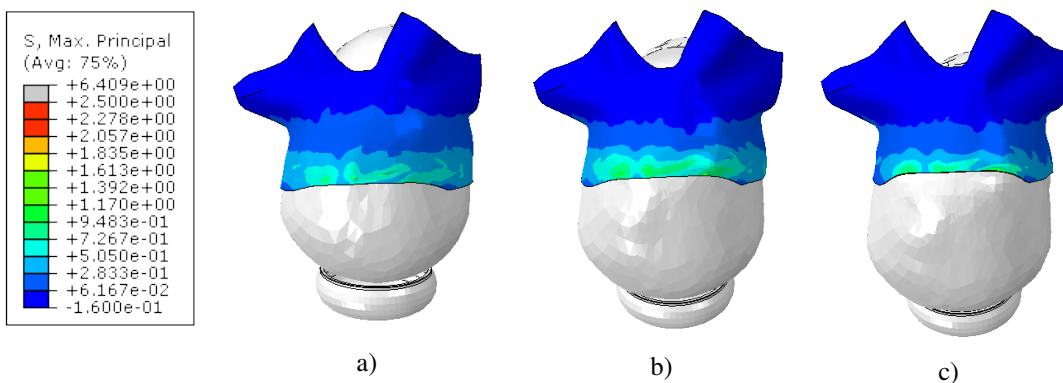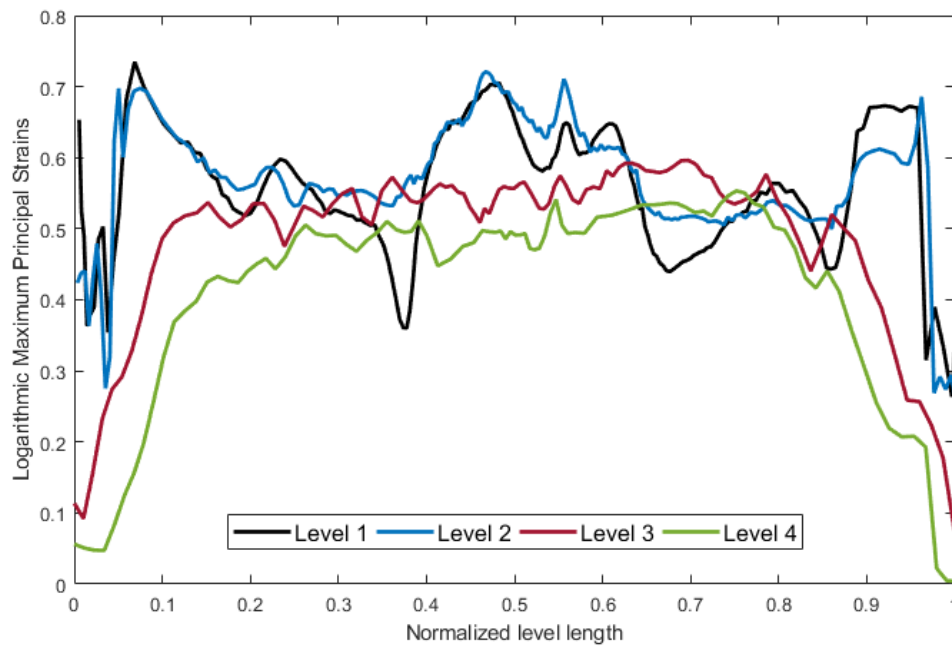Figure 5.17: Logarithmic maximum principal strains obtained along the normalized length in the different levels of the pelvic floor muscles for a vertical displacement of the fetus head of 83 mm.

5.4.2 Vacuum Extractor

The reaction forces applied to the suction cup of the vacuum extractor were also evaluated during the simulation while it pulled the fetus head through the birth canal. In Figure 5.18, the magnitude of forces during the vertical displacement of the fetus head is represented.

The suction cup was applied to the fetus head when the head was engaged in the maternal pelvis, that is, for a vertical displacement of 45 mm. Therefore until 45 mm there was no suction cup to evaluate the forces. A maximum value of force of nearly 300 N was obtained for a fetus descent of approximately 55 mm. Other studies that performed simulations with normal vaginal deliveries, like Borges et al. [102] and Oliveira et al. [84], evaluated the forces on the fetus head, obtaining maximum reaction forces of 175 N and 202 N, respectively. Therefore we can say that

the forces applied in the suction cup are slightly higher than the forces that the fetus head has to do in a normal delivery.
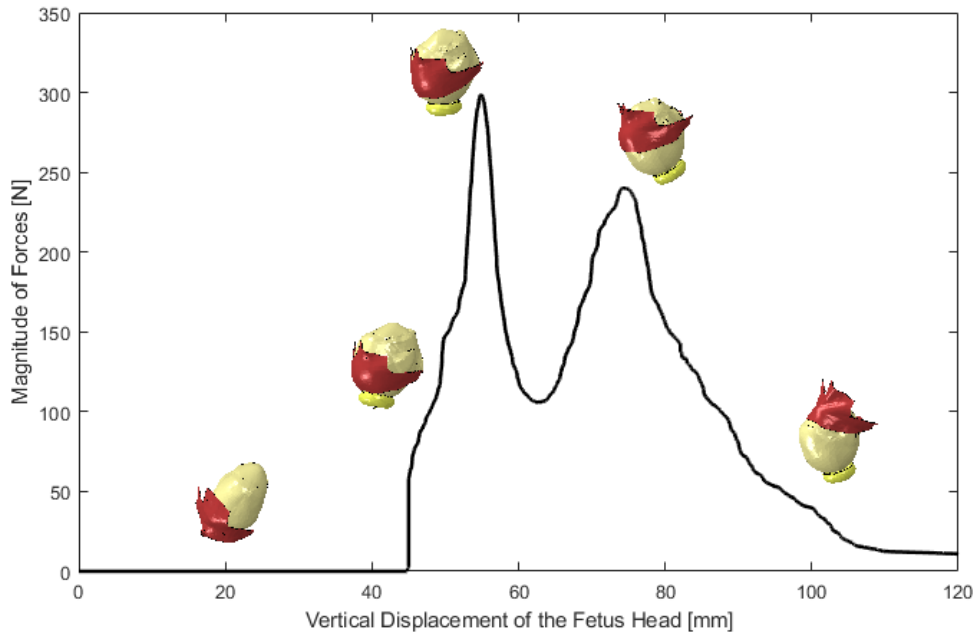
Figure 5.18: Magnitude of forces applied in the suction cup during the vertical displacement of the fetus head.

5.4.3 Pelvic Bones

5.4.3.1 Pubic Symphysis

The pubic symphysis is a cartilaginous joint that has the ability to widen during pregnancy and labor, making it easier for the fetus to pass through the maternal pelvis. To analyze this change in the pubic symphysis, and already knowing the pubic initial gap (4.05 mm), the distance between the narrowest points of the gap was determined and the gap widening was evaluated and is shown in Figure 5.19.

The maximum value obtained for the widening of the pubic symphysis was 2.7 mm for a vertical displacement of the fetus head of 73 mm. This value is still in the range of a normal widening of 2 to 3 mm that can happen during labor, without feeling pain [33]. Therefore, in this simulation, it can be claimed that in a vacuum-assisted vaginal delivery, a diastasis of the symphysis pubis did not occur, like it can happen when an instrumental delivery is performed [32].

Figure 5.19: Widening of pubic symphysis during the vertical displacement of the fetus head.

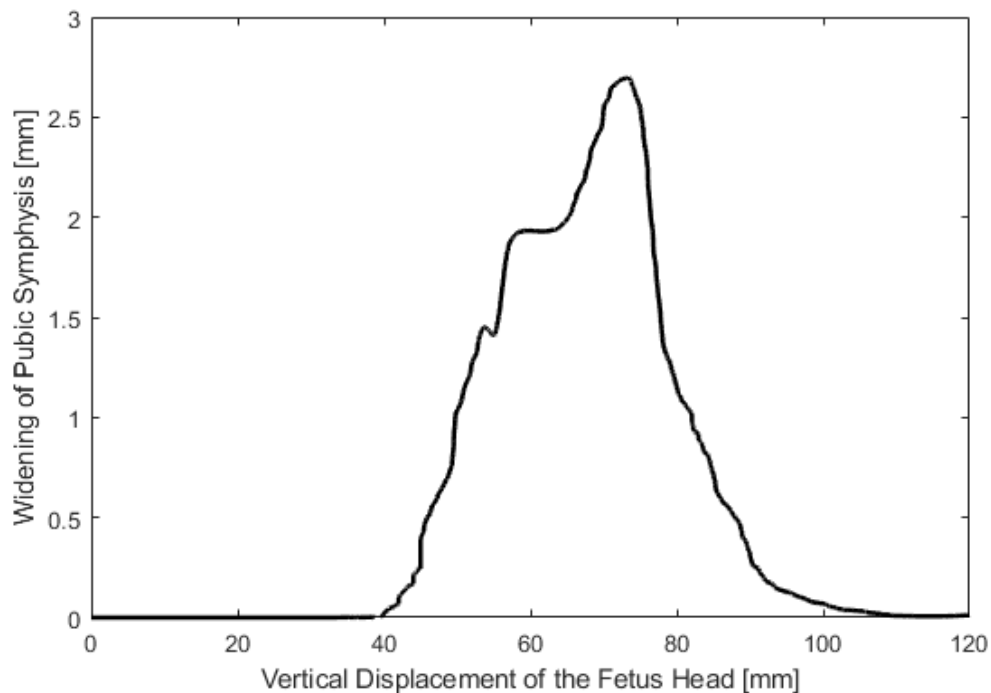In the pubic ligaments, the maximum principal stresses were also evaluated during the descent of the fetus head (Figure 5.20). It can be observed that the evolution of the maximum principal stresses in both superior and inferior public ligaments are similar to the widening of the pubic symphysis. The maximum values in both ligaments occur at the same vertical displacement of the fetus head of 73 mm, which is coincident with the vertical descent of the fetus head for the widening of the symphysis pubis. In the superior pubic ligament, the maximum value obtained was 9.3 MPa, while in the inferior pubic ligament it was approximately 2 MPa. This large difference can be explained because, in the pelvic model used, the elements obtained to measure the stresses in these ligaments are narrower in the superior pubic ligament than in the inferior pubic ligaments, therefore presenting greater stresses in the superior ligaments.

5.4.3.2   Sacrum and Coccyx

In this work, it is possible to analyze the results in the coccyx and in the sacrum, since the joint between them, the sacrococcygeal joint, can move by flexing or extending. When the sacrococcygeal joint moves in an anterior and cranial direction, due to the descent of the fetus head, flexion in the coccyx occurs. Whereas, in the extension, the coccyx moves in a posterior and caudal direction [102].

To measure the movement of the coccyx, the reference line represented in Figure 5.21 was used. This line starts on the inferior border of the pubic symphysis and goes to the inferior border
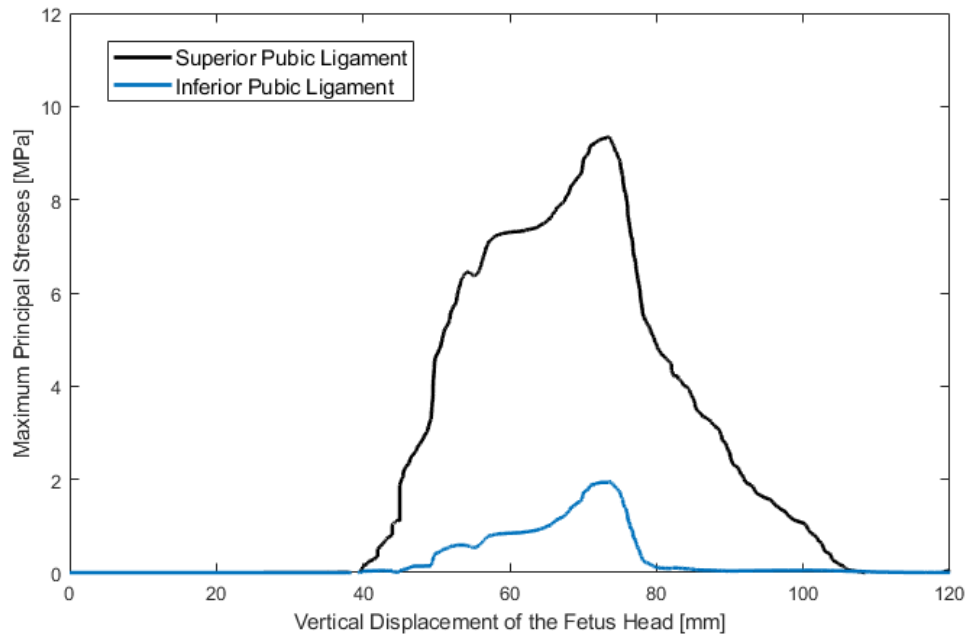
Figure 5.20: Maximum principal stresses in both superior and inferior public ligaments during the vertical displacement of the fetus head.

of the sacrum. Then, with equation 5.9, the distance from the tip of the coccyx to this reference line was calculated, obtaining the difference movement of the coccyx.
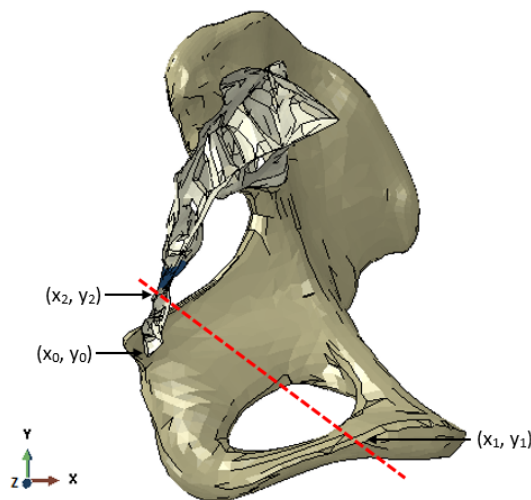
Figure 5.21: Reference line used for the calculation of the coccyx movement.

$$dist((x_1,y_1),(x_2,y_2),(x_0,y_0)) = \frac{|(y_2-y_1)x_0 - (x_2-x_1)y_0 + x_2y_1 - y_2x_1|}{\sqrt{(y_2-y_1)^2 + (x_2-x_1)^2}} \tag{5.9}$$

The movement of the coccyx during the vertical displacement of the fetus head is shown in Figure 5.22. Although the maximum value slightly varies between a vertical descent of the fetus head of 58 mm and 71 mm, the maximum movement of the coccyx obtained was approximately 3.3 mm for a vertical displacement of 58 mm. It is at this moment that the fetus starts the cardinal movement of the head extension and touches the inferior border of the sacrum (point (x_2, y_2) in Figure 5.21). Borges et al. [102] also calculated this value for a normal delivery and obtained a maximum value of 3.3 mm, but for a vertical descent of the fetus head of 65 mm. Therefore, in this simulation, the head extension occurred sooner than with a normal delivery.
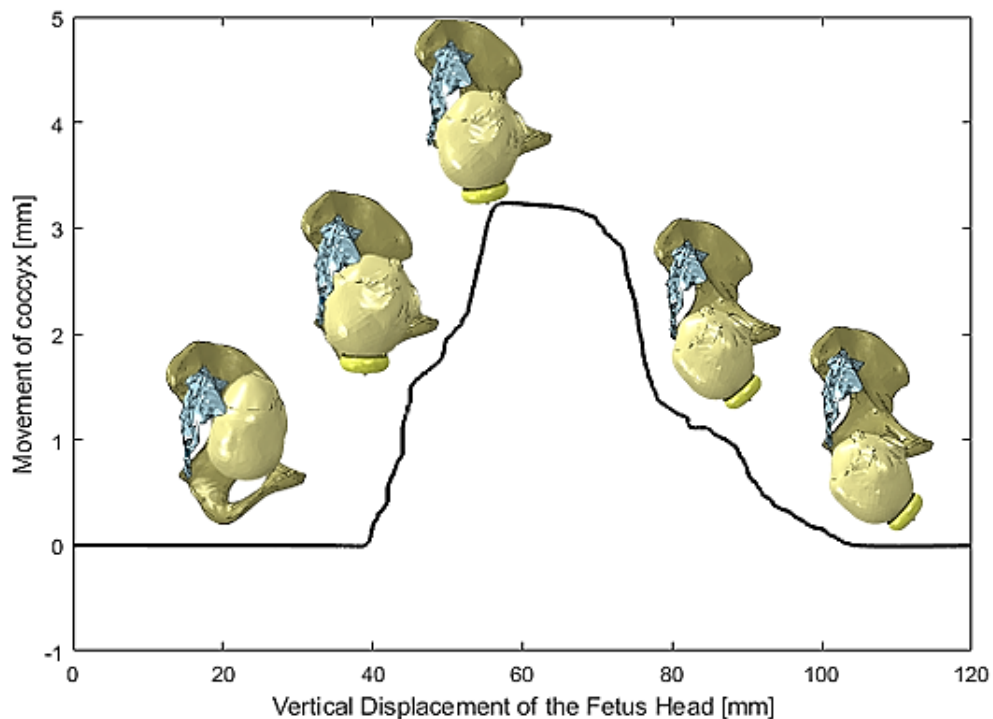
Figure 5.22: Movement of the coccyx during the vertical displacement of the fetus head.

In order to evaluate the rotation of the coccyx, its tip (point (x_0, y_0) in Figure 5.21) rotation along the z axis was determined and the results are shown in Figure 5.23.

The maximum value of the coccyx rotation obtained was approximately 17° for a vertical displacement of the fetus head of 66 mm. It is at this moment that the fetus head touches the tip of the coccyx while performing the head extension. The negative value presented at the end of the simulation is explained by a coccyx flexion, which is returning to the original position since not all ligaments of the sacrococcygeal joint are present in this model. According to Woon et al. [34], during labor, the maximum rotation that the coccyx can suffer without fracturing is 22°. Thus, in this vacuum-assisted vaginal delivery simulation, the coccyx did not fracture like it can happen in an instrumental delivery [35]. Borges et al. [102] obtained a coccyx rotation of 15.7° for a normal vaginal delivery which is slightly lower than the value obtained in this vacuum-assisted simulation.
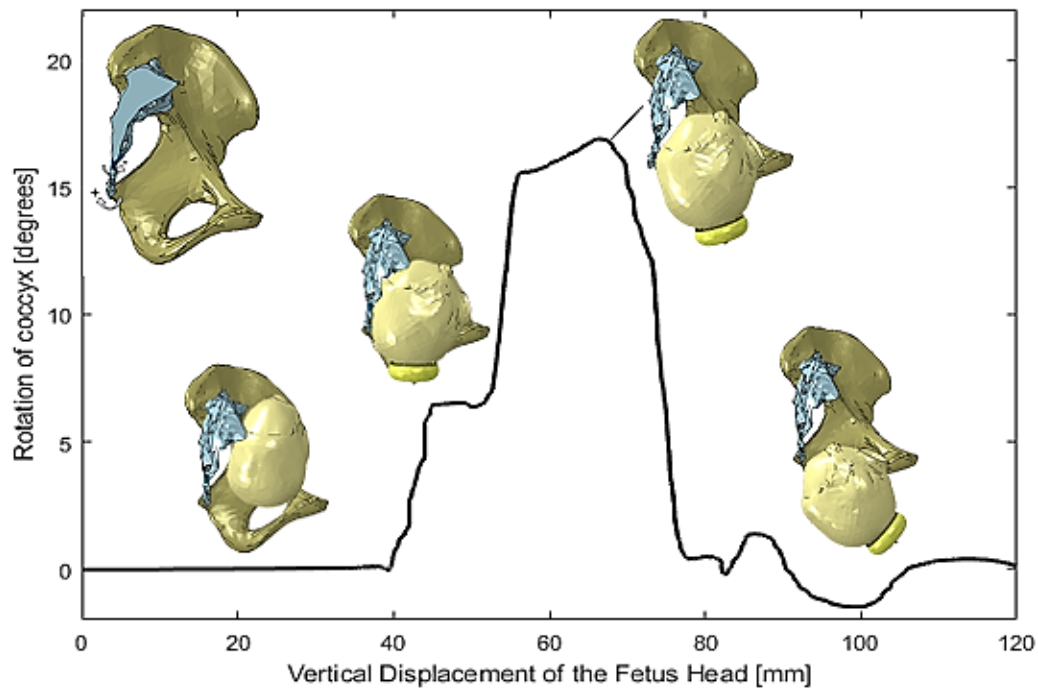
Figure 5.23: Rotation of the coccyx during the vertical displacement of the fetus head.

To obtain the displacement of the sacrum and coccyx along the x-axis, a path was defined in the sagittal plane of these bones, which is represented in Figure 5.24. The displacements are represented in Figure 5.25, where the black dashed line represents the beginning of the sacrococcygeal joint (corresponding to a normalized length of 0.72). Here, two lines are shown, representing two different situations of the simulation. One was obtained at the beginning of the coccyx movement, for a vertical descent of the fetus head of 41 mm, and the other at the peak value of coccyx movement, for a vertical descent of the fetus head 58 mm.
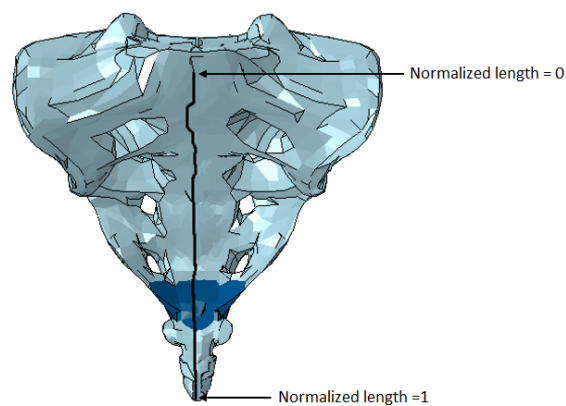
Figure 5.24: Path used to measure the displacement of the sacrum and coccyx.
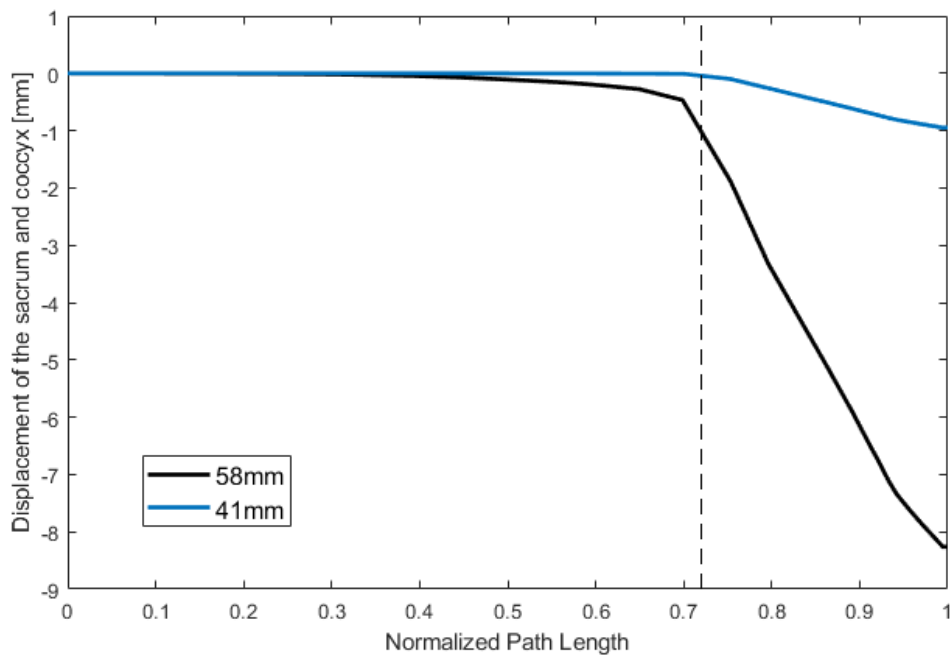
Figure 5.25: Displacement of the sacrum and coccyx in x-axis obtained along the normalized length for a vertical displacement of the fetus head of 41 mm and 58 mm. The black dashed line represents the beginning of the sacrococcygeal joint.

Analyzing Figure 5.25, it can be observed that a higher displacement of the coccyx and the sacrum takes place when the sacrococcygeal joint appears, in both moments. Therefore, it can be stated that the coccyx is more affected than the sacrum when the fetus head is negotiating to pass through the maternal pelvis. For a vertical displacement of the fetus head of 41 mm, a displacement of 0.95 mm occurs, while for a vertical descent of the fetus head of 58 mm, this value is 8.26 mm. As expected, at the moment of the maximum movement of the coccyx (58 mm), the sacrum and coccyx displacement is higher than when the coccyx starts to move (41 mm), being consistent with the results of the movement and rotation of the coccyx.

Chapter 6

Conclusions

This chapter will sum up the principal ideas of this work. It also describes ways in which this study could be improved as future works.

6.1 Conclusions

During vaginal delivery, to facilitate the passage of the fetus through the birth canal, the maternal pelvis undergoes some modifications. In addition, the pelvic floor muscles go through a series of stretches and strains that can cause severe deformations and damage, and muscles can even rupture. In chapter 3, every study that analyzed this problem found a stretch ratio of the LAM avulsion superior to 1.5, which is considered the permissible noninjurious length stretch of the muscle. It was also found that this value increased when an assisted vaginal delivery was performed, especially with a forceps delivery because of the risk of injury to the fetus and maternal morbidity. As a consequence, vacuum extractor became the technique of choice when in need of an assisted vaginal delivery.

Therefore, in this work, a noninvasive procedure with a biomechanical numerical simulation was performed. A finite element model of the fetal head was used to simulate the cardinal movements that the fetus has to perform in the second stage of labor, in a vertex presentation and in an occiput anterior position. Then the suction cup of the vacuum extractor was placed in the flexion point of the fetus head. A left OA position was used to successfully complete the simulation, because of constraints imposed by the pelvic bones and pelvic floor.

In the results obtained in this vacuum-assisted vaginal delivery simulation, a stretch ratio superior than the permissible noninjurious length stretch of the muscle occurred in the lower part of the pelvic floor muscles. Therefore, concluding that the inferior part of the levator ani muscle, especially the pubococcygeus muscle is the most affected muscle during the delivery and so where injuries are most prone to occur. As expected, this was also confirmed when evaluating the maximum stresses and strains on the PFM. In the suction cup of the vacuum extractor, it can be assumed that the forces needed to pull the fetus head are slightly higher than the forces that the fetus does by itself in a normal delivery. Regarding the pelvic bones, both the pubic symphysis

widening and the movement and rotation of the coccyx were in their permissible values that can occur during labor. Thus, concluding that a diastasis of the symphysis pubic and a coccyx fracture did not occur, as it can happen during instrumental vaginal deliveries.

Comparing these results with simulations performed with normal vaginal deliveries, there were not found many significant differences. This may have happened because, in this simulation, the coccyx could move freely as the suction cup pulled the fetus through the available space in the pelvis. However, instrumental vaginal deliveries are usually performed with a bed under the mother, making the coccyx more restricted to movement. Therefore, a different birthing position in which the coccyx could not move would probably cause some dysfunctions in the mother, and a pubic symphysis diastasis or even the fracture of the coccyx could occur.

The problem study in this work is of great complexity, so it presents some limitations that one should pay attention to. The suction cup was tied to the fetal head, but the effect of suction was not considered. The change in the hormones that happen during pregnancy and labor were not taken into consideration, but they can change some of the characteristics of the pelvic bones and ligaments. Also, during the delivery, fetal head molding occurs and modifies the head diameters, making it easier to pass through the birth canal, which was not considered.

6.2   Future Work

This work has given some encouraging results. We already have an idea of the impact that a vacuum-assisted vaginal delivery can cause on the maternal pelvic floor muscles and bones, so for future works, it would be important to test the impact of the suction cup in the fetal head. For this, the head would not be considered a rigid structure and fetal head molding would have to be taken into consideration. The effect of suction in the vacuum extractor would also be relevant to perceive the impact on the fetal head.

Additionally, it would be interesting to test a simulation with a coccyx more restricted to movement, as an instrumental delivery should happen. Perform simulations where hormonal changes are present would also be significant for future studies to evaluate the changes in the pelvic bones and ligaments during labor.

References

[1] H. U. Memon and V. L. Handa. Vaginal childbirth and pelvic floor disorders. *Women's Health*, 9(3):265–272, 2013.

[2] D. A. Oliveira, M. P. L. Parente, B. Calvo, T. Mascarenhas, and R. M. Natal Jorge. The management of episiotomy technique and its effect on pelvic floor muscles during a malposition childbirth. *Computer Methods in Biomechanics and Biomedical Engineering*, 20(11):1249–1259, 2017.

[3] H. Feltovich. Labour and delivery: A clinician's perspective on a biomechanics problem. *Interface Focus*, 9(5):1–7, 2019.

[4] WHO. *Managing Prolonged and Obstructed Labour*. WHO Library Cataloguing, Geneva, 2nd edition, 2008.

[5] A. Sharma. *Labour Room Emergencies*. Springer, Singapore, 1st edition, 2020.

[6] B. Nolens, T. Van den Akker, J. Lule, S. Twinomuhangi, J. Van Roosmalen, and J. Byamugisha. Women's recommendations: vacuum extraction or caesarean section for prolonged second stage of labour, a prospective cohort study in Uganda. *Tropical Medicine and International Health*, 24(5):553–562, 2019.

[7] H. Chen and D. Tan. Cesarean section or natural childbirth? Cesarean birth may damage your health. *Frontiers in Psychology*, 10(351):1–7, 2019.

[8] I. Coelho da Costa, C. S. Nunes, and H. S. Machado. Mode of Delivery and Labour Analgesia: A Study of Preference in Portuguese Pregnant Women. *Journal of Anesthesia & Clinical Research*, 09(08):1–11, 2018.

[9] Ulla Korhonen. Maternal Pelvis, Feto-pelvic Index and Labor Dystocia. Master's thesis, Faculty of Health Sciences, University of Eastern Filand, Kuopio, Finland, 2014.

[10] Gaspar Roriz. Parto computacional assistido. Master's thesis, FEUP, UP, Porto, Portugal, 2015.

[11] R. Lapeer, Z. Gerikhanov, and V. Audinis. A computer-based simulation of vacuum extraction during childbirth. In *Conference: SIMULIA UK Regional User Meeting*, pages 1–12, Norwich, 2014. University of East Anglia.

[12] D. A. Becker, C. T. Blanchard, J. M. Szychowski, S. L. Rogers, C. G. Brumfield, and A. Subramaniam. Resident Operative Vaginal Delivery Volume after Educational Curriculum Implementation. *American Journal of Perinatology*, 2020.

[13] D. J. Murphy, B. K. Strachan, and R. Bahl. Assisted Vaginal Birth. *BJOG: An International Journal of Obstetrics and Gynaecology*, (26):1–43, 2020.

[14] P. E. Bailey, J. Van Roosmalen, G. Mola, C. Evans, L. de Bernis, and B. Dao. Assisted vaginal delivery in low and middle income countries: an overview. *BJOG: An International Journal of Obstetrics and Gynaecology*, 124(9):1335–1344, 2017.

[15] Frédéric Michas. Percentage of births delivered by forceps or vacuum extraction in the United States from 1990 to 2018, 2019. URL: https://www.statista.com/statistics/276067/us-births-delivered-by-forceps-or-vacuum-extraction/{#}statisticContainer, accessed Jan. 03, 2021.

[16] D. Oliveira, M. Silva, M. Vila Pouca, M. Parente, T. Mascarenhas, and R. Jorge. Biomechanical Simulation of Vaginal Childbirth: The Colors of the Pelvic Floor Muscles. In Springer, editor, *Computational Biomechanics for Medicine: Personalisation, Validation and Therapy*, chapter I, pages 1–17. 2020.

[17] M. A.T. Bortolini, H. P. Drutz, D. Lovatsis, and M. Alarab. Vaginal delivery and pelvic floor dysfunction: current evidence and implications for future research. *International Urogynecology Journal*, 21(8):1025–1030, 2010.

[18] G. Rostaminia and S. Abramowitch. Finite Element Modeling in Female Pelvic Floor Medicine: a Literature Review. *Current Obstetrics and Gynecology Reports*, 4(2):125–131, 2015.

[19] D. Oliveira, M. Parente, T. Mascarenhas, and R. Natal Jorge. Biomechanical analysis of the damage in the pelvic floor muscles during childbirth. *Lecture Notes in Computational Vision and Biomechanics*, 29:133–142, 2018.

[20] B. T. Haylen, D. de Ridder, R. M. Freeman, S. E. Swift, B. Berghmans, J. Lee, A. Monga, E. Petri, D. E. Rizk, P. K. Sand, and G. N. Schaer. An International Urogynecological Association (IUGA)/International Continence Society (ICS) Joint Report on the Terminology for Female Pelvic Floor Dysfunction. *Neurourology and Urodynamics*, 29:4–20, 2010.

[21] M. Alperin, M. Cook, L. J. Tuttle, M. C. Esparza, and R. L. Lieber. Impact of vaginal parity and aging on the architectural design of pelvic floor muscles. *American Journal of Obstetrics and Gynecology*, 215(3):312.e1–312.e9, 2016.

[22] A. L. Olsen, V. J. Smith, J. O. Bergstrom, J. C. Colling, and A. L. Clark. Epidemiology of surgically managed pelvic organ prolapse and urinary incontinence. *Obstetrics and Gynecology*, 89(4):501–506, 1997.

[23] K. C. Lien, D. M. Morgan, J. O. L. Delancey, and J. A. Ashton-Miller. Pudendal nerve stretch during vaginal birth: A 3D computer simulation. *American Journal of Obstetrics and Gynecology*, 192(5 SPEC. ISS.):1669–1676, 2005.

[24] I. Nygaard, M. D. Barber, K. L. Burgio, K. Kenton, S. Meikle, J. Schaffer, C. Spino, W. E. Whitehead, J. Wu, and D. J. Brody. Prevalence of Symptomatic Pelvic Floor Disorders in US Women. *American Medical Association*, 300(11):1311–1316, 2008.

[25] G. Hilde, J. Stær-Jensen, F. Siafarikas, M. E. Engh, I. H. Brækken, and K. Bo. Impact of childbirth and mode of delivery on vaginal resting pressure and on pelvic floor muscle strength and endurance. *American Journal of Obstetrics and Gynecology*, 208(1):50.e1–50.e7, 2013.

[26] P. Rahmanou, J. Caudwell-Hall, I. Kamisan Atan, and H. P. Dietz. The association between maternal age at first delivery and risk of obstetric trauma. *American Journal of Obstetrics and Gynecology*, pages 3–15, 2016.

[27] R. Warren and S. Arulkumaran. *Best Practice in Labour and Delivery*. Cambridge University Press, London, 2nd edition, 2016.

[28] J. M. DeSilva and K. R. Rosenberg. Anatomy, Development, and Function of the Human Pelvis. *The Anatomical Record*, 300:628–632, 2017.

[29] A. Graziottin and D. Gambini. Anatomy and Physiology of Genital Organs - Women. In *Handbook of Clinical Neurology*, volume 130, chapter 4, pages 39–60. Elsevier B.V., 2015.

[30] R. L. Drake, W. A. Vogl, and A. W. M. Mitchell. Pelvis and Perineum. In *Gray's Anatomy For Students*, pages 423–456. Chruchill Livingstone - Elsevier, 3rd edition, 2014.

[31] K. L. Moore, A. M. R. Agur, and A. F. Dalley. Pelvis and Perineum. In *Moore's Essential Clinical Anatomy*, pages 195–206. Wolters Kluwer Health, 5th edition, 2015.

[32] B. Sujana, A. Keepanasseril, and D. Maurya. Diastasis of the pubic symphysis following vaginal delivery. *International Journal of Gynecology & Obstetrics*, 131(1):102–103, 2017.

[33] S. Jain, P. Eedarapalli, P. Jamjute, and R. Sawdy. Symphysis pubis dysfunction: a practical approach to management. *The Obstetrician & Gynaecologist*, 8(3):153–158, 2006.

[34] J. T. K. Woon and M. D. Stringer. Clinical anatomy of the coccyx: A systematic review. *Clinical Anatomy*, 25(2):158–167, 2011.

[35] J. Y. Maigne, F. Rusakiewicz, and M. Diouf. Postpartum coccydynia: A case series study of 57 women. *European Journal of Physical and Rehabilitation Medicine*, 48(3):387–392, 2012.

[36] S. G. Gabble, J. R. Niebyl, J. L. Simpson, M. B. Landon, H. L. Galan, E. R. M. Jauniaux, D. A. Driscoll, V. Berghella, and W. A. Grobman. *Obstetrics Normal and Problem Pregnancies*. Elsevier, Philadelphia, 7th edition, 2017.

[37] G. D. Posner, J. Dy, A. Y. Black, and G. D. Jones. *Human Labor & Birth*. 6th edition, 2013.

[38] J. Stoker and C. Wallner. The Anatomy of the Pelvic Floor and Sphincters. In *Imaging Pelvic Floor Disorders*, pages 1–29. Springer, Berlin, Heidelberg, 2008.

[39] L. Crumbie and A. Osika. Muscles of the pelvic floor. kenhub, 2020. URL: https://www.kenhub.com/en/library/anatomy/muscles-of-the-pelvic-floor, accessed Dec. 03, 2020.

[40] Marco Paulo Lages Parente. *Biomechanics of the pelvic floor during vaginal delivery*. PhD thesis, FEUP, UP, Porto, Portugal, 2008.

[41] R. Natal Jorge, S. Brandão, T. Da Roza, M. Parente, and T. Mascarenhas. Biomechanical Childbirth Simulations. In *Biomechanics of the Female Pelvic Floor*, chapter Chapter Two, pages 415–431. Elsevier Inc., Porto, 2016.

[42] H. Rather, J. Muglu, L. Veluthar, and K. Sivanesan. The art of performing a safe forceps delivery: A skill to revitalise. *European Journal of Obstetrics and Gynecology and Reproductive Biology*, 199:49–54, 2016.

[43] A. M. Dückelmann and K. Kalache. Fetal Progression in Birth Canal: State of the Art. In *Intrapartum Ultrasonography for Labor Management*, chapter 13, pages 159–181. Springer, Berlin, 2013.

[44] M. P. Parente, R. M. Natal Jorge, T. Mascarenhas, and A. L. Silva-Filho. The influence of pelvic muscle activation during vaginal delivery. *Obstetrics and Gynecology*, 115(4):804–808, 2010.

[45] R. Armbrust, W. Henrich, L. Hinkson, C. Grieser, and J. P. Siedentopf. Correlation of intrapartum translabial ultrasound parameters with computed tomographic 3D reconstruction of the female pelvis. *Journal of Perinatal Medicine*, 44(5):1–5, 2016.

[46] Y. M. Cargill and C. J. MacKinnon. Guidelines for Operative Vaginal Birth. *Journal of Obstetrics and Gynaecology Canada*, 40(2):e74–e80, 2018.

[47] U. A. Ali and E. R. Norwitz. Vacuum-Assisted Vaginal Delivery. *Reviews In Obstetrics & Gynecology*, 2(1):5–17, 2009.

[48] D. Goordyal, J. Anderson, A. Alazmani, and P. Culmer. An engineering perspective of vacuum assisted delivery devices in obstetrics: A review. *Proceedings of the Institution of Mechanical Engineers, Part H: Journal of Engineering in Medicine*, pages 1–14, 2020.

[49] American College of Obstetricians and Gynecologists. Operative Vaginal Birth: ACOG Practice Bulletin, No. 219. *Obstetrics & Gynecology*, 135(4):e149–59, 2020.

[50] H. Sekia and S. Takedab. A review of prerequisites for vacuum extraction: Appropriate position of the fetal head for vacuum extraction from a forceps delivery perspective. *Medical & Clinical Reviews*, 02(02):1–5, 2016.

[51] J. Unuigbe, G. Agbon-Ojeme, R. Erhatiemwomon, and K. Maduako. Instrumental vaginal deliveries: A review. *Tropical Journal of Obstetrics and Gynaecology*, 35(2):99–107, 2018.

[52] S. Turkmen. Maternal and neonatal outcomes in vacuum-assisted delivery with the Kiwi OmniCup and Malmström metal cup. *Journal of Obstetrics and Gynaecology Research*, 41(2):207–213, 2015.

[53] Peter de Jong. *Vacuum Assisted Delivery Procedures*. Medela AG, Cape Town, South Africa, 2015.

[54] World Health Organization. *Managing Complications in Pregnancy and Childbirth: A guide for midwives and doctors*. 2nd edition, 2017.

[55] I. Kepenekci, B. Keskinkilic, F. Akinsu, P. Cakir, A. H. Elhan, A. B. Erkek, and M. A. Kuzu. Prevalence of Pelvic Floor Disorders in the Female Population and the Impact of Age, Mode of Delivery, and Parity. *Diseases of the Colon and Rectum*, 54(1):85–94, 2011.

[56] J. A. Sainz, E. González-Diaz, A. M. Martínez, I. Ortega, C. Fernández-Fernández, A. F. Palacín, and J. A. García-Mejido. Prevalence of levator hiatal overdistension after vacuum and forceps deliveries. *Neurourology and Urodynamics*, 39(2):841–846, 2020.

[57] J. Cassadó, M. Simó, N. Rodríguez, O. Porta, E. Huguet, I. Mora, M. Girvent, R. Fernández, and I. Gich. Prevalence of levator ani avulsion in a multicenter study (PAMELA study). *Archives of Gynecology and Obstetrics*, 302(1):273–280, 2020.

[58] K. L. Shek and H. P. Dietz. The effect of childbirth on hiatal dimensions. *Obstetrics and Gynecology*, 113(6):1272–1278, 2009.

[59] K. Svabík, K. L. Shek, and H. P. Dietz. How much does the levator hiatus have to stretch during childbirth? *BJOG: An International Journal of Obstetrics and Gynaecology*, 116(12):1657–1662, 2009.

[60] I. Volløyhaug, S. Mørkved, and K. Salvesen. Forceps delivery is associated with increased risk of pelvic organ prolapse and muscle trauma: A cross-sectional study 16-24 years after first delivery. *Ultrasound in Obstetrics and Gynecology*, 46(4):487–495, 2015.

[61] C. M. Durnea, B. A. O'Reilly, A. S. Khashan, L. C. Kenny, U. A. Durnea, M. M. Smyth, and H. P. Dietz. Status of the pelvic floor in young primiparous women. *Ultrasound in Obstetrics and Gynecology*, 46(3):356–362, 2015.

[62] G. Trutnovsky, I. Kamisan Atan, A. Martin, and H. P. Dietz. Delivery mode and pelvic organ prolapse: a retrospective observational study. *BJOG: An International Journal of Obstetrics and Gynaecology*, 123(9):1551–1556, 2015.

[63] R. Kearney, J. M. Miller, J. A. Ashton-Miller, and J. O. L. DeLancey. Obstetric factors associated with levator ani muscle injury after vaginal birth. *Obstetrics and Gynecology*, 107(1):144–149, 2006.

[64] S. Friedman, J. L. Blomquist, J. M. Nugent, K. C. McDermott, A. Muñoz, and V. L. Handa. Pelvic muscle strength after Childbirth. *Obstetrics and Gynecology*, 120(5):1021–1028, 2012.

[65] H. U. Memon, J. L. Blomquist, H. P. Dietz, C. B. Pierce, M. M. Weinstein, and V. L. Handa. Comparison of levator ni muscle avulsion injury after forceps-assisted and vacuum-assisted vaginal childbirth. *Obstetricians and Gynecologists*, 125(5):1080–1087, 2015.

[66] K. L. Shek and H. P. Dietz. Intrapartum risk factors for levator trauma. *BJOG: An International Journal of Obstetrics and Gynaecology*, 117(12):1485–1492, 2010.

[67] J. A. García-Mejido, A. Martín-Martínez, E. González-Diaz, C. Fernández-Fernández, I. Ortega, M. Medina, A. Fernández-Corona, A. Fernández-Palacín, and J. A. Sainz. Malmström vacuum or Kielland forceps: which causes more damage to pelvic floor? *Ultrasound in Obstetrics and Gynecology*, 55(2):257–263, 2020.

[68] J. A. Garcia-Mejido, L. Gutierrez, A. Fernandez-Palacín, A. Aquise, and J. A. Sainz. Levator ani muscle injuries associated with vaginal vacuum assisted delivery determined by 3/4D transperineal ultrasound. *Journal of Maternal-Fetal and Neonatal Medicine*, 30(16):1891–1896, 2017.

[69] U. M. Peschers, A. H. Sultan, K. Jundt, A. Mayer, V. Drinovac, and T. Dimpfl. Urinary and anal incontinence after vacuum delivery. *European Journal of Obstetrics & Gynecology and Reproductive Biology*, 110:39–42, 2003.

[70] I. Michalec, O. Simetka, M. Navratilova, M. Tomanova, M. Gartner, D. Salounova, M. Prochazka, and M. Kacerovsky. Vacuum-assisted vaginal delivery and levator ani avulsion in primiparous women. *Journal of Maternal-Fetal and Neonatal Medicine*, 29(16):2715–2718, 2016.

[71] K. Jundt, I. Scheer, B. Schiessl, K. Karl, K. Friese, and M. Peschers. Incontinence, Bladder Neck Mobility, and Sphincter Ruptures in Primiparous Women. *European Journal of Medical Research*, 15:246–252, 2010.

[72] E. Ashwal, A. Wertheimer, A. Aviram, H. Pauzner, A. Wiznitzer, Y. Yogev, and L. Hiersch. The association between fetal head position prior to vacuum extraction and pregnancy outcome. *Archives of Gynecology and Obstetrics*, 293(3):567–573, 2016.

[73] E. González-Diaz, J. A. García-Mejido, A. Martín-Martínez, C. Fernández-Fernández, I. Ortega, M. Medina, A. Fernández-Corona, A. Fernández-Palacín, and J. A. Sainz. Are there differences in the damage to the pelvic floor between malmstrom's and kiwi omnicup vacuums? A multicenter study. *Neurourology and Urodynamics*, 39(1):190–196, 2020.

[74] J. A. García-Mejido, A. Fernández-Palacín, M. J. Bonomi Barby, L. Castro, A. Aquise, and J. A. Sainz. A comparable rate of levator ani muscle injury in operative vaginal delivery (forceps and vacuum) according to the characteristics of the instrumentation. *Acta Obstetricia et Gynecologica Scandinavica*, 98(6):729–736, 2019.

[75] X. Li, J. A. Kruger, M. P. Nash, and P. M. F. Nielsen. Modeling childbirth: Elucidating the mechanisms of labor. *Wiley Interdisciplinary Reviews: Systems Biology and Medicine*, 2(4):460–470, 2010.

[76] X. Li, J. A. Kruger, M. P. Nash, and P. M. F. Nielsen. Effects of nonlinear muscle elasticity on pelvic floor mechanics during vaginal childbirth. *Journal of Biomechanical Engineering*, 132(11):1–6, 2010.

[77] E. Jean Dit Gautier, O. Mayeur, J. Lepage, M. Brieu, M. Cosson, and C. Rubod. Pregnancy impact on uterosacral ligament and pelvic muscles using a 3D numerical and finite element model: preliminary results. *International Urogynecology Journal*, 29(3):425–430, 2018.

[78] K. C. Lien, B. Mooney, J. O. L. DeLancey, and J. A. Ashton-Miller. Levator ani muscle stretch induced by simulated vaginal birth. *Obstetrics and Gynecology*, 103(1):31–40, 2004.

[79] M. P. L. Parente, R. M. Natal Jorge, T. Mascarenhas, A. A. Fernandes, and J. A. C. Martins. Deformation of the pelvic floor muscles during a vaginal delivery. *International Urogynecology Journal*, 19(1):65–71, 2008.

[80] J. A. C. Martins, M. P. M. Pato, E. B. Pires, R. M. Natal Jorge, M. Parente, and T. Mascarenhas. Finite element studies of the deformation of the pelvic floor. *Annals of the New York Academy of Sciences*, 1101:316–334, 2007.

[81] L. Hoyte, M. S. Damaser, S. K. Warfield, G. Chukkapalli, A. Majumdar, D. J. Choi, A. Trivedi, and P. Krysl. Quantity and distribution of levator ani stretch during simulated vaginal childbirth. *American Journal of Obstetrics and Gynecology*, 199(2):198.e1–198.e5, 2008.

[82] P. Y. Noritomi, J. V. Lopes Da Silva, R. C. A. Dellai, A. Fiorentino, L. Giorleo, and E. Ceretti. Virtual modeling of a female pelvic floor and hypothesis for simulating biomechanical behavior during natural delivery. *Procedia CIRP*, 5:300–304, 2013.

[83] L. Krofta, L. Havelková, I. Urbánková, M. Krčmář, L. Hynčík, and J. Feyereisl. Finite element model focused on stress distribution in the levator ani muscle during vaginal delivery. *International Urogynecology Journal*, 28(2):275–284, 2017.

[84] D. A. Oliveira, M. P. L. Parente, B. Calvo, T. Mascarenhas, and R. M. Natal Jorge. Numerical simulation of the damage evolution in the pelvic floor muscles during childbirth. *Journal of Biomechanics*, 49(4):594–601, 2016.

[85] M. P.L. Parente, R. M. Natal Jorge, T. Mascarenhas, A. A. Fernandes, and J. A.C. Martins. The influence of the material properties on the biomechanical behavior of the pelvic floor muscles during vaginal delivery. *Journal of Biomechanics*, 42(9):1301–1306, 2009.

[86] D. Jing, J. A. Ashton-Miller, and J. O. L. DeLancey. A subject-specific anisotropic visco-hyperelastic finite element model of female pelvic floor stress and strain during the second stage of labor. *Journal of Biomechanics*, 45(3):455–460, 2012.

[87] X. Li, J. A. Kruger, M. P. Nash, and P. M. F. Nielsen. Anisotropic effects of the levator ani muscle during childbirth. *Biomechanics and Modeling in Mechanobiology*, 10(4):485–494, 2011.

[88] M. C. P. Vila Pouca, J. P. S. Ferreira, D. A. Oliveira, M. P. L. Parente, and R. M. Natal Jorge. Viscous effects in pelvic floor muscles during childbirth: A numerical study. *International Journal for Numerical Methods in Biomedical Engineering*, 34(3):1–10, 2018.

[89] M. C.P. Vila Pouca, J. P.S. Ferreira, D. A. Oliveira, M. P. L. Parente, and R. M. Mascarenhas, T.and Natal Jorge. On the effect of labour durations using an anisotropic visco-hyperelastic-damage approach to simulate vaginal deliveries. *Journal of the Mechanical Behavior of Biomedical Materials*, 88:120–126, 2018.

[90] X. Li, J. A. Kruger, J. Chung, M. P. Nash, and P. M. F. Nielsen. Modelling Childbirth: Comparing Athlete and Non-athlete Pelvic Floor Mechanics. In *Medical Image Computing and Computer-Assisted Intervention - MICCAI 2008. Lecture Notes in Computer Science.*, volume 5242, pages 750–757. Springer Berlin Heidelberg, part ii edition, 2008.

[91] X. Li, J. A. Kruger, J. Chung, M. P. Nash, and P. M. F. Nielsen. Modelling the pelvic floor for investigating difficulties during childbirth. *Medical Imaging 2008: Physiology, Function, and Structure from Medical Images*, 6916, 2008.

[92] M. P. L. Parente, R. M. Natal Jorge, T. Mascarenhas, A. A. Fernandes, and J. A. C. Martins. The influence of an occipito-posterior malposition on the biomechanical behavior of the pelvic floor. *European Journal of Obstetrics and Gynecology and Reproductive Biology*, 144S:S166–S169, 2009.

[93] Maria Elisabete Teixeira Silva. Estudo Biomecânico de um Feto Durante um Parto Vaginal. Master's thesis, FEUP, UP, Porto, Portugal, 2012.

[94] M. P. Parente, R. M. Natal Jorge, T. Mascarenhas, A. A. Fernandes, and A. L. Silva-Filho. Computational modeling approach to study the effects of fetal head flexion during vaginal delivery. *American Journal of Obstetrics and Gynecology*, 203(3):217.e1–217.e6, 2010.

[95] M. E.T. Silva, D. A. Oliveira, T. H. Roza, S. Brandão, M. P.L. Parente, T. Mascarenhas, and R. M. Natal Jorge. Study on the influence of the fetus head molding on the biomechanical behavior of the pelvic floor muscles, during vaginal delivery. *Journal of Biomechanics*, 48(9):1600–1605, 2015.

[96] J. A. Ashton-Miller and J. O. L. DeLancey. On the biomechanics of vaginal birth and common sequelae. *Annual Review of Biomedical Engineering*, 11:163–176, 2009.

[97] M. Bozkurt. Pelvic floor dysfunction, and effects of pregnancy and mode of delivery on pelvic floor. *Taiwanese Journal of Obstetrics & Gynecology*, 53:452–458, 2014.

[98] Gerhard Holzapfel. *Nonlinear Solid Mechanics: A Continuum Approach for Engineering Science*, volume 37. John Wiley & Sons, Ltd, 2002.

[99] J. Bonet and R. Wood. *Nonlinear Continuum Mechanics for Finite Element Analysis*. Cambridge University Press, 2nd edition, 2008.

[100] Allan Bower. *Applied Mechanics of Solids*. Taylor & Francis, 2010.

[101] S. Janda, F. C. T. Van Der Helm, and S. B. De Blok. Measuring morphological parameters of the pelvic floor for finite element modelling purposes. *Journal of Biomechanics*, 36(6):749–757, 2003.

[102] M. Borges, R. Moura, D. Oliveira, M. Parente, T. Mascarenhas, and R. Natal. Effect of the birthing position on its evolution from a biomechanical point of view. *Computer Methods and Programs in Biomedicine*, 200, 2021.

[103] Nam Ho Kim. *Introduction to Nonlinear Finite Element Analysis*. Springer, 2015.

Appendix A

A.1 Paper submitted and accepted at the "Congresso Nacional de Biomecânica"

Considerações preliminares para simulações numéricas no parto assistido

Beatriz Estêvão[1], Dulce Oliveira[2], Marco Parente[3]
[1]Faculdade de Engenharia, Universidade do Porto, Portugal, up201909421@fe.up.pt
[2]INEGI, Universidade do Porto, Portugal, doliveira@fe.up.pt
[3]INEGI, FEUP, Universidade do Porto, Portugal, mparente@fe.up.pt

RESUMO

O parto vaginal é considerado a principal causa de disfunção do pavimento pélvico. Quando é necessário auxiliar o parto vaginal, os obstetras utilizam ventosas. Neste estudo, foram analisadas considerações iniciais para a simulação numérica do parto vaginal assistido. Foram feitas simulações numéricas para avaliar tensões e deformações nos músculos do pavimento pélvico materno. A análise dos gráficos obtidos mostra que para um deslocamento vertical da cabeça do feto de aproximadamente 60 mm, as tensões máximas nos músculos do pavimento pélvico foram de 0,82 e 0,29 MPa para uma distância normalizada de 0 e 0,47 respetivamente. Nas deformações, os valores máximos foram 0,70 e 0,49 para os mesmos valores das distâncias normalizadas das tensões. Esses valores máximos correspondem aos músculos associados a lesões que ocorrem durante o parto.

Palavras-chave: Simulação de Parto, Método dos Elementos Finitos, Ventosa Kiwi Omnicup, Ventosa Malmström.

INTRODUÇÃO

Qualquer problema que impeça a progressão do parto natural requer medidas para acelerar o parto, uma das quais é o parto vaginal assistido, que segundo a Organização Mundial de Saúde, corresponde a 2 a 23% dos partos em todo o mundo [1]. Nos últimos anos, embora a taxa total de partos

81

vaginais assistidos tenha diminuído, o uso de ventosas aumentou e representa quase 4 vezes a taxa de partos com o uso de fórceps [2].

Durante o parto vaginal, quando o feto passa pelo canal de parto, o risco de lesões musculares do pavimento pélvico aumenta [3], sendo o parto vaginal considerado a principal causa de disfunção do pavimento pélvico [4].

Os principais objetivos deste estudo são a familiarização com os modelos computacionais e a análise numérica com os softwares Abaqus e SolidWorks. Assim, o parto normal foi simulado e o impacto nos músculos do pavimento pélvico avaliado. Considerações preliminares foram ainda analisadas para a simulação do parto vaginal assistido.

MATERIAIS E MÉTODOS

O método dos elementos finitos (MEF) foi utilizado, para medir tensões e deformações nos músculos do pavimento pélvico durante o parto. O modelo de elementos finitos do pavimento pélvico e do feto foi desenvolvido no trabalho de Parente et al. [5].

As ventosas são o dispositivo mais utilizado no parto vaginal devido à facilidade de uso, segurança e eficácia [6]. Dois tipos de ventosas foram modelados durante este estudo: a ventosa Kiwi Omnicup e a ventosa Malmström. Na literatura foi verificado que a ventosa Kiwi Omnicup possui diâmetro de 50 mm [2]. Este também é um dos diâmetros disponíveis na ventosa Malmström [7]. A malha de elementos finitos da ventosa Kiwi Omnicup foi criada por Roriz [8]. A ventosa Malmström foi criada utilizando o software SolidWorks (Figura 1a). De seguida, este modelo foi importado para o ABAQUS e a malha do objeto foi criada (Figura 1b).

Figura 1. a. Modelo da ventosa Malmström em 3D. b. Malha de elementos finitos.

No parto vaginal assistido, a ventosa é colocada após o início do parto. Para mimetizar este momento, estudaram-se diferentes abordagens como o comando *MODEL CHANGE*, que permite desativar e reativar elementos para simular a remoção ou inserção do modelo. Também é necessário estabelecer a união entre o modelo de ventosa e a cabeça do feto, e isso é feito a partir do comando *TIE*.

RESULTADOS E DISCUSSÃO

A Figura 2a mostra a distribuição das tensões principais máximas obtidas no pavimento pélvico, para um deslocamento vertical da cabeça do feto de aproximadamente 60 mm. Na Figura 2b,

observam-se as deformações máximas no pavimento pélvico, para o mesmo deslocamento vertical da cabeça do feto. Ambos os gráficos foram obtidos sem ventosas.
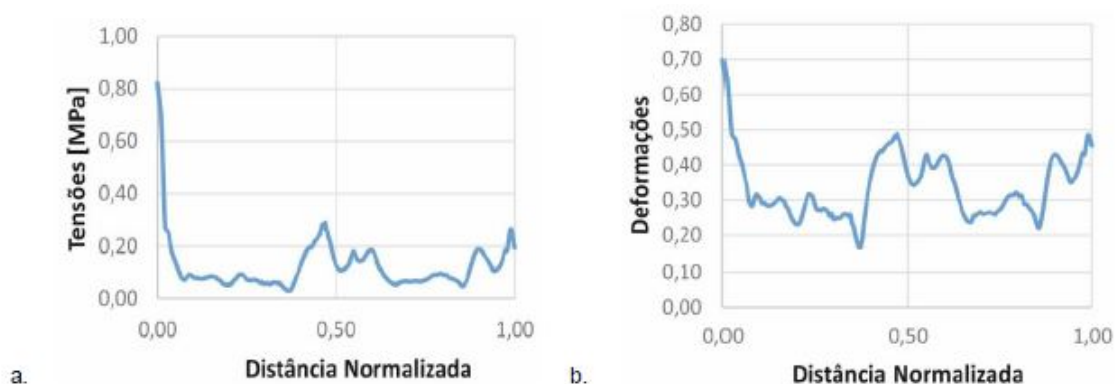

Figura 2. a. Tensões máximas e b. deformações máximas no pavimento pélvico para um deslocamento vertical da cabeça do feto de aproximadamente 60 mm, sem ventosa.

Como pode ser visto na Figura 2a, as tensões máximas foram obtidas quando a distância normalizada estava em 0 e 0,47 e a tensão correspondente aos valores são 0,82 e 0,29 MPa. Esses dois pontos coincidem com a fixação do pavimento pélvico à estrutura óssea e ao ponto intermédio do músculo elevador do ânus, respetivamente. Estas zonas estão associados a lesões que ocorrem durante o parto [4]. A Figura 2b também apresenta dois pontos onde a deformação é máxima. Esses pontos, são quando a distância normalizada está em 0 e 0,47 que, tal como dito, são locais associados a lesões durante o parto vaginal. As respetivas deformações máximas são 0,70 e 0,49.

CONCLUSÃO

O risco de lesões nos músculos do pavimento pélvico aumenta durante o parto vaginal. Estes músculos, estão sujeitos a altos valores de tensões e deformações quando o feto passa pelo canal do parto. Ambos os valores máximos obtidos nos gráficos de tensões e deformações correspondem aos músculos que estão associados a lesões durante o parto vaginal.

REFERÊNCIAS

[1] Odon, J. (2011). Assisted vaginal delivery instrument. *World Health Organization*. http://www.who.int/medical_devices/en/index.html.

[2] Ali, U.A., Norwitz, E.R. (2009). Vacuum-Assisted Vaginal Delivery. Reviews in Obstetrics & Gynecology, 2(1), 5–17.

[3] Natal Jorge, R.M., Brandão, S., Da Roza, T., Parente, M., Mascarenhas, T. (2016). Biomechanical Childbirth Simulations. In *Biomechanics of the Female Pelvic Floor*. Elsevier Inc. 415–431.

[4] Oliveira, D.A., Silva, M.E.T., Vila-Pouca, M., Parente, M.P.L., Mascarenhas, T., Natal Jorge, R.M. (2020). Biomechanical Simulation of Vaginal Childbirth: The Colors of the Pelvic Floor Muscles. In *Computational Biomechanics for Medicine*, MICCAI 2019, Nash, M., Nielsen, P., Wittek, A., Miller, K., Joldes,

G. (Eds), Springer,978-3-030-15922-1.

[5] Parente, M.P.L. (2008). *Biomechanics of the Pelvic Floor during Vaginal delivery*. (PhD thesis, Universidade do Porto).

[6] Unuigbe, J., Agbon-Ojeme, G., Erhatiemwomon, R., Maduako, K. (2018). Instrumental vaginal deliveries: A review. Tropical Journal of Obstetrics and Gynaecology, 35(2), 99–107.

[7] González-Diaz, E., García-Mejido, J.A., Martín-Martínez, A., Fernández-Fernández, C., Ortega, I., Medina, M., Fernández-Corona, A., Fernández-Palacín, A., Sainz, J.A. (2020). Are there differences in the damage to the pelvic floor between malmstrom's and kiwi omnicup vacuums? A multicenter study. Neurourology and Urodynamics, 39(1), 190–196.

[8] Roriz, G. (2015). *Parto computacional assistido*. (MSc thesis, Universidade do Porto).